5-24-1971

EPR study of some d5 transition elements in single crystals

Mahmoud Gawish

Follow this and additional works at: https://fount.aucegypt.edu/retro_etds

Recommended Citation
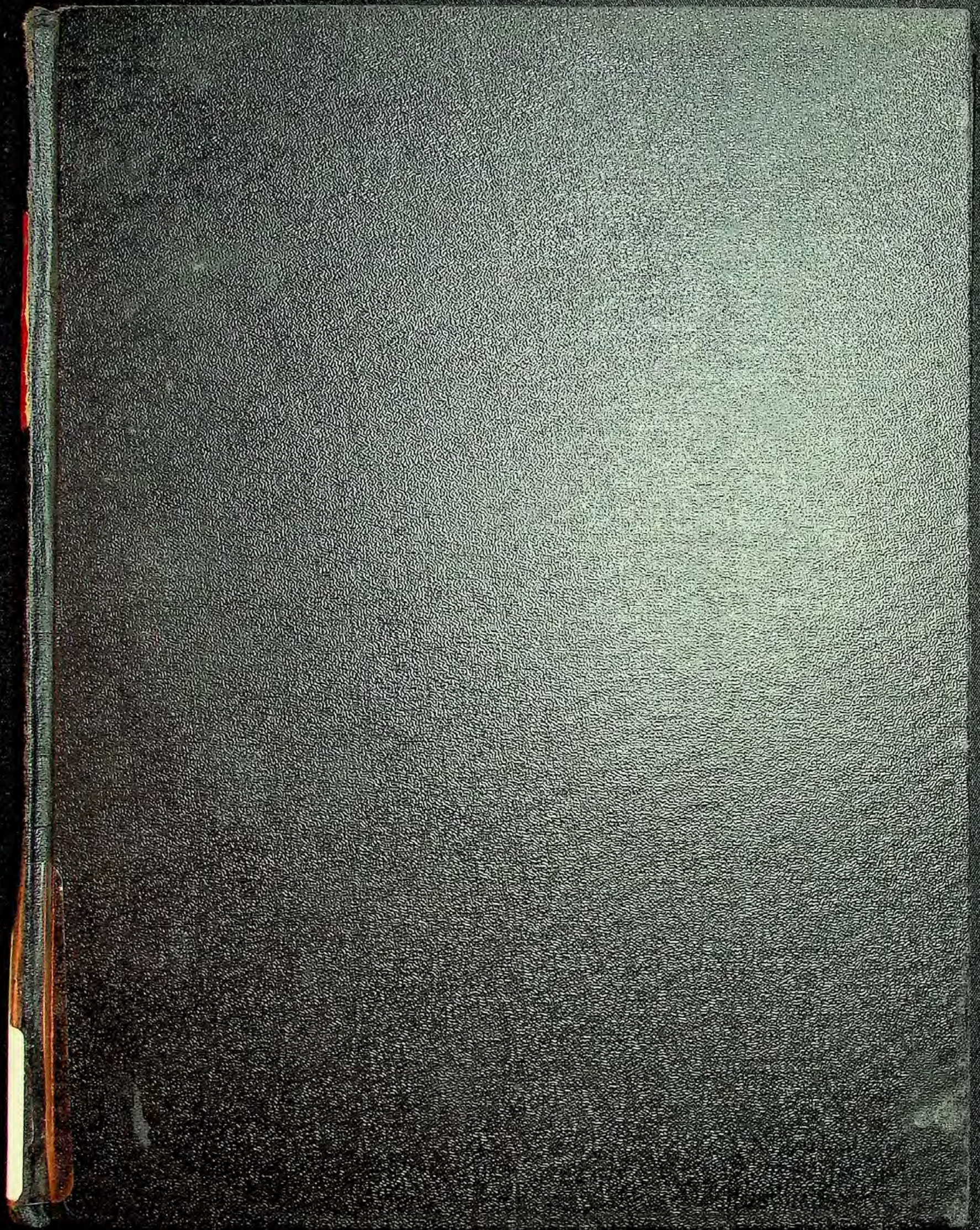
The Committee consisting of Professors Richard Borg, Ezzat Abdel Aziz, Youssef Leito, Robert Weeks, Eugene Loh, Salah Arafa, Fadel Assabghy and Adli Bishay examined today Mr. Mahmoud M. Gawish orally in his M.Sc. Thesis entitled: "EPR STUDY OF SOME d^5 TRANSITION ELEMENTS IN SINGLE CRYSTALS".

The student answered the questions adequately, and the Committee recommends that his thesis is definitely of the level of Master of Science in Solid State Science.

May 24, 1971.

EPR STUDY

OF SOME d^5 TRANSITION ELEMENTS IN SINGLE CRYSTALS.

BY

MAHMOUD GAWISH

THESIS

SUBMITTED IN PARTIAL FULFILLMENT OF THE
REQUIREMENTS FOR THE DEGREE OF MASTER OF
SCIENCE IN SOLID STATE PHYSICS IN THE GRADUATE
COLLEGE OF THE

American University in Cairo,

1971.

ii

ABSTRACT

The electron paramagnetic resonance of Mn^{2+} and Fe^{3+} in single crystals of $BaTiO_3$ and Mg_2SiO_4 has been studied at 9.5 Gc. The spectra are interpreted in terms of a spin Hamiltonian of the form $H = gBH.S + D\left[S_z^2 - \frac{1}{3}(S+1)\right] + E(S_x^2 - S_y^2)$. Two different sites which could be occupied by either Mn^{2+} or Fe^{3+} ions are found in both crystals. The Ba^{2+} and Ti^{4+} sites in $BaTiO_3$, and the M(1) and M(2) sites in Mg_2SiO_4. Mn^{2+} ions occupy the Ti^{4+} site in $BaTiO_3$. An additional impurity was found to be present in the $BaTiO_3$ crystal and is attributed to Fe^{3+} ion in the Ti^{4+} sites also. In Mg_2SiO_4 crystal the Fe^{3+} ions occupy the M(2) site. Temperature variation showed that $BaTiO_3$ undergoes three phase transitions, above $120^{\circ}C$ it is in the cubic phase, between 120° and $5^{\circ}C$ it is in the tetragonal phase, below $5^{\circ}C$ it is in the orthorhombic phase. But no site disordering was observed for $BaTiO_3$ for any temperature range. Mg_2SiO_4 showed local disordering above $400^{\circ}C$.

X-ray irradiation did not show disordering of the $BaTiO_3$, but just a decrease in the intensity of the Mn^{2+} and Fe^{3+} lines attributed to the change of valency of small percentages of the doped Mn^{2+} ions and the Fe^{3+} impurity ions. While the Fe^{3+} lines in Mg_2SiO_4 were not detected after X-ray irradiation, attributed to the change of valency of the Fe^{3+} ion.

iii

TABLE OF CONTENTS

Figure Captions

ACKNOWLEDGMENT

I wish here to express my thanks and gratitude to Professor Dr. Adli Bishay, Chairman of the Material Engineering and Physical Sciences Department for his constant encouragement and deep interest in research.

It is my pleasure to express my deep gratitude and thanks to Professor R.A. Weeks and Dr. S. Arafa for supervising the conduct of this work. Without the benefit of their guidance, their valuable discussion and advice and above all their constant encouragement, this thesis could not have been completed.

Thanks are due to the A.U.C. for the facilities made available during the course of this research.

Finally I wish to thank Mr. Fredrick Shafik for expert technical assistance in the ESR Laboratory, and Mr. Aziz Kirolos for typing this thesis.

CHAPTER I

Introduction

Much interest has been centered on the interpretation of the several kinds of EPR spectra which can be observed for d^5 electronic states, notably in crystal systems containing Fe^{3+} and Mn^{2+}. The spin Hamiltonian usually used to fit the spectra is:

$$\mathcal{H} = \beta \, H.g.S + D\left[S_z^2 - \tfrac{1}{3} S(S+1)\right] + E\,(S_x^2 - S_y^2) \qquad (1)$$

originally proposed by Bleaney and Stevens[1]. Some authors also include quartic terms but these are usually small when the symmetry of the electric field, with which the d^5 electrons interact, is lower than cubic and are justifiably omitted. The values of the terms D and E reflects the symmetry of the electric field.

R.D. Dowsing and J.F. Gibson[2] by the use of the above spin Hamiltonian and the ratio of $\frac{E}{D}$, denoted by λ, computed the transition probabilities within and between the three Kramers doublets for the d^5 electronic states ions. Thus predicting for a given microwave frequency, where EPR lines are to be expected for various values of D and λ.

Recently, ions of the d^5 system have been used to study the order-disorder transformations in crystals. This is done

by making use of the fact that a crystal has a well-defined long-range order but also contains many local perturbations of this order. So, electron paramagnetic resonance of substitutional magnetic ions can be used to provide information about the crystal field environment of these ions. There are two types of disorder; the first type is that for which there are two or more sites in a crystal differing in their crystalline electric fields, which may be occupied by either of two ions. The second has one type of site in a crystal which is perturbed in various degrees from one point in the crystal to the next. This second type of disorder has been studied by A. Chatelain and R.A. Weeks in 1969[3] in which they used the divalent Mn^{2+} as a probe of the single crystal, polycrystal, and glass of zinc chloride. Again A. Chatelain and R.A. Weeks in 1970[4] used the spectrum of divalent Mn^{2+} in Mg_2SiO_4 single crystals to determine whether the Mn^{2+} was ordered in the sense of the first type.

Purpose of research

The present paper reports on the electron paramagnetic resonance of the high-spin d^5 transition ions Mn^{2+} and Fe^{3+} in single crystals of $BaTiO_3$ and Mg_2SiO_4 respectively. The EPR spectra of Mn^{2+} ions in $BaTiO_3$ single crystals in the

cubic, tetragonal and orthorhombic phases, forbidden lines and their orientation dependance in the hyperfine structure of these spectra in the three phases, are discussed.

The EPR spectra of impurities in a nominally pure Mg_2SiO_4 synthetic single crystal are also presented. The symmetries in these spectra observed at different temperatures are considered. The temperature dependance of the spectra exhibits anomalus behaviour, and possible reasons for this are discussed. Estimates of the spin Hamiltonian parameters of both Mn^{2+} and Fe^{3+}, from the observed EPR spectra, are made. These parameters are compared with those published in other papers.

Ordering of the paramagnetic ions are considered for the Ba and Ti sites in $BaTiO_3$ and for the two different Mg sites, M(1) and M(2) in Mg_2SiO_4.

X-ray irradiation of each crystal followed by EPR measurements is made, in order to determine whether a change of valency of the impurity ions in Mg_2SiO_4 and the doped ions in $BaTiO_3$ occurs.

Thermal annealing of the Mg_2SiO_4 and $BaTiO_3$ single crystals at a temperature of 300°C was performed to determine whether the valency changes produced by X-ray irradiation are

reversible. The Mg_2SiO_4 crystal was annealed at higher temperatures to determine whether disordering occurred.

Previous Research

1- $BaTiO_3$

Barium titanate single crystals have been the subject of many EPR studies. The first of which was by A.W. Hornig and E.T. Jaynes in 1954[5]. In which they observed the EPR in $BaTiO_3$ single crystal containing small amounts of iron. They concluded that the iron present was not a ferric ion with $^6S_{5/2}$ basic level, but a ferrous ion with a $^5D_4$ basic level located at the barium position in the lattice. Sakudo[6] in 1963 made EPR measurements of Fe^{3+} in $BaTiO_3$ at low temperatures. He discussed the experimental results at the temperatures of orthorhombic and rombohedral phases. He reported the difference in spectra for the three phases. Above 120°C, the crystal possess a cubic perovskite structure (m3m), being paraelectric. Below 120°C, it transforms to a tetragonal modification (4mm) with spontaneous polarization along [100] direction. Below 0°C, it transforms to an orthorhombic modification. Again Sakudo, Unoki and Mackaw in 1963[7] made EPR measurements near the Curie temperature, and observed the effect of a d.c electric field on the resonance spectra. Denis in 1965[8] made an EPR observation

of oxygen vacancies in iron-doped $BaTiO_3$. From a considera-
tion of the symmetry characteristics of the spectrum and
ionic size, he assumed that Fe^{3+} substitutes for Ti^{4+} in the
lattice, and that oxygen vacancies are randomly distributed
throughout the crystal and provide the necessary charge
compensation. Hiroshi Ikushima and Shigeru Hayakwa in 1965[9]
observed the "forbidden" doublets in the hyperfine spectrum
of bivalent manganese ion (Mn^{2+}) in $BaTiO_3$ single cyrstal
and calculated the splittings to third order in a perturbation
calculation. Finally Hiroshi Ikushima in 1966[10] presented
the experimental results of ESR of Mn^{2+} in $BaTiO_3$ single
crystal at cubic and tetragonal phases and discussed the
forbidden lines in the hyperfine structure at both phases in
detail.

2- Mg_2SiO_4

Forsterite (Mg_2SiO_4) has a crystal structure belonging
to the olivine group, the most recent and complete analysis
of which has been done by Birle, Gibbs, Moore, and Smith[11].
Such crystals belonging to the olivine group and containing
metallic atoms in the molecule has been the subject of many
studies. H. Onken in 1965[12] showed that in monticellite,
Ca $MgSiO_4$, Mg, and Ca are ordered in the M(1) and M(2) sites

respectively. S. Geller and Durand in 1960[13] showed that in lithiophilite, Li Mn PO_4, Li occupies the smaller M(1) and Mn the larger M(2) sites. Eliseev in 1958[14] concluded that $(Fe_x Mg_{1-x}) SiO_4$ system disobeys Vegard's law and he proposed Fe^{2+} - Mg^{2+} ordering. Independent measurements by several authors contradict these conclusions for ordering. In general it is found that the olivine system shows ideal substitution for Mg, Mn, Fe and Ca ions. Complete references are given in the paper published by Birle et al[11]. These authors interpreted their results as indicating disorder of Mg and Fe atoms. However, they did not exclude the possibility of minor cations such as Ca and Mn occupying one site prefrentially.

Recently, J. Michoulier, J.M. Gaite and B. Maffeo in 1969[15], and A. Chatelain, R.A. Weeks in 1970[4], reported on the electron paramagnetic resonance of Mn^{2+} ions in natural forsterite and showed unequivocally that these ions occupy only one of the two M sites.

CHAPTER II

EPR Theory and Technique

A- EPR Theory

II.1. Introduction

An electron travels in an orbit around a nucleus, and consequently has orbital angular momentum. Within this orbit, it also spins about its own axis, and has spin momentum. This spinning charge gives rise to a magnetic dipole.

If this magnetic dipole is placed in an external magnetic field, it will orient itself in discrete directions. One orientation is that parallel to the magnetic field and is equivalent to the lowest energy position. The antiparallel direction will be the state equivalent to the highest energy position.

The lower energy state of the split energy levels has a greater population than the higher energy state, and the technique of ESR is to produce transitions from the lower level, to the higher level (see Fig. 2-1). If the two energy levels in question are E_1 and E_2, then the energy required to produce one transition from E_1 to E_2 is:

$$E_2 - E_1 = h\nu \qquad (2-1)$$
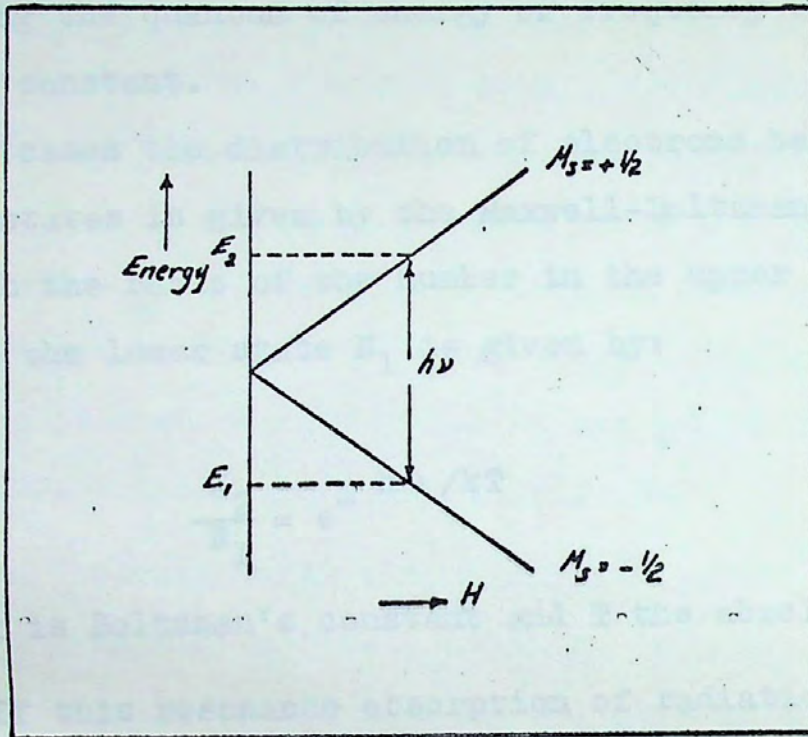
Fig. 2-1

The Zeeman splitting of an energy level.

h ν being the quantum of energy of frequency ν where h is
Plank's constant.

In most cases the distribution of electrons between the two
energy states is given by the Maxwell-Boltzmann expression,
in which the ratio of the number in the upper state N_2 to
that in the lower state N_1 is given by:

$$\frac{N_2}{N_1} = e^{-h\nu/kT} \qquad (2-2)$$

where k is Boltzman's constant and T the absolute temperature.

If this resonance absorption of radiation is to continue,
there must be some other mechanism which allows electrons in
the upper energy state to loose energy and drop back to the
lower state. This mechanism must allow energy transfer of hν
by interaction with some system other than the incident
radiation. If this were not so, the larger number of electrons
absorbing energy in the ground state would rapidly tend to
equalize N_1 and N_2 and so no further absorption would occur.
The ways in which electrons may loose energy and fulfil this
condition are termed "relaxation processes".

In the simplest of atoms only two basic levels are
involved. The number of levels is determined by the value
of the spin quantum number M_s, which may take any integral

or half-integral value from S, S-1,... to -S, i.e. (2 S+1) values, S being the electron spin. The Pauli exclusion principle allows transitions between spin levels only where

$M_S = \pm 1$. In the simplest case where $S = \frac{1}{2}$, the possible values are $+ \frac{1}{2}$ or $- \frac{1}{2}$ and a transition between these two levels is permitted, M_S being unity. The spin of the electron is then characterised by its projection M_S along the magnetic field, as shown in Fig. 2-1.

We have seen that the spinning electron has orbital motion around the nucleus. Consider this system placed in a steady magnetic field H, with the axis of the spin rotation inclined at some angle to the applied field. The spinning electron acting as a small magnetic dipole will experience a torque tending to turn it into alignment with the field, but this alignment cannot take place as the electron spin has orbital momentum about the nucleus. The axis of the spinning electron will then precess around the magnetic field axis. This precession motion is analogous to a gyroscope. The frequency of precession is the Larmor precession frequency $w \ (= 2\pi\nu)$, and is related to the applied magnetic field by the relation

$$w = \gamma H \qquad (2\text{-}3)$$

where γ is the magnetogyric ratio of the electron and is the ratio of magnetic moment to mechanical moment of inertia. Inserting known values of fundamental units into these quantities gives:

$$\gamma = \frac{g\beta}{h/2\pi} \qquad (2\text{-}4)$$

and, putting these values in equation (2-3), the basic energy equation becomes

$$h\nu = g\beta H \qquad (2\text{-}5)$$

where β is the magnetic moment of the electron, the Bohr magneton, and g is the spectroscopic splitting factor, or Landé factor. The g value is nearly equal to 2.00 for a free electron[1]. It should be noted that this equation ignores other energy terms, which, in some circumstances are far from negligible. As we shall see in this chapter, the expression (2-5) actually arises from one term of the spin Hamiltonian.

II-2. The Spin Hamiltonian

The general Hamiltonian[2,3,4] including magnetic as well as electric interactions can be written:

$$\mathcal{H} = H_1 + H_2 + H_{LS} + H_Z + H_{SS} + H_{SI} + H_Q + H_I + H_{LI} \qquad (2\text{-}6)$$

$\underline{H_1}$ represents that part of the Hamiltonian of the free ion which is spin independent and is largely kinetic energy:

$$H_1 = \sum \left(\frac{P_i^2}{2m_0} - \frac{Z e^2}{r_i} \right) + \sum_{i < k} \frac{e^2}{r_{ik}} \qquad (2\text{-}7)$$

This is usually by far the most dominant term in the overall Hamiltonian, but plays no part in the spin Hamiltonian.

H_2 is that part of the potential energy which arises from the electrostatic field Φ_c of the neighbouring atoms, with which each electron $- e_i$ interacts.

$$H_2 = -e_i \; \Phi_c \; (r_i) \qquad (2\text{-}8)$$

This crystal electric field plays a large part in the study of single crystals.

H_{LS} refers to spin-orbit coupling and may be represented by:

$$H_{LS} = \lambda \, L.S \qquad (2\text{-}9)$$

i.e. an interaction of orbital angular momentum L with electron spin S. The constant λ may be positive or negative, and is the spin orbit coupling constant derived from optical spectroscopy.

H_Z is the term mainly responsible for the paramagnetism, the Zeeman term, and may be expressed by:

$$H_Z = \beta H \; (L + 2S) \qquad (2\text{-}10)$$

If the expectation value of the orbital magnetic moment L is zero, then,

$$H_Z = 2\beta HS$$

$\underline{H_{SS}}$ represents small terms involving magnetic interactions between electrons.

$$H_{SS} = (2\beta)^2 \sum_{j > k} \left[r_{jk}^2 (S_j \cdot S_k) - 3(S_j \cdot r_{jk})(S_k \cdot r_{jk}) \right] r_{jk}^{-5} \quad (2\text{-}11)$$

This term is often small enough to be ignored but it may be important in some transition metal ions.

$\underline{H_{SI}}$ expresses the magnetic interaction of the electron of interest with the magnetic moment of nearby nuclei, i.e., electron spin – nuclear spin interaction.

$$H_{SI} = - g g_N \beta \beta_N \left[\frac{S \cdot I}{r^3} - \frac{3(S \cdot r)(I \cdot r)}{r^5} - \frac{8\pi}{3} S \cdot I \, \delta(r) \right] \quad (2\text{-}12)$$

where g and g_N are the electronic and nuclear g-values, β and β_N are the electronic and nuclear magnetic moments, r is the distance between electron and nucleus, and $\delta(r)$ is the Dirac delta function. The first two terms produce an anisotropy in the spectrum. The term $\frac{8\pi}{3} g g_N \beta \beta_N \, I \cdot S \, \delta(r)$ may be written as $A \cdot I \cdot S$, the contact hyperfine interaction and produces an isotropic splitting of the Zeeman levels.

$\underline{H_Q}$ is the term representing electrostatic interaction with the electric quadrupole moment Q of the nucleus.

$$H_Q = \frac{e^2 Q}{2I(2I-1)} \left[\frac{I(I+1)}{r^3} - \frac{3(r.I)^2}{r^5} \right] \qquad (2\text{-}13)$$

where Q is the electric quadrupole moment of nucleus ℓ.

H_I is the nuclear contribution, which is extremely small and may be considered negligible. It may be expressed as:

$$H_I = \sum g_N \beta_N \, H.I \qquad (2\text{-}14)$$

H_{LI} is the nuclear spin-orbit interaction

$$H_{LI} = g \, g_N \, \beta \beta_N \sum_{i,k} \left(\frac{I_{ik} \, I_i}{r_{ik}^3} \right) \qquad (2\text{-}15)$$

This term is important only in that it gives a second-order contribution to the hyperfine interaction by allowing the nuclear spin and electron spin to couple indirectly through the orbital momentum.

The orders of magnitude of these various interactions are as follows[3]:

H_1	Spin-independent term.	10^5 cm^{-1}
H_2	Crystal field.	10^4
H_{LS}	Spin-orbit interaction.	10^2
H_Z	Zeeman term.	1
H_{SS}	Magnetic interaction between electrons.	1
$H_{SI}+H_Q$	Interaction with nuclear spins.	10^{-2}
H_I	Nuclear contribution	10^{-3}

The lowest group of energy levels, i.e. the ones
between which microwave transitions are induced, depend in
a complicated way on the particular ion, the symmetry and
strength of the crystalline electric field, the spin-orbit
coupling, and other effects such as the hyperfine interaction
between electrons and nucleus. However, these energy levels,
can be described by the use of a spin Hamiltonian in a fairly
simple way that requires no detailed knowledge of the above
effects[3].

We may now consider the individual components collect-
ively. The term H_1 is of no interest to us as it is spin
independent. H_2, H_{LS}, H_Z, H_{SI}, H_Q and H_I are important in
E.S.R. studies of crystals. The other components are small
compared with H_2, H_{LS}, H_Z, H_{SI}, H_Q & H_I and will not be
considered.
The total spin Hamiltonian is then:

$$\mathcal{H} = H_2 + H_{LS} + H_Z + H_{SI} + H_Q + H_I \qquad (2\text{-}16)$$

II-3. Orbital level splitting in Crystal Fields.

If the atom under investigation is situated in a
crystalline lattice, as is the case here, there will be
strong crystalline electric fields acting on it, produced
by the electrons of the surrounding ligand atoms. These

electric fields produce a Stark-effect splitting on the
electron states of the atom being considered and the first
problem is to decide which orbital level will be lowest for
a given electron configuration in a crystalline field of
given symmetry.

The wave function of an atomic orbital may be expressed in
spherical coordinates (r, θ, ϕ) as[5]:

$$= R(r) \cdot \Theta(\theta) \cdot \Phi(\varphi) \cdot \Psi_s \qquad (2\text{-}17)$$

i.e, the product of a function of r alone, another of θ
alone, another of φ alone and a function Ψ_s accounting for
the spin of the electron. The function $R(r)$ has spherical
symmetry and is not affected by operations of symmetry. The
function Ψ_s accounts for the spin wave functions, the
degeneracy of which according to Kramer's theorem[3], cannot
be removed by an electrostatic field. The discussion may be
restricted to the angular functions $\Theta(\theta)$ and $\Phi(\varphi)$ expressed
in the form of spherical harmonics:

$$y_{1, \pm m}(\theta, \varphi) = \Theta(\theta) \cdot \Phi(\varphi) \qquad (2\text{-}18)$$

meaning the probability of finding the electron at a distance
between r and r + dr from the nucleus, with its angular
coordinates having values between θ and $\theta + d\theta$, and φ and
$\varphi + d\varphi$, is:

$$\psi^* \psi \, d\tau = \left[R_{n,l} (r) \right]^2 \left[Y_{l, \pm m} (\theta, \varphi) \right]^2 r^2 \sin \theta \, dr \, d\theta \, d\varphi$$

and the electron will have a spatial distribution whose density at each point is given by:

$$\vartheta (r) = \psi^* \psi \qquad (2\text{-}19)$$

The angular factors associated with d-orbitals may be written in spherical coordinates as[4]:

$$d \, (m_l = + 2) \propto e^{2i\varphi} \sin^2 \theta$$

$$d \, (m_l = + 1) \propto e^{i\varphi} \sin \theta \cos \theta$$

$$d \, (m_l = 0) \propto (3 \cos^2 \theta - 1) \qquad (2\text{-}20)$$

$$d \, (m_l = -1) \propto e^{-i\varphi} \sin \theta \cos \theta$$

$$d \, (m_l = -2) \propto e^{-2i\varphi} \sin^2 \theta \cos \theta$$

Replacing these functions by linear combinations in orthogonal coordinates, they take the form[4]:

$$d_{3z^2 - r^2} = d(0) \qquad \propto 3 \cos^2 \theta - 1 \quad \propto 3z^2 - r^2$$

$$d_{xz} = \frac{d(+1) + d(-1)}{\sqrt{2}} \qquad \propto \sin \theta \cos \theta \cos \varphi \propto xz$$

$$d_{yz} = -i \frac{d(+1) - d(-1)}{\sqrt{2}} \qquad \propto \sin \theta \cos \theta \sin \varphi \propto yz \qquad (2\text{-}21)$$

$$d_{x^2 - y^2} = \frac{d(+2) + d(-2)}{\sqrt{2}} \qquad \propto \sin^2 \theta \cos 2\varphi \propto x^2 - y^2$$

$$d_{xy} = -i \frac{d(+2) - d(-2)}{\sqrt{2}} \qquad \propto \sin^2 \theta \sin 2\varphi \propto xy$$

The spatial distributions of the electron densities for these d-orbital levels are shown in Fig. 2.2. In the absence of an external electric or magnetic field, these orbitals will have the same energy, i.e. the free-ion d-levels are five-fold orbitally degenerate. Interaction with a cubic crystalline field can be easily shown by reference to the character of the group (appendix II). The d-level is broken into a two-fold orbitally degenerate e_g-level and a three-fold orbitally degenerate t_{2g}-level. The triple degeneracy of the t_{2g}-level arises from d_{xy}, d_{yz}, d_{zx}, while in cubic fields, from the equivalence of $d_{3z^2-r^2}$. The degeneracy of the e_g-levels, $d_{x^2-y^2}$ and $d_{3z^2-r^2}$, is apparent if we recall that the orbital function $d_{3z^2-r^2}$ may be written in terms of the angular functions x^2-y^2 and $3z^2-r^2$, as the linear combination

$$(3z^2-r^2) + (x^2-y^2) = 2z^2 - x^2 - y^2$$

$$= 3z^2 - (x^2+y^2+z^2)$$

$$= 3z^2 - r^2 = d_{3z^2-r^2} \qquad (2.6)$$

Any symmetry operation that exchanges x,y,z will similarly exchange $3z^2-r^2$, $3x^2-r^2$ and x^2-y^2. A simple choice of the linear combination then will reproduce $d_{3z^2-r^2}$

FIG. 2.2 Typical orbital electron clouds.

$d_{x^2-y^2}$ d_{yz} d_{xz} $d_{3z^2-r^2}$ d_{xy}

The spatial distributions of the electron densities for these
d-orbital levels are shown in Fig. 2-2.

In the absence of any perturbing electric or magnetic field,
these orbitals will all have the same energy, i.e. the free-
ion d-levels are five-fold orbitally degenerate.

Interaction with a cubic octahedral environment is easily
shown by resorting to the character table of the O_h point
group (Appendix III). The d-level is found to split into a
two-fold orbitally degenerate e_g-level and a three-fold
orbitally degenerate t_{2g}-level. The triple degeneracy of the
t_{2g}-level arises from the equivalence of xy, yz and zx, which
in turn results, from the equivalence of x,y and z. The
degeneracy of the e_g-levels, $d_{3z^2-r^2}$ and $d_{x^2-y^2}$ is understood
if we recall that the orbital function $d_{3z^2-r^2}$ may be put in
terms of the angular functions z^2-y^2 and z^2-x^2, as the linear
combination

$$(z^2-x^2) + (z^2-y^2) = 2z^2 - x^2-y^2$$

$$= 3z^2 - (x^2+y^2+z^2)$$

$$= 3z^2 - r^2 \propto d_{3z^2-r^2} \qquad (2-22)$$

Any symmetry operation that exchanges x,y,z will similarly
exchange z^2-x^2, z^2-y^2 and x^2-y^2. A simple choice of the
linear combination that will reproduce $d_{3z^2-r^2}$ after a

symmetry operation that exchanges x,y and Z will then show
that the orbital angular functions $d_{3Z^2-r^2}$ and $d_{x^2-y^2}$ have
orbital degeneracy in cubic groups.

The obvious question now is which one of the t_{2g} and
e_g-levels will have the higher energy. The answer is
illustrated in Fig. 2-3. In the case of an octahedron,
where the ligand molecules have the coordinates $(\frac{1}{2},\frac{1}{2},0)$,
$(\frac{1}{2},0,\frac{1}{2})$, $(0,\frac{1}{2},\frac{1}{2})$ referred to the edges of the cube shown
in solid lines, the e_g-levels experience the strongest
interaction, while the t_{2g}-levels experience the weakest
interaction. It should be remembered that the interaction
between an electron in an orbital and a ligand molecule is
repulsive, since it arises from interaction between electric
charges of the same sign. Therefore, the potential energy
of the e_g-levels must be higher than the potential energy of
the t_{2g}-levels. The two levels are represented in the same
figure, together with five-fold orbitally degenerate levels
corresponding to a spherical field, $\langle O_h \rangle$, of the same
average strength. The average potential energy of the
electron in the split levels must be equal to the energy of
degenerate levels in spherical symmetry. The separation
between the t_{2g}-level and the spherical-field, five fold
degenerate level must then be equal to two- thirds the
separation of the e_g-level.

e_g

$(3z^2 - r^2,\ x^2 - y^2)$

$\langle o_h \rangle$

O_h

free
ion

Δ_o

t_{2g}

(xy, yz, xz)

d_{3z^2, r^2}

d_{xz}

t_2

(xy, yz, xz)

$\langle T_d \rangle$

T_d

free
ion

Δ_t

e

$(3z^2 - r^2,\ x^2 - y^2)$

d_{xz}

$d_{3z^2 - r^2}$

Fig. 2-3

The splitting of the d-levels by a regular tetrahedron leads to the opposite situation, as illustrated in Fig. 2-3.

It is clear that the study of the symmetry alone does not suffice for determining the energy of the levels. In order to do this, it is necessary to find an expression for the crystal-field term:

$$H_2 = - e_i \; \phi_c \; (r_i)$$

of the Hamiltonian of equation (2-6).

It is to be noted that H_1 and H_2 terms in the total Hamiltonian are so big with respect to the other terms that H_1 and H_2 can be cut out from the total Hamiltonian, and the other terms are correlated in another Hamiltonian called the spin Hamiltonian.

But again the crystal field effect appears in the spin Hamiltonian due to the symmetries involved. So this crystal field secondary effect is treated as a perturbation with respect to the Zeeman term, if it is smaller than the Zeeman term.

II-4. The crystal field potential

The electrostatic potential at an ion, due to ligand molecules, may be expanded in powers of x, y, Z and combinations thereof. There are symmetry arguments that impose

conditions on the expansion of the potential term $\Phi(r)$ of
equation (2-8). A cubic environment reduces the number of
terms as follows. Since in any cubic group there are two-
fold axes coincident with x,y and Z, or symmetry planes
perpendicular to them, or both, the function:

$$\Phi(r) = \Phi(x,y,Z) \qquad (2-23)$$

must be even in x,y, and Z, since it must remain invariant
under the operations of symmetry referred to above, which
in turn change the sign of each coordinate. Therefore, only
even powers of x,y and Z have to be considered in the
expansion. Zeroth-order terms in x,y or Z have spherical
symmetry and have no bearing in symmetry considerations.
The second-order terms may be written

$$c_1 x^2 + c_2 y^2 + c_3 z^2 \qquad (2-24)$$

Terms in xy, yz, and xz are odd in each coordinate and
cannot appear. For cubic symmetry, four-fold proper and
improper rotations and the four three-fold proper rotations
make x,y and Z equivalent. Therefore $c_1 = c_2 = c_3 = c$ and
equation (2-24) reduces to:

$$c (x^2 + y^2 + Z^2) = cr^2 \qquad (2-25)$$

which is again a spherical function. The next term to
consider is the fourth-order, which can be written:

$$A'_1 x^4 + A'_2 y^4 + A'_3 z^4 + A'_{12} x^2 y^2 + A'_{23} y^2 z^2 + A'_{31} z^2 x^2$$

$$(2\text{-}26)$$

Application of the three-fold proper rotations reduces equation (2-26) to:

$$A' (x^4 + y^4 + z^4) + A_1 (x^2 y^2 + y^2 z^2 + z^2 x^2) \quad (2\text{-}27)$$

which is invariant under the operations of the cubic group. Higher-order terms, such as $x^2 y^2 z^2$, ..., are also invariant.

It is usually sufficient to consider the term

$$= A' (x^4 + y^4 + z^4) \qquad (2\text{-}28)$$

For lower symmetries, the second order terms are:

$$\Phi = C_1 x^2 + C_2 y^2 + C_3 z^2 \text{ for orthorhombic symmetry } (2\text{-}29)$$

and the expression reduces to:

$$\Phi = C_\perp (x^2 + y^2) + C_{||} (z^2) \text{ for axial symmetry } (2\text{-}30)$$

Strictly speaking, equations (2-29) and (2-30) should be added, in each case, to the term of equation (2-28). However this latter often represents a negligible effect and hence may be neglected.

In the case of cubic symmetry, the coefficient A' is related to the splitting of the d-levels shown in Fig. 2-3 by:

$$\Delta_0 = 10 A'$$

II-5. Electronic Splitting and the crystal field spin Hamiltonian

Transition group atoms often have more than one unpaired electron associated with them, and in the first transition group (3d shell) up to five unpaired electrons occur, e.g Mn^{2+} and Fe^{3+} both have five unpaired electrons which half fill the d-shell, hence $S = \frac{5}{2}, L = 0$ and $J = \frac{5}{2}$ (Hund's Rules[3]). Such atoms $S \geqslant 1$ will undergo splitting of the m_s states due to the internal crystalline, or molecular, field Fig. 2-4. If there is an odd number of unpaired electrons associated with the atom, the internal crystalline field will leave the levels, according to Kramer's theorem[3], at least two fold degenerate (e.g. it cannot split the $M_3 = \pm \frac{1}{2}$ or $M_3 = \pm \frac{3}{2}$ levels of the Mn^{2+} or Fe^{3+} ions). If on the other hand, there is an even number of unpaired electrons associated with the atom then it is possible for the internal field to remove all the degeneracy completely.

The term of the effective spin Hamiltonian that removes the degeneracy in systems of $S \geqslant 1$ is:

$$S \cdot \Phi \cdot S = [S_x \ S_y \ S_z] \cdot \{\Phi_{ij}\} \begin{bmatrix} S_x \\ S_y \\ S_z \end{bmatrix} \qquad (2-31)$$

which was introduced in equation (2-16).
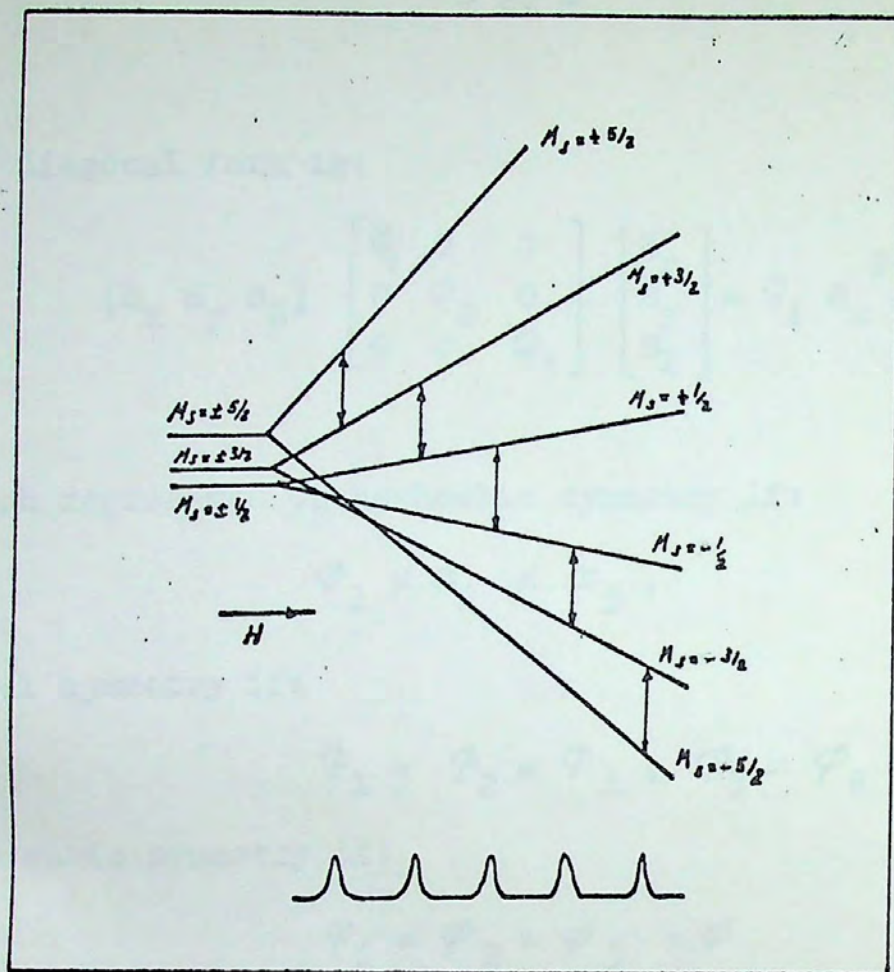
Fig. 2-4

Energy level diagram of d^5 ion with S = $\frac{5}{2}$, with zero field splitting.

The diagonal form is:

$$[S_x \ S_y \ S_z] \begin{bmatrix} \varphi_1 & 0 & 0 \\ 0 & \varphi_2 & 0 \\ 0 & 0 & \varphi_3 \end{bmatrix} \cdot \begin{bmatrix} S_x \\ S_y \\ S_z \end{bmatrix} = \varphi_1 \ S_x^2 + \varphi_2 \ S_y^2 + \varphi_3 S_z^2$$

(2-32)

which represents orthorhombic symmetry if:

$$\varphi_1 \neq \varphi_2 \neq \varphi_3 , \tag{2-33}$$

axial symmetry if:

$$\varphi_1 = \varphi_2 = \varphi_\perp , \quad \varphi_3 = \varphi_\parallel , \tag{2-34}$$

and cubic symmetry if:

$$\varphi_1 = \varphi_2 = \varphi_3 = \varphi \tag{2-35}$$

In the latter case, equation (2-31) simplifies to:

$$S \cdot \bar{\varphi} \cdot S = \varphi \ (S_x^2 + S_y^2 + S_z^2) = \varphi \ S \ (S+1) \tag{2-36}$$

and the term accounts for an equal displacement of each preexistent level. Therefore, a cubic field does not remove, to the second order in S, the spin degeneracy. Consideration of equation (2-36), which states a condition that must be satisfied by the spin components, reduces the number of independent parameters to two. If one writes:

$$\varphi_1 \ S_x^2 + \varphi_2 \ S_y^2 = \frac{1}{2} \ (\varphi_1 + \varphi_2) \ (S_x^2 + S_y^2)$$

$$+ \frac{1}{2} \ (\varphi_1 - \varphi_2) \ (S_x^2 - S_y^2) \tag{2-37}$$

one may define the new parameters

$$E = \tfrac{1}{2} (\varphi_1 - \varphi_2) \qquad (2\text{-}38)$$

$$D = \varphi_3 - \tfrac{1}{2} (\varphi_1 + \varphi_2) \qquad (2\text{-}39)$$

Clearly, E vanishes for axial symmetry since $\varphi_1 = \varphi_2$, and both parameters vanish for cubic symmetry, in view of equation (2-35). Now, the average energy of the crystal field is

$$(\tfrac{1}{3}) (\varphi_1 + \varphi_2 + \varphi_3) S(S+1) \qquad (2\text{-}40)$$

and equally displaces all levels. One may then subtract it from the Hamiltonian, for it will not affect the energy of the transitions. Taking into account the definition of D, equation (2-40) may be written as:

$$\left[\tfrac{1}{3} D + \tfrac{1}{2} (\varphi_1 + \varphi_2) \right] S(S+1) \qquad (2\text{-}41)$$

If equations (2-38) and (2-39) are taken into account, the crystal field term, after some algebraic handling, may be written as:

$$D \left[S_z^2 - \tfrac{1}{3} S(S+1) \right] + E (S_x^2 - S_y^2) \qquad (2\text{-}42)$$

In case of axial symmetry, the term $D \left[S_z^2 - \tfrac{1}{3} S(S+1) \right]$ directly gives the zero-field splitting, for H does not appear in the term. It implies, for example, that for H = 0

and $S = \frac{3}{2}$, the zero-field splitting is given by $D\left[(\frac{3}{2})^2 - (\frac{1}{2})^2\right]$ = 2D. The crystal field terms gives a zero-field spin degeneracy for levels of $m_s \neq 0$ since the crystal field does not distinguish between $+m_s$ and $-m_s$. This degeneracy is actually lifted by the magnetic field through the Zeeman term giving rise to two levels: $+m_s$ and $-m_s$, which may in turn be split by hyperfine interaction.

It is found that, to second order in S, the levels of the D term are[15]:

$$D(m_s - \tfrac{1}{2})\left[3\ \frac{g_{//}^2}{g_H^2}\ \cos^2\theta -1\right] \quad (2\text{-}43)$$

where m_s stands for the spin magnetic quantum number, and θ is the angle between the magnetic field and the symmetry axis.

For an S state ion (as Mn^{2+} and Fe^{3+}) the g-value is isotropic, and hence $g_{//} = g_{\perp} = g_H$, and equation (2-43) reduces to: $D(m_s-\tfrac{1}{2})\left[3\cos^2\theta -1\right]$. The variation of the crystal field spectrum, usually known as "fine structure", then follows a:

$$\left[3\cos^2\theta -1\right]$$

law.

It is to be noted that for S-ions, like Mn^{2+} and Fe^{3+} (d^5 ions) in which no splitting of the levels to the second order in S occurs for cubic fields, it is necessary to consider the forth order term:

$$\frac{a}{6} (x^4 + y^4 + z^4) \qquad (2-44)$$

The parameter a is usually two orders of magnitude smaller than $D^{(5)}$.

II-6. Electronic Splitting of Mn^{2+} and Fe^{3+} ions

The Mn^{2+} and Fe^{3+} ions are in a ^6S spectroscopic state, with five unpaired electrons giving $S = \frac{5}{2}$ (for an S-state ion $L = 0$). Electronic splittings are produced between the three doublets corresponding to $M_s = \pm \frac{1}{2}, \pm \frac{3}{2}$ and $\pm \frac{5}{2}$. In this case the $M_s = \pm \frac{1}{2}$ components lie lowest, with the $\pm \frac{3}{2}$ and $\pm \frac{5}{2}$ some 0.05 and 0.15 cm^{-1} above them for the Mn^{2+} ion[16], and 0.07 and 0.68 cm^{-1} for the Fe^{3+} ion[16] in cubic electric fields. These splittings are, in fact, the electronic splitting referred to in the Spin Hamiltonian derivation, and is denoted by the parameter A'.

The three doublets can therefore be represented in zero-magnetic field to a first approximation as shown on the left-hand side of Fig. 2-5, and the way in which they separate as
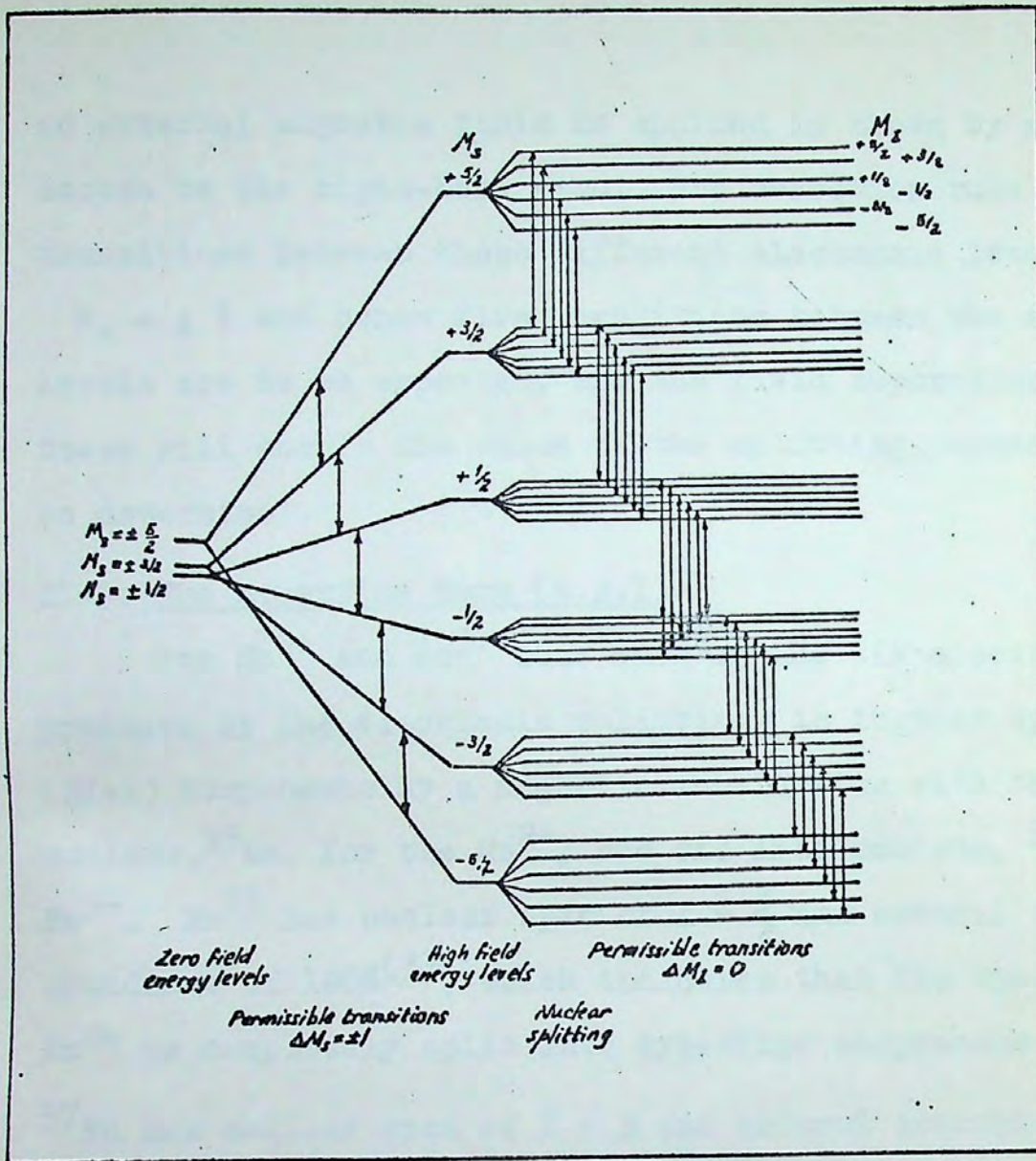
Fig. 2-5

Energy level diagram showing zero field splitting of
the Mn^{2+} ion, which has an electron spin of 5/2 and a
nuclear spin of 5/2. The thirty permissible transitions
are indicated by arrows.

an external magnetic field is applied is shown by moving
across to the right-hand side. The selection rule for
transitions between these different electronic levels is

$M_S = \pm 1$ and hence five transitions between the six
levels are to be expected, and the field separations between
these will enable the value of the splitting parameter D, to
be determined.

II-7. The hyperfine term (S.A.I)

For Mn^{2+} and Fe^{3+} ions each of the six electronic levels
produced by the electronic splitting, is further split into
$(2I+1)$ components by a magnetic interaction with the manganese
nucleus, ^{55}Mn, for the Mn^{2+}, and the iron nucleus, ^{57}Fe for the
Fe^{3+}. Mn^{55} has nuclear spin of $I = \frac{5}{2}$ and natural isotopic
abundance of 100%[3], which indicates that the spectrum of
Mn^{2+} is completely split into hyperfine components by ^{55}Mn.

^{57}Fe has nuclear spin of $I = \frac{1}{2}$ and natural isotopic abundance
of 2.14%[3], hence each fine structure transition will be
flanked by two hyperfine lines whose intensity will be $\sim 1\%$
of the intensity of the fine structure line. The selection
rule for transitions between the levels is $M_I = 0$, and hence
six hyperfine components are now expected on each electronic
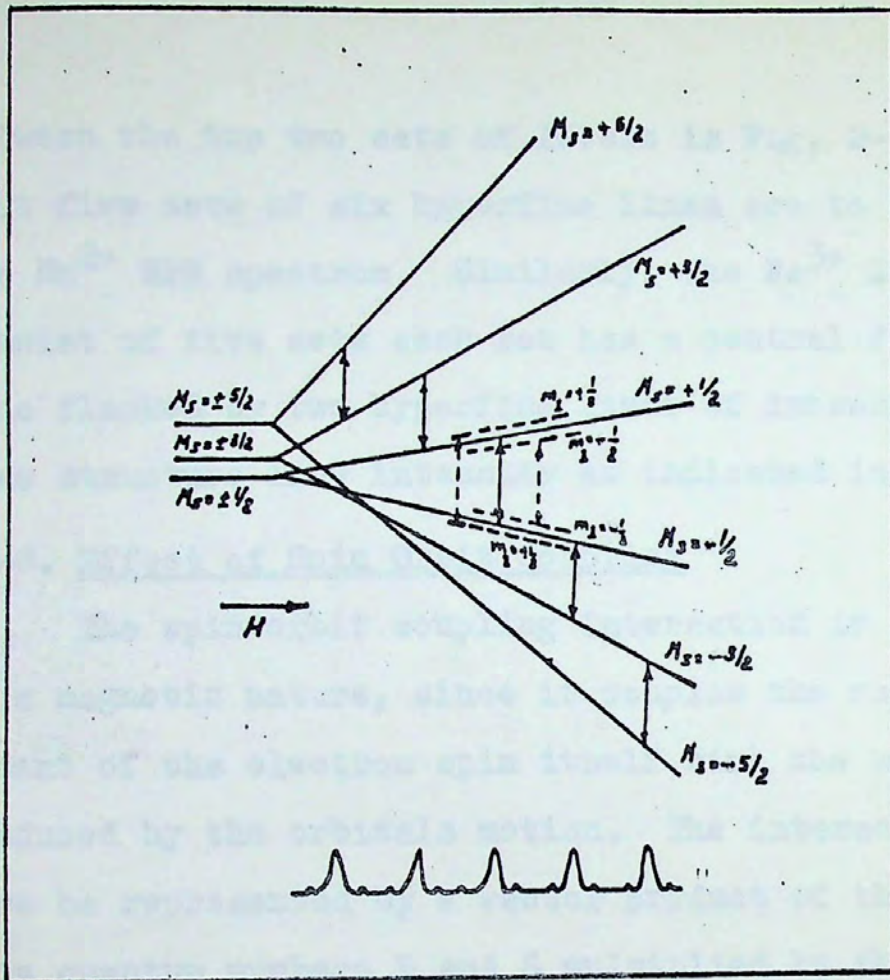transition of the Mn^{2+}, as indicated by the vertical arrows

Fig. 2-6

Energy level diagram showing zero field
splitting of the Fe^{3+} ion, which has an electron
spin of 5/2 and a nuclear spin of 1/2. The five
fine structure lines with the flanking hyperfines
are shown.

between the top two sets of levels is Fig. 2-5. It follows
that five sets of six hyperfine lines are to be expected for
the Mn^{2+} EPR spectrum. Similarly, the Fe^{3+} EPR spectrum will
consist of five sets each set has a central fine structure
line flanked by two hyperfine lines of intensity $\sim 1\%$ of the
fine structure line intensity as indicated in Fig. 2-6.

II-8. Effect of Spin Orbit Coupling

The spin orbit coupling interaction is essentially one
of a magnetic nature, since it couples the magnetic dipole
moment of the electron spin itself with the magnetic field
produced by the orbitals motion. The interaction can there-
fore be represented by a vector product of the orbital and
spin quantum numbers L and S multiplied by the interaction
constant which is normally denoted by λ. This energy of
interaction, which can thus be represented as $\lambda.L.S$ will now
act as a perturbation on the energy splittings that have
already been produced by the effect of the crystalline
electric field. For an S state ion L = 0 and the spin orbit
coupling (first order) term will be zero, but the second order
term of the spin-orbit coupling effect will account for the
shift of the g-value from the free electron spin value of 2.0023.

II-9. Appropriate Spin Hamiltonian

A spin Hamiltonian which adequantely fits a d^5 system and a crystal field of orthorhombic (or lower) symmetry is[6]:

$$\mathcal{H} = g\beta H.S + D\left[S_z^2 - \frac{1}{3}S(S+1)\right] + E\left[S_x^2 - S_y^2\right] + AI.S \qquad (2-45)$$

where all symbols have their usual meaning and the hyperfine term is for the manganese nucleus only in case of $BaTiO_3$ single crystal, and for the iron nucleus only in case of Mg_2SiO_4 crystal.

It is assumed that g and A are isotropic, which is a good approximation for an S state ion of $3d^5$ configuration.

i) If D and E are zero

Then an isotropic absorption line with a g-value slightly greater than 2 is expected. However, higher order terms occur in a cubic symmetry which produce a small splitting of the electronic states.

ii) If D and E are finite but small (0.001-0.1 cm^{-1})

Then five EPR transitions are observed and are well understood[7].

iii) If $D \gg g\beta H$ and E=0

Then the electronic levels of equation (2-45) in zero magnetic field are found to be three Kramers doublets. The lowest doublet has the effective[8] g-values, $g_{\parallel} = 2$, $g_{\perp} = 6$

and is exemplified experimentally in strong axially symmetric electric fields, e.g., in Fe^{3+} impurities in strontium titanate[9].

iv) If $E \gg g\beta H$ and D very small (around zero)

Then the electronic levels of equation (2-45) in zero magnetic field are found to be three Kramers doublets. The middle doublet has an isotropic effective g value of 4.29. Castner et al[10] were the first to propose (D=0, E ≠ 0) to account for the g = 4.27 spectrum found for ferric ions in glass. Griffith[11] defended this original interpretation of the g = 4.29 signal but showed that so long as the environment of the d^5 ion is more symmetric than the over-all symmetry group of the site in a special way, then D need not be zero but shall be small. The special environments are tetrahedral $MA_2B_2(C_{2v})$, distorted octahedral $MA_6(D_{2h})$, and octahedral $MA_3B_3(C_{2v})$, in all of which the excited $^4T_1$ state is split into three equally spaced components.

v) If both D & $E \gg \beta gH$

For this case, various authors[6,12,13,14] have shown that the g = 4.29 signal can arise if λ , the ratio of E to D, is $\frac{1}{3}$. It was pointed out by Blumberg[15] that if $\lambda = 0$ represents axial symmetry (D ≠ 0, E = 0), then an increase in λ represents

a departure towards rhombic symmetry. $\lambda = \frac{1}{3}$ represents
maximum possible rhombic symmetry with equally spaced
Kramers doublets and values of λ greater than $\frac{1}{3}$ represent
a convergence towards axial symmetry again, with $\lambda = 1$
representing entirely axial symmetry. Thus ESR signals near
g = 4.29 are expected if λ is near $\frac{1}{3}$. But it is to be
noted[11] that equally spaced energy levels do not necessarily
imply complete rhombic symmetry.

B- EPR Technique

EPR SPECTROMETER

The two main requirements for an EPR experiment are a large uniform magnetic field, and a stabilized frequency source in the right wavelength region. The way in which these are related in an actual spectrometer can be represented schematically as in Fig. 2-7.

The basic items of any electron spin resonance spectrometer are the microwave radiation source, an absorption cell, in which the specimen is inserted, a large uniform magnetic field into which the absorption cell containing the specimen is inserted; and some means of detecting the level of the microwave radiation in the absorption cell cavity and determining whether any absorption has, in fact, taken place as the magnetic field is varied.

a- The absorption cell

The absorption cell takes the form of a cavity resonator, which is a space enclosed by conducting walls and possesses a resonant frequency for each particular type of field configuration that can exist in the space. Its behaviour is analogous to that of a parallel tuned circuit containing an inductance and a capacitor. At microwave
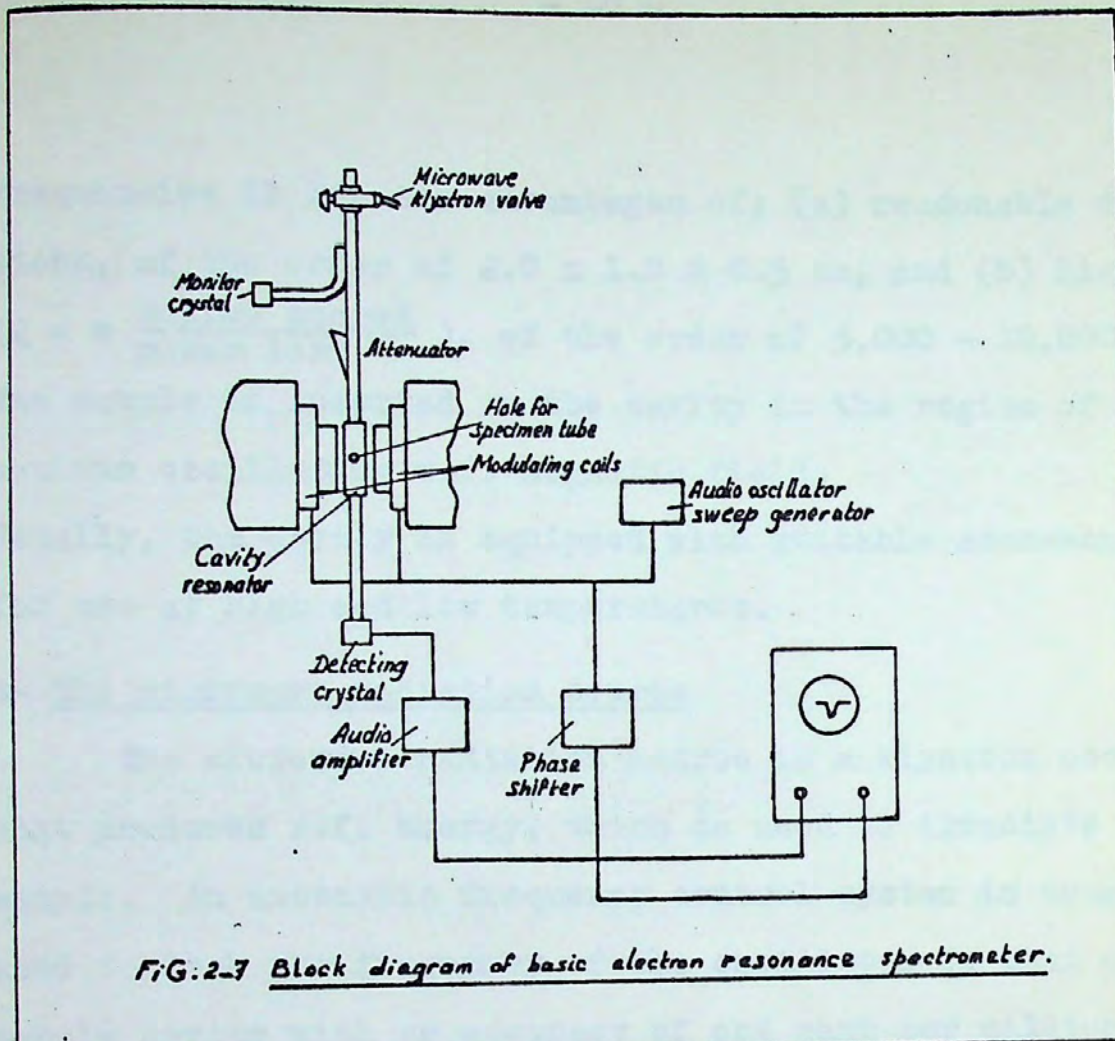
FIG. 2-7 Block diagram of basic electron resonance spectrometer.
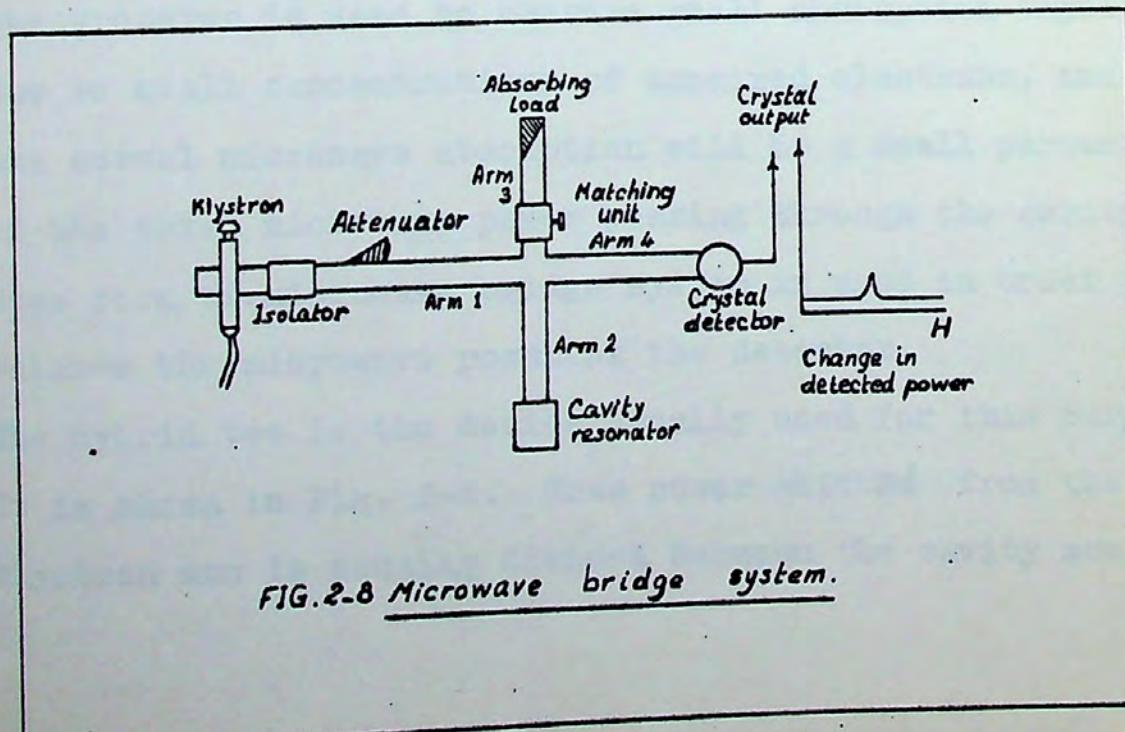
FIG. 2-8 Microwave bridge system.

frequencies it has the advantages of; (a) reasonable dimen-
sions, of the order of 2.0 x 1.0 x 0.5 cm, and (b) high Q
($Q = w \frac{energy\ stored}{power\ lost}$), of the order of 5,000 - 10,000.
The sample is inserted in the cavity in the region of
maximum oscillating r.f. magnetic field.
Usually, the cavity is equipped with suitable accessories
for use at high and low temperatures.

b- The microwave radiation source

The microwave radiation source is a klystron oscillator
that produces r.f. energy, which is used to irradiate the
sample. An automatic frequency control system is usually
used to lock the frequency of the oscillator to that of the
sample cavity with an accuracy of one part per million.
In most practical applications, the electron resonance
spectrometer is used to measure small absorption signals,
due to small concentrations of unpaired electrons, and thus
the actual microwave absorption will be a small percentage
of the total microwave power passing through the cavity.
Some form of microwave bridge system is used in order to
balance the microwave power at the detector.
The hybrid tee is the device usually used for this purpose.
It is shown in Fig. 2-8. Thus power emitted from the
klystron arm is equally divided between the cavity arm and

the matching load arm. If all the power is absorbed and none reflected, then no power enters the detector arm; thus the crystal detector receives no energy. The hybrid tee can now be considered similar to a balanced bridge, since any change in the terminating impedance of the cavity arm and the load arm will unbalance it and result in energy reaching the crystal detector.

c- The uniform magnetic field

An electromagnet provides a homogeneous magnetic field which can be varied from near zero to about 10,000 gauss. The magnet power supply provides a stable, controlled current to the energizing coils of the electromagnet.

Since the magnetic field is to be varied for determining the absorption, therefore, it is equipped with a scanning unit. The scanning unit supplies a control voltage to the input of the current regulated magnet power supply. This control voltage can be varied linearly with respect to time, thus resulting in a linear sweep of the magnetic field. 100 kc sweep generator provides modulation of the static magnetic field at the sample location within the cavity, to facilitate the detection of the EPR resonance.

d- The Detection System

A crystal diode is used as a detector in one arm of the hybrid tee bridge.

This diode requires a bias current to be passing through it if it is to be sensitive to the signals which is expected to detect. The needed bias current is provided by adjusting the balance of hybrid tee bridge so that a small amount of microwave energy is reflected from the cavity to the crystal detector.

By slowly varying the magnetic field until the proper value for resonance is reached, a signal will appear on the scope. This signal is the result of using a modulation and phase detection method of observing the resonance signal, which is explained as follows:

The static magnetic field is positioned on one side of the resonance line. Superimposed on that field is a sine wave modulation at frequency of 100 kc. As a result of this 100 kc field sweep, and the EPR resonance, the microwave energy in the cavity is modulated. The phase and amplitude of this modulation is dependent on the EPR resonance line and the value of the static magnetic field with superimposed modulation relative to the resonance line, Fig. 2-9. The microwave energy (modulated by a 100 kc voltage which contains

EPR RESONANCE SIGNAL

SIGNAL "A"

SWEEP MODULATION
VOLTAGE
(CONSTANT PHASE)

① ② ① ②

SIGNAL "A"
INPUT

SIGNAL "A"
OUTPUT

EPR RESONANCE SIGNAL

SIGNAL "B"

SWEEP
MODULATION
VOLTAGE
(CONSTANT PHASE)
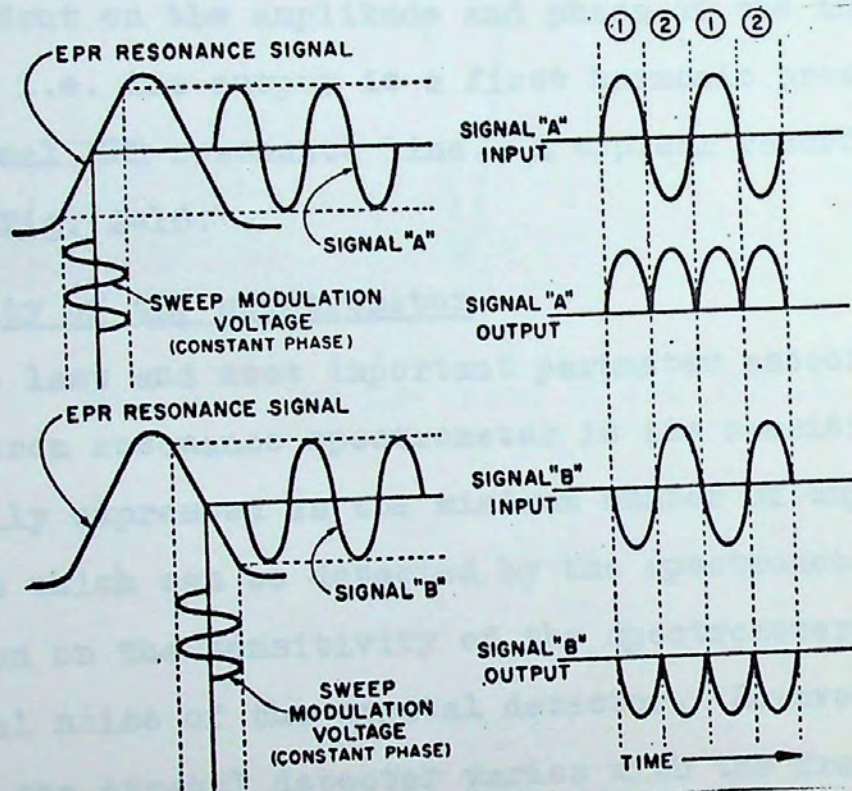
SIGNAL "B"
INPUT

SIGNAL "B"
OUTPUT

TIME

Fig. 2-9: Input and output signals of phase detector.

the EPR signal information) strikes the crystal diode in one arm of the hybrid tee. The signal information is then amplified and carried to the input of the phase detector. The phase detector is supplied by a phase reference voltage from the same 100 kc oscillator used to supply modulation to the EPR cavity. The output developed by the phase detector is a d-c output voltage, the amplitude and polarity of which are dependent on the amplitude and phase of the input voltage, Fig. 2-9. i.e. The output is a first harmonic presentation of the original EPR resonance line. A typical recorder trace is shown in Fig. 2-10.

Sensitivity of the spectrometer

The last and most important parameter associated with any electron resonance spectrometer is its sensitivity. This is normally expressed as the minimum number of unpaired electrons which can be detected by the spectrometer. The main limitation on the sensitivity of the spectrometer is the additional noise of the crystal detector. However, the excess noise of the crystal detector varies with the frequency of modulation and there is an inverse relation between it and the frequency. It follows that high sensitivity, in which negligible noise is added by the detecting system, will only be obtained if modulation frequencies of much higher value then the audio range are employed.
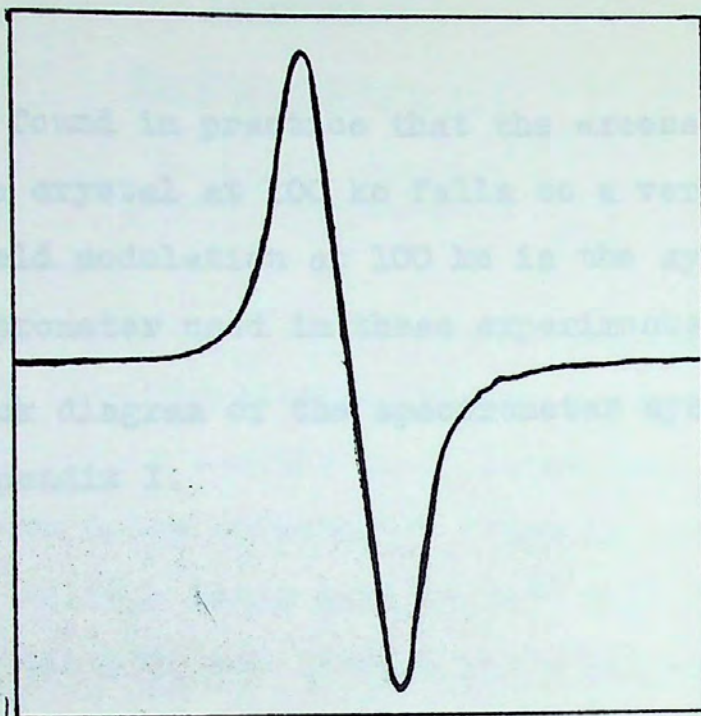
Fig. 2.10
Typical recorder trace of EPR signal.

- 46 -

It is found in practice that the excess noise contributed by the crystal at 100 kc falls to a very small amount. Magnetic field modulation at 100 kc is the system employed in the spectrometer used in these experiments.

A block diagram of the spectrometer system used is shown in Appendix I.

CHAPTER III

Crystal Structures

A- $BaTiO_3$ Crystal

The basic lattice of $BaTiO_3$, existing above 120°C and slightly below this temperature, may be regarded as a simple cubic array of corner sharing $Ti-O_6$ octahedra, with barium ions filling the holes between[1]. This is the "perovskite" structure, of chiefly ionic nature: Ba^{2+} Ti^{4+} $O_3^=$, Fig. 3-1. Between 120°C and 5°C, the lattice has a slight tetragonal distortion and a spontaneous polarization associated with a displacement of the Ti^{4+} ion away from the center of the unit cell. The spontaneous polarization produces a bound surface charge of the order of 10^{-5} coulomb/cm^2[2,3]. This value is due partly to the displacement of the Ti^{4+} ion with respect to its surroundings, and partly to the polarization of the highly polarizable oxygens resulting from the displacement of the Ti^{4+}.

The polar, optic and c-axes in the tetragonal crystal system are all in the same direction. In the tetragonal phase, one axis has expanded, forming the c-axis.
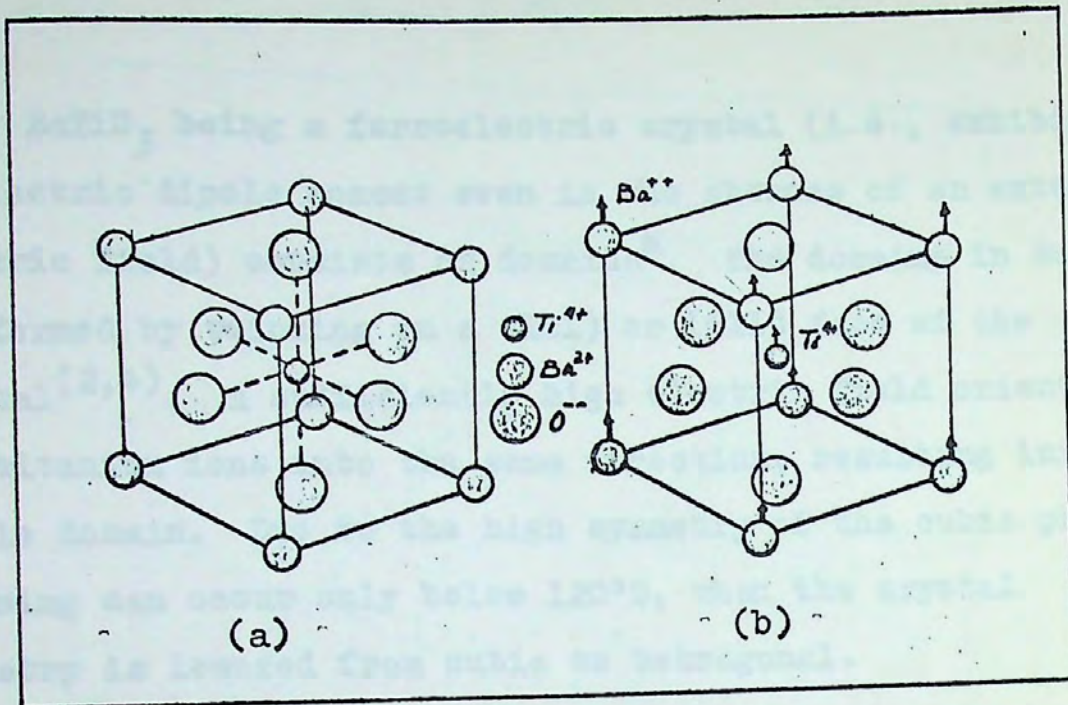
Fig. 3-1

(a) The perovskite structure of barium titanate. The structure is cubic, with Ba^{2+} ions at the cube corners, O^{2-} ions at the face centers, and a Ti^{4+} ion at the body center. (b) Below the Curie temperature the structure is slightly deformed, with Ba^{++} and Ti^{4+} ions displaced relative to the O^{--} ions, thereby developing a dipole moment.

BaTiO$_3$ being a ferroelectric crystal (i.e., exhibits an electric dipole moment even in the absence of an external electric field) consists of domains[*]. The domains in BaTiO$_3$ are formed by twinning on a (101) or (011) face of the crystal[2,4]. A sufficiently high electric field orients all titanium ions into the same direction, resulting into a single domain. Due to the high symmetry of the cubic phase, twinning can occur only below 120°C, when the crystal symmetry is lowered from cubic to tetragonal. Crystal plates which are a single domain at room temperature, occur with their optic axis either in the plane of the plate (in which case it is called "a-domain crystal plate"), or perpendicular to the plane of the plate (in which case it is called "C-domain crystal plate"), Fig. 3-2.

There are two other phase transitions in BaTiO$_3$ near 5°C and -70°C respectively. Lowering the temperature below 5°C BaTiO$_3$ undergoes a phase transition from tetragonal to orthorhombic, and the axis of polarization will be along a cell-face diagonal. Below -70°C BaTiO$_3$ undergoes a phase transition from orthorhombic to trigonal, and its polarization will be along a cell body diagonal[5].

---

[*] A ferroelectric crystal generally consists of regions called "DOMAINS" within each of which the polarization is in the same direction, but in adjacent domains the polarization is in different directions.
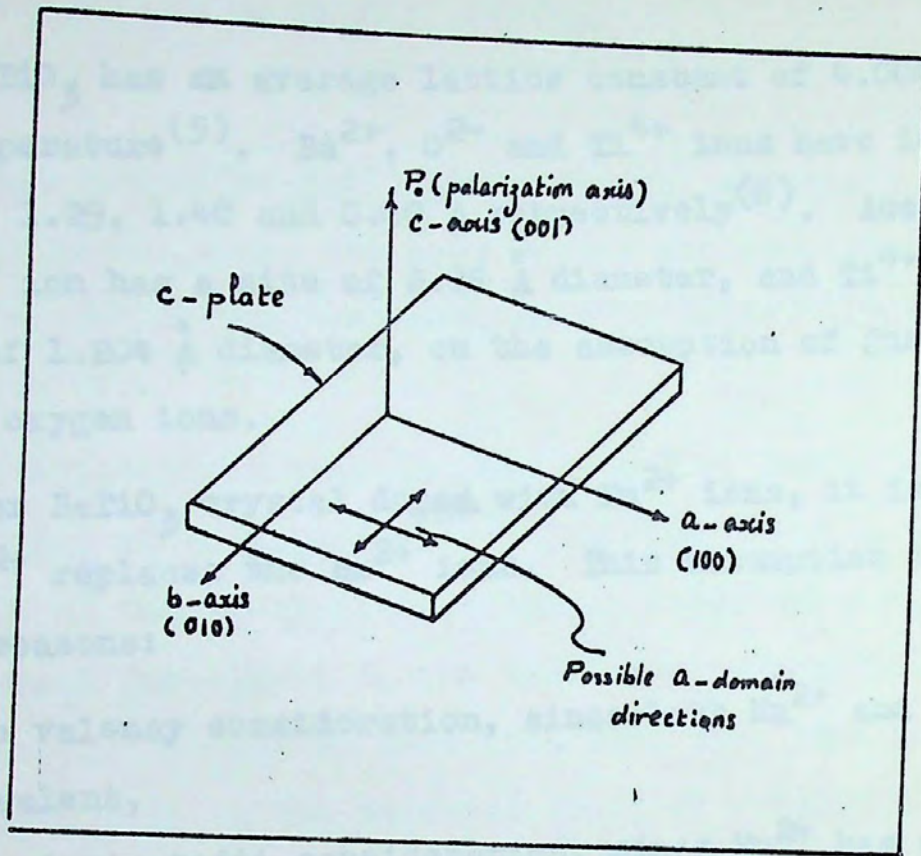
Fig. 3-2

Barium titanate crystal axes and domains.

BaTiO$_3$ has an average lattice constant of 4.004 Å at room temperature[5]. Ba^{2+}, O^{2-} and Ti^{4+} ions have ionic radii of 1.29, 1.40 and 0.60 Å respectively[6]. Accordingly, the Ba^{2+} ion has a site of 2.86 Å diameter, and Ti^{4+} ion has a site of 1.204 Å diameter, on the assumption of just touching the oxygen ions.

For BaTiO$_3$ crystal doped with Mn^{2+} ions, it is expected that Mn^{2+} replaces the Ba^{2+} ions. This assumption is based on two reasons:

i) the valency consideration, since both Mn^{2+} and Ba^{2+} are divalent,

ii) the ionic radii consideration, since Mn^{2+} has an ionic diameter of 1.6 Å and Ba^{2+} ion has a site diameter of 2.86 Å.

If EPR measurements are made, the expected spectra has to reveal cubic symmetry for the Ba^{2+} or Mn^{2+} site, and also cubic symmetry for the Ti^{4+} site.

B- Mg_2SiO_4 crystal

Forsterite (Mg_2SiO_4) has a crystal structure belonging to the olivine group, the most recent and complete analysis of its structure has been published by Birle, Gibbs, Moore and Smith[7].

The idealized olivine structure Fig. 3-3 consists of a hexagonal close packed array of oxygen atoms in which one-half of the available octahedral voids are occupied by M atoms and one-eighth of the available tetrahedral voids by Si atoms. It may be seen from Fig. 3-3, that the key structural unit is the serrated chain of octahedra lying parallel to the z-axis. In any one yz layer only half the octahedral voids are occupied resulting in a serrated chain of unoccupied octahedra whose shape is the same as that of the occupied band, but which is displaced b/2 (see also Fig. 3-4). The next layer of occupied octahedra is displaced a/2 from the first layer. The occupied serrated chain lies directly above the unoccupied serrated chain of the first layer, and is related to the occupied chain of the first layer by the b glide plane. Accordingly, none of the octa-hedra share faces. The serrated chains are joined together by silicon centered tetrahedra which share a triangle of
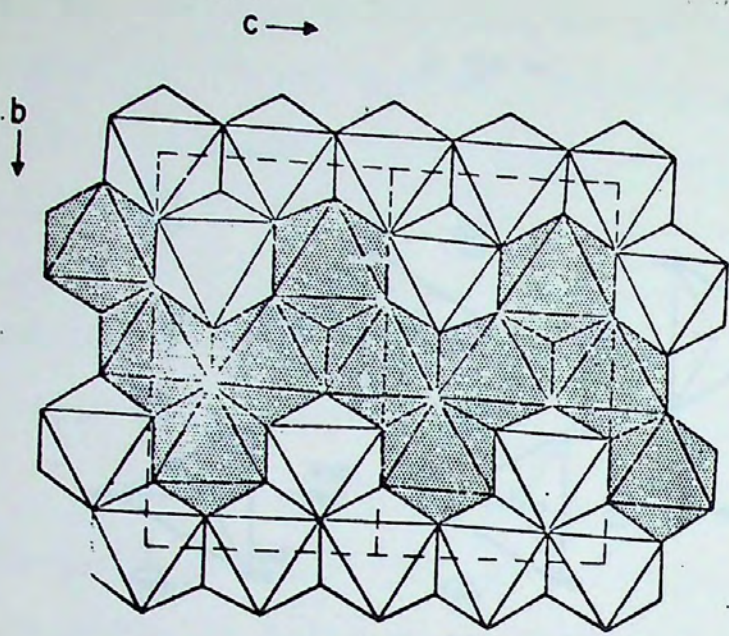
Fig. 3-3

Octahedral populations in the crystal
structure of olivine. Shaded and
unshaded octahedra distinguish the two
levels normal to the plane of the
drawing.

(a)

(b)
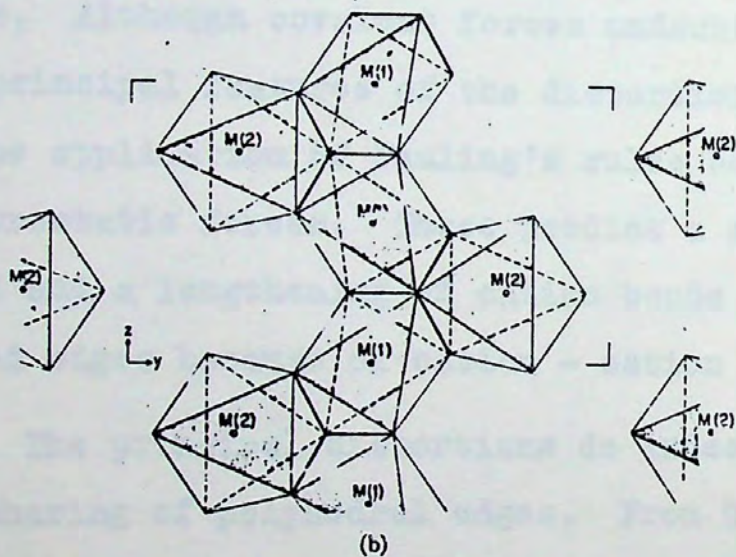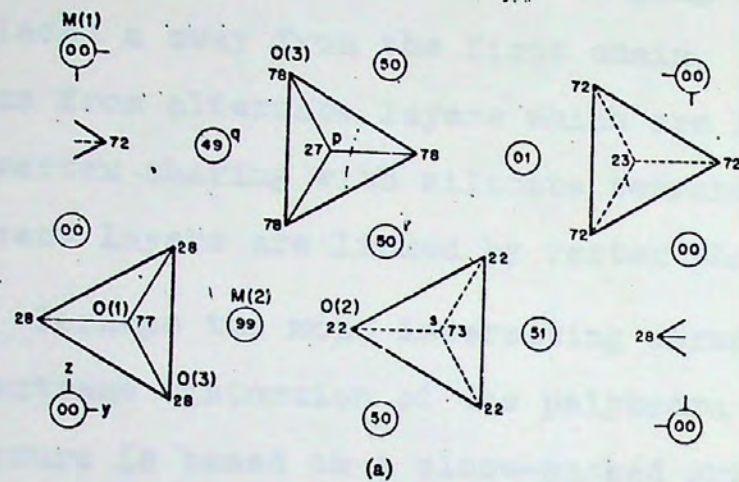
Fig. 3-4

(a) Tetrahedral arrangements and the neighbouring octahedral sites.

(b) Actual distortions observed for olivine in a portion of an octahedral serrated band.

edges with octahedra from one serrated chain and which share the vertex opposing the triangle with a vertex from each of three octahedra belonging to a serrated chain displaced a away from the first chain. In contrast to the chains from alternate layers which are linked by this edge and vertex sharing with silicate tetrahedra, chains of adjacent layers are linked by vertex sharing of octahedra.

Perhaps the most interesting structural feature is the extreme distortion of the polyhedra even though the structure is based on a close-packed arrangement of oxygen atoms. Although covalent forces undoubtedly contribute, the principal features of the distortions can be explained by the application of Pauling's rules based on simple electrostatic forces. These predict a shortening of shared edges and a lengthening of cation bonds to oxygen atoms of shared edges because of cation - cation repulsion.

The principal distortions do indeed correlate with the sharing of polyhedral edges. From Table 3-1 the distortions may be seen.

From Fig. 3-5 it may be seen that the silicon tetrahedron is almost a trigonal pyramid elongated parallel to the x-axis. The M(1) octahedron which lies on an inversion

Table 3-1

Interatomic Distances (Å) in Forsterite

Atoms		Interatomic distance A	Atoms		Interatomic distance A
		Si-tetrahedron			
1Si	O(1)	1.614	1 O(1) - O(2)		2.743
1	O(2)	1.6 54	2	O(3)	2.757
2	- O(3)	1.635	2 O(2) - O(3)[a]		2.556
			1 O(3) - O(3)[a]		2.586
	mean	1.634		mean	2.659
	M(1) octahedron			**M(2) octahedron**	
2M(1)	- O(1)	2.091	1M(2) - O(1)		2.177
2	- O(2)	2.075	1	- O(2)	2.059
2	- O(3)	2.142	2	- O(3)	2.217
	mean	2.103	2	- O(3)	2.070
2O(1)	- O(2)[b]			mean	2.135
2	O(2)		2O(1) - O(3)[b]		2.857
2	O(3)[b]		2	- O(3)	3.028
2	O(3)		2O(2) - O(3)		3.194
2O(2)	- O(3)[a]		2	- O(3)	2.937
2	O(3)		1O(3) - O(3)[a]		2.586
			2	- O(3)	3.408
			2	- O(3)	2.995
	mean	2.964		mean	3.001

a = edges shared between tetrahedron and octahedron.

b = edges shared between octahedra.

M(1) ● 50
3.01

SI J3 2.72
07 3.27

M(2) ● 49
3.23

O(1)
27
2.85
O(2)
78
M(2) ● 01 3.66
101 3.59

2.87
2.56
3.14
3.39

O(3)
78
2.09
2.09
3.04

3.04
2.16
M(1)
50
2.16
O(3)
22

3.39
2.09 2.09
3.14
2.58
2.87

M(2) ● 99 3.59
01 3.66
O(2)
22
2.85
O(1)
93
M(2) ● 51
3.23

SI 07 2.72
107. 3.27

(a)

SI ● 43
3.40

100 3.66
M(1) ●
00 3.59

O(3)
28
3.00
O(3)
78
M(1) ● 50
3.23

2.93
3.22
3.04
2.87

SI ● 57
3.28
O(2)
72
2.06 2.24
207 M(2) 75
3.41
2.19
2.60
O(1)
27
SI 93 2.82
07 3.27

2.08 2.24
3.22
3.04
2.87

2.93

00 3.59
M(1) ●
100 3.60
O(3)
28
3.00
O(3)
78
M(1) ● 50
3.23

(b)

M(1) ● 00
4.44
O(3)
78
M(1) ● 50 2.72
150 3.27

2.76
1.63
2.56

M(2) ● 49 2.82
149. 3.27
2.60
SI
93
O(1)
27 2.14
1.62 1.65
O(2)
78
M(2) ● 01
3.28

2.76
1.63
2.56

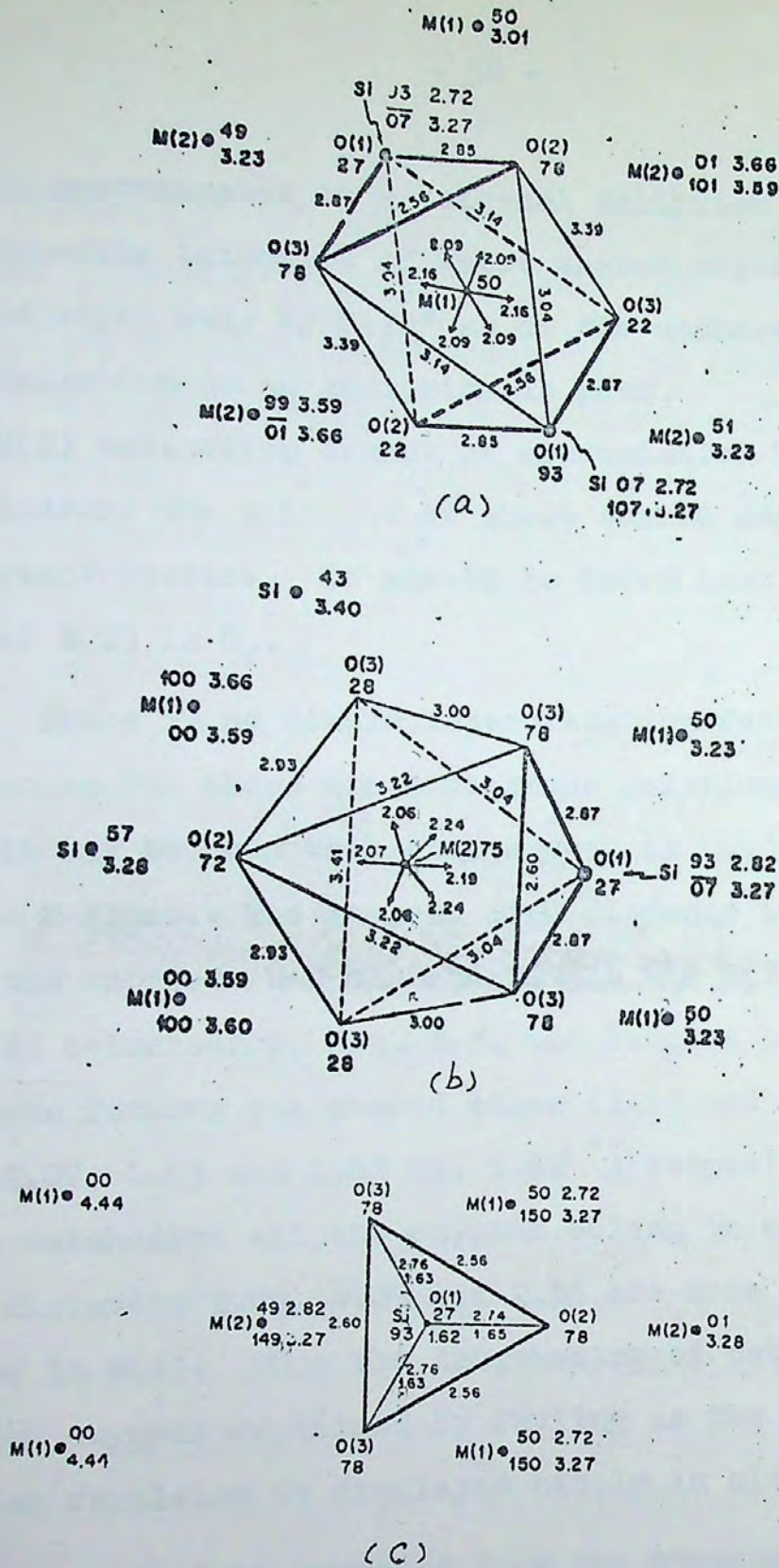M(1) ● 00
4.41
O(3)
78
M(1) ● 50 2.72
150 3.27

(c)

Fig. 3_5 (a) Interatomic distances about the M(1)
octahedron.

(b) Interatomic distances about the M(2)
octahedron.

(c) Interatomic distances about the Si
tetrahedron.

centre approximates to a trigonal antiprism because of the
two opposing triangles of short shared edges. However the
shared edges vary by $0.3A^\circ$ as do the unshared edges so the
approximation to an antiprism is poor.

The M(2) octahedron cannot be approximated by any symmetrical
polyhedron: the triangle of short shared edges is the most
important feature. It should be noted that the point symme-
try of M(2) is C_v.

There is no simple interpretation for the cation-oxygen
distances but there are some crude relationships. From Table
3.1 it may be seen that each oxygen is bonded to one Si and
three M atoms. The longest Si-O distance is to O(2) which
has the shortest M-O distances. In the M(2) octahedron and
the Si tetrahedron, Fig. 3-5, the longest bonds are to
oxygens forming the shared edges (2.19 and 2.24 vs. 2.06
and 2.07; 1.63 and 1.63 vs. 1.62 $\overset{\circ}{A}$ respectively. In the
M(1) octahedron all the oxygens belong to shared edges, and
the distances 2.09, 2.09 and 2.16 are more regular than
those in M(2). Thus the lengthening of cation bonds to
shared oxygens explained by Pauling as the result of cation-
cation repulsion is displayed nicely in olivine.

As might be expected from the greater charge on the
silicon ion, the edge shared between a tetrahedron and an

octahedron (2.56 and 2.60 A°) are shorter than those shared
between octahedra (2.87 and 2.89 A°). Unshared edges are
all larger than the shared edges in the same polyhedron :-
Si tetrahedron, 2.73 and 2.76; octahedra, 2.94 to 3.44 A°
respectively. Although the shared edges are shorter than
the unshared edges, the great variation in the lengths of
the unshared edges in the octahedron shows that the situat-
ion is actually more complex. Comparison of Fig. 3.5b with
Fig. 3.4b shows that shortening of the O(3)-O(3) edge shared
between the M(2) and Si polyhedra results in a **lengthening**
of the other O(3)-O(3) edge which lies parallel to the
z-axis: this arises because these two O(3)-O(3) edges add
up to yield the c repeat distance which is not completely
free to shorten upon sharing of the first edge because of
the geometrical requirements of the M(1) octahedra. Indeed
comparison of Fig. 3-5a with Fig. 3-4b shows that the c
repeat distance is also determined in part by the O(1)-O(2)
edges of two M(1) octahedra. These edges are the shortest
of the unshared edges of the M(1) octahedron. Thus one can
envisage a compromise between conflicting electrostatic and
spatial factors such that the first O(3)-O(3) edge shortens
and the second one lengthens while the two O(1)-O(2) edges
shorten somewhat. Of course a detailed analysis would
require simultaneous consideration of all the edges.

Mg_2SiO_4 crystal has an average lattice constants of $a = 4.662$ A°, $b = 10.225$ A° and $c = 5.994$ A°[7]. Inspection of Fig. 3-5a, Fig. 3-5b and Table 3-1 reveals that the M(1) site diameter is 1.38 A°, and the M(2) site diameter is 1.46 A°, on the assumption of just touching the oxygen ions. Hence an impurity can occupy any of these sites, if its ionic diameter fits the site diameters listed above.

If EPR measurements are made, the expected spectra will reveal; inversion center symmetry if the impurity present occupies the M(1) sites, and C_{2v} point symmetry if the impurities occupy the M(2) sites.

CHAPTER IV

Experimental Procedure

A- Samples

The samples studied are:

(a) $BaTiO_3$ single crystals dopped with Mn^{2+} ions.[x]

Two samples were used for the study. They are crystal
plates of dimensions 7x3x0.2 mm, and of the a-domain
structure. Their direction of polarization is along
the surface of the crystal plate (which is parallel to
the a-axis), and has been detected optically through
the use of crossed polaroids. The colour of the crystal
is orange.

Fig. 4-1a, illustrates the $BaTiO_3$ crystal plate indicat-
ing its axes and the direction of polarization.

(b) Mg_2SiO_4 single crystal with various impurities.[+]

One sample was used for the study. Its shape is nearly
quarter of a sphere of 10 mm diameter. Its crystallo-
graphic axes are known, and are shown in Fig. 4-1b. The
crystal is colourless, but has a misty appearance.

The crystal has been cut to five pieces to fit the
experiments performed.

----

[x] These crystals were prepared by Dr. M. Shabana in Harvard
University during his study for Ph.D. degree.

[+] This crystal was prepared by Mr. Cabell Finch at Oak Ridge
National Laboratory. It was grown by pulling a seed from
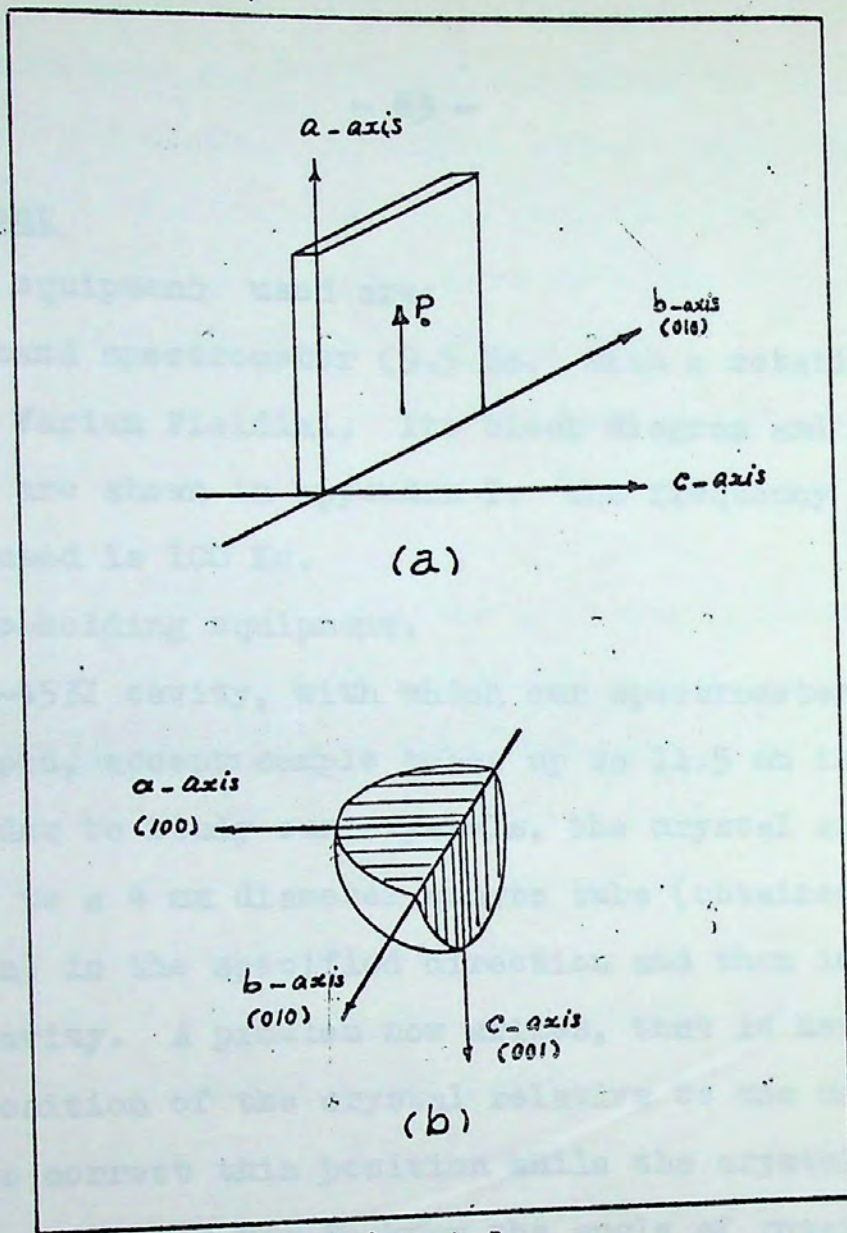a melt in an iridium crucible at a temp. of 1900°C and in
oxygen atmosphere.

Fig. 4-1

(a) BaTiO$_3$ crystal plate indicating its axes and the direction of polarization.

(b) Mg$_2$SiO$_4$ crystal indicating its crystallographic axes.

B- Equipment

The equipment used are:

(a) An X-band spectrometer (9.5 Gc.) with a rotating magnet and a Varian Fieldial. Its block diagram and specifications are shown in appendix I. The frequency of modulation used is 100 Kc.

(b) Sample-holding equipment.

The V-4531 cavity, with which our spectrometer system is equipped, accepts sample tubes up to 11.5 mm in diameter. In order to study our crystals, the crystal sample was glued to a 4 mm diameter quartz tube (obtained from Varian) in the specified direction and then inserted into the cavity. A problem now arises, that is how to measure the position of the crystal relative to the magnetic field, how to correct this position while the crystal is inside the cavity, and how to know the angle of rotation? These problems have been solved partially by certain types of the Varian spectrometer systems in which the d.c. magnet can rotate around its vertical axis.

Our V-4502 spectrometer system has this facility, but the sizes of the TE_{102} cavity and the air gap between the magnet poles make it impossible for the magnet to rotate through angles of more than $\pm 15°$.

A goniometer was built which enables the crystal to be
fixed in any **desir**ed direction, and to rotate it either:

  i) around a vertical axis perpendicular to the d.c
     magnetic field, as shown in Figs. 4-2a & 4-2b
     called the θ-rotation.

 ii) around a horizontal axis parallel to the d.c
     magnetic field, as shown in Fig. 4-2c, called the
     Φ- rotation.

iii) in a combined rotation of i and ii above.

The goniometer is shown in appendix-II. All its parts
are made of a plastic free of EPR signals except that of
the sample, and at the same time causes only a small
disturbance of the field in the cavity.

(c) Variable temperature accessory.

The Model V-4557 variable temperature accessory
automatically controls the temperature of an EPR sample
within the range of - 185°C to + 300°C. It was used for
the low temperature measurements.

C- Experiments performed

The experiments that have been done are:

I- **EPr** BaTiO$_3$ single crystal.

  (1) Choice of the suitable power attenuation, modulat-
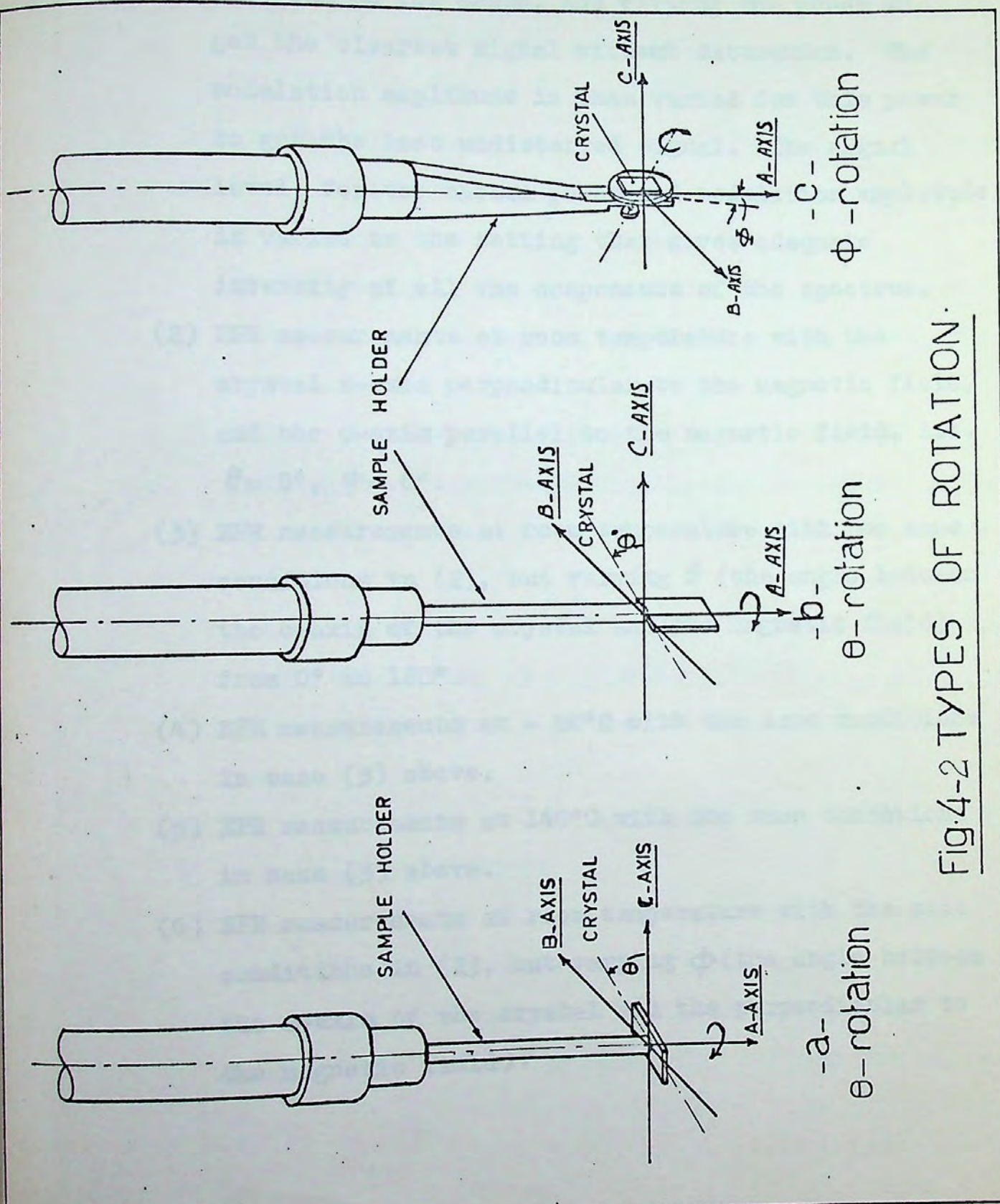   ion amplitude and signal level. This is done by

Fig.4-2 TYPES OF ROTATION.

fixing one of the absorption lines of the EPR
spectrum on the scope, and varying the power to
get the clearest signal without saturation. The
modulation amplitude is then varied for this power
to get the best undistorted signal. The signal
level, for the chosen power and modulation amplitude,
is varied to the setting that gives adequate
intensity of all the components of the spectrum.

(2) EPR measurements at room temperature with the
crystal a-axis perpendicular to the magnetic field,
and the c-axis parallel to the magnetic field, i.e.
$\theta = 0°$, $\phi = 0°$.

(3) EPR measurements at room temperature with the same
conditions in (2), but varying θ (the angle between
the c-axis of the crystal and the magnetic field)
from 0° to 180°.

(4) EPR measurements at - 40°C with the same conditions
in case (3) above.

(5) EPR measurements at 140°C with the same conditions
in case (3) above.

(6) EPR measurements at room temperature with the same
conditions in (2), but varying ϕ (the angle between
the a-axis of the crystal and the perpendicular to
the magnetic field).

(7) EPR measurements at room temperature with the same
conditions in case (2), but after irradiating the
crystal with X-rays for 3 hours.

II- For Mg_2SiO_4 Single Crystal

(8) Samé as (1) for $BaTiO_3$ crystal mentioned above.

(9) EPR measurements at room temperature with the
crystal c-axis perpendicular to the magnetic field,
and rotating the crystal in the ab plane around the
c-axis.

(10) EPR measurements at room temperature with the
crystal b-axis perpendicular to the magnetic field,
and rotating the crystal in the ac plane around the
b-axis.

(11) EPR measurements at room temperature with the crystal
a-axis perpendicular to the magnetic field, and
rotating the crystal in the bc plane around the
a-axis.

(12) EPR measurments for the same conditions in case (10)
above but at - 160°C.

(13) EPR measurements for the crystal with its b-axis
perpendicular to the magnetic field and the c-axis
parallel to the magnetic field, and varying the
temperature from - 160° gradually to room temperature.

(14) EPR measurements at room temperature for the
powder of a crushed piece of the crystal.

(15) EPR measurements for the powder of the crystal
while varying the temperature from - 160°C to
room temp.

(16) EPR measurements at room temperature with the
same conditions in (9), but after irradiating
the crystal with X-rays for 60 minutes, and
subsequent annealing to temperatures ranging from
300° to 500°C.

N.B.   EPR measurement of the "1% pitch in KCl" standard
sample was made under the same conditions of each
experiment to insure adequate calculations and results.

CHAPTER V

## RESULTS AND DISCUSSION

A- BaTiO$_3$ Crystal

I- Results

a- General

The EPR spectrum obtained for the crystal at room temperature, from experiment No. 2 mentioned in Chapter IV, is shown in Fig. 5-1. The spectrum consists of several components:

i) A six line spectrum having separations of about 80 gauss between lines, with equal intensities, and line width of 6 gauss. The g-value at the center of gravity of the six lines is equal to 2.004 ± 0.001.

ii) Inner resonance lines, in the form of doublets between the lines of the six line spectrum. The separation between the two lines of each doublet varies from 15 to 25 gauss. Their intensity is 1/50 of the intensity of the six-line spectrum when the crystal (C) axis is parallel to the magnetic field H.

iii) A single line, of intensity about four times that of the 6-line spectrum, and a line width of about 11 gauss. It has a g-value of 2.000 ± 0.001.
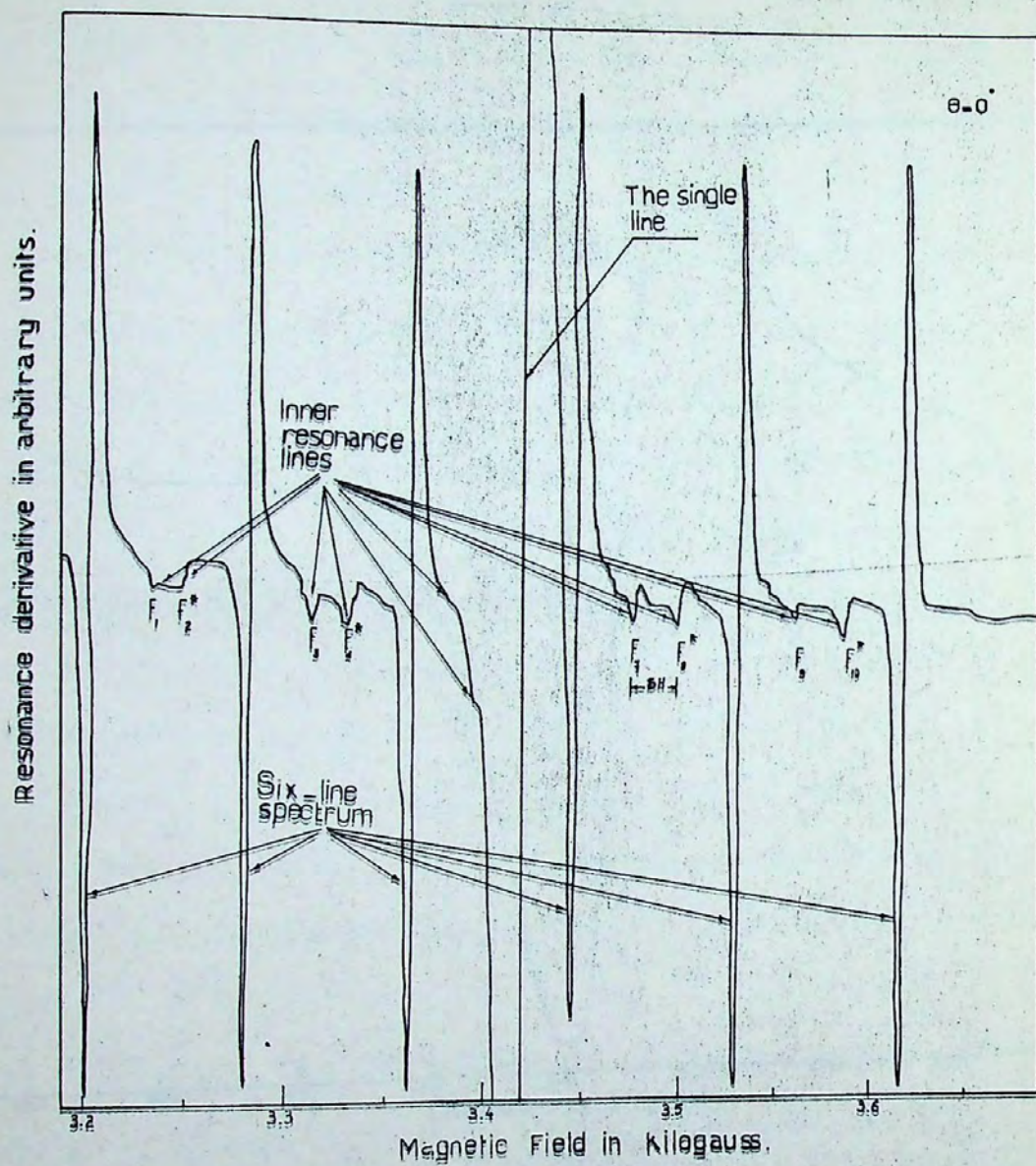
[a]

Fig. 5.1: EPR spectra of BaTiO$_3$ crystal at 25°C
with H parallel to the c-axis, and a-axis
perpendicular to H.
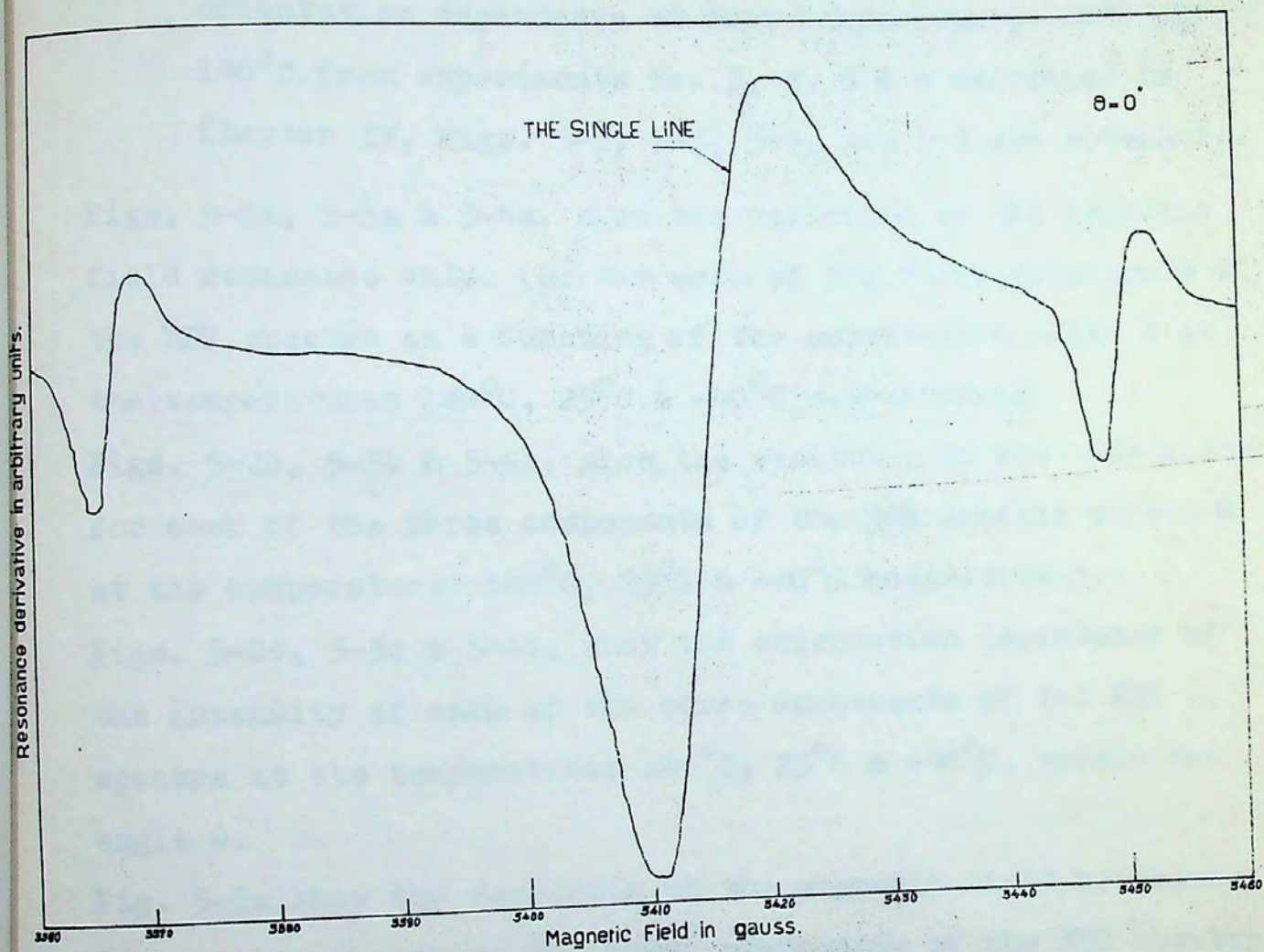
Fig. 5.1b: The single line enlarged.

iv) No other transitions were detected over the field range 0-10 K.Gauss. From the EPR spectra (for the same spectrometer conditions) obtained for the crystal orientation dependence at room temperature, -40°C and 140°C, from experiments No. 3, 4, 5 & 6 mentioned in Chapter IV, Figs. 5-2, 5-3, 5-4, and 5-5 are obtained.

Figs. 5-2a, 5-3a & 5-4a, show the variation of the magnetic field resonance value (H) for each of the three components of the EPR spectra as a function of the orientation angle θ at the temperatures 140°C, 25°C & -40°C respectively.

Figs. 5-2b, 5-3b & 5-4b, show the variation of the line width for each of the three components of the EPR spectra versus θ at the temperatures 140°C, 25°C & -40°C respectively.

Figs. 5-2c, 5-3c & 5-4c, show the orientation dependence of the intensity of each of the three components of the EPR spectra at the temperatures 140°C, 25°C & -40°C, versus the angle θ.

Fig. 5-5a show the variation of the magnetic field resonance value (H) for each of the three components of the EPR spectra as a function of the orientation angle $\emptyset$ at room temperature, and $\theta = 0°$.

Fig. 5-5b, show the variation of the line width for each of the three components of the EPR spectra as a function of the

Fig. 5.2: Orientation dependence of the parameters of EPR spectra components of BaTiO$_3$ at 140°C & θ-rotation.

Fig. 5.3: Orientation dependence of the parameters of EPR spectra components of BaTiO₃ at 25°C & θ-rotation.

Fig. 5.4: Orientation dependence of the parameters of EPR spectra components of BaTiO$_3$ at -40°C & θ-rotation.
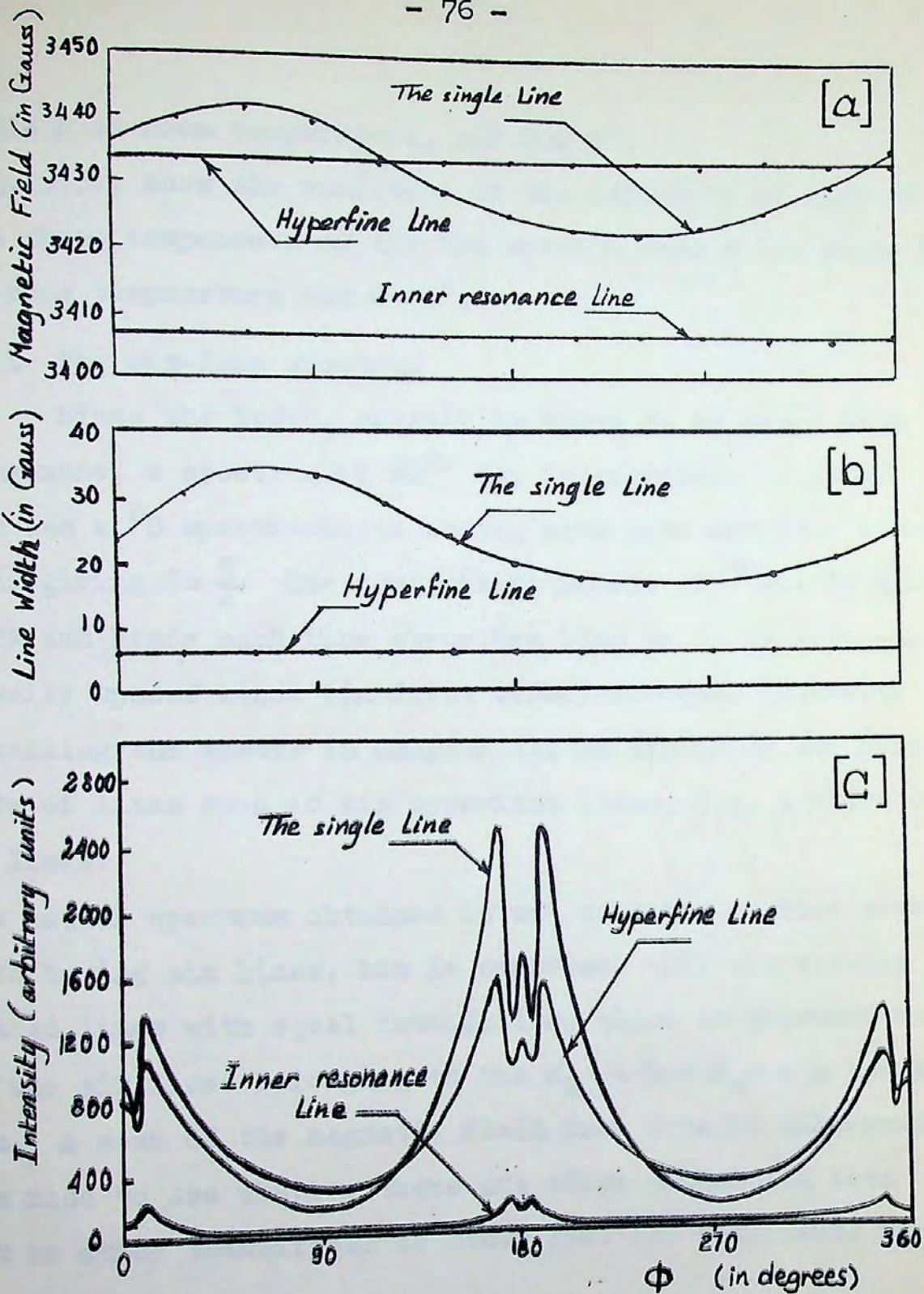
Fig. 5.5

angle $\emptyset$ at room temperature, and $\Theta = 0^\circ$.

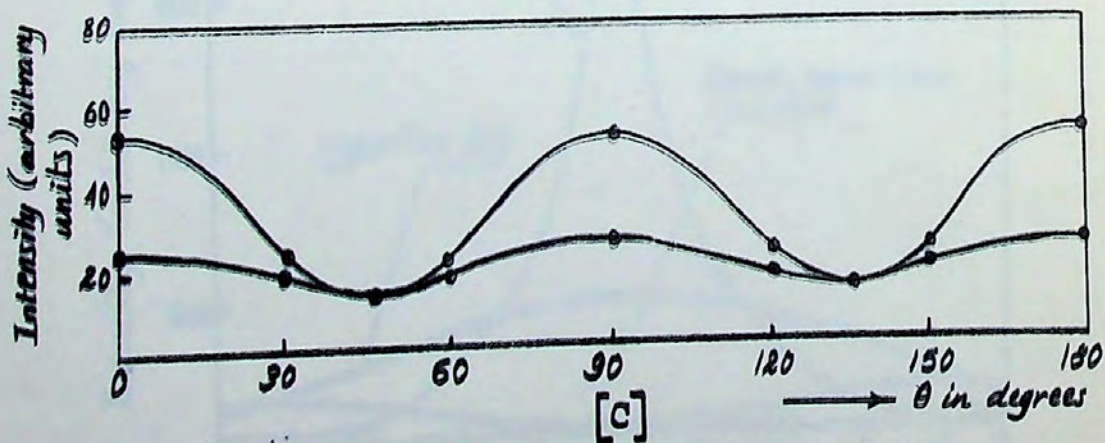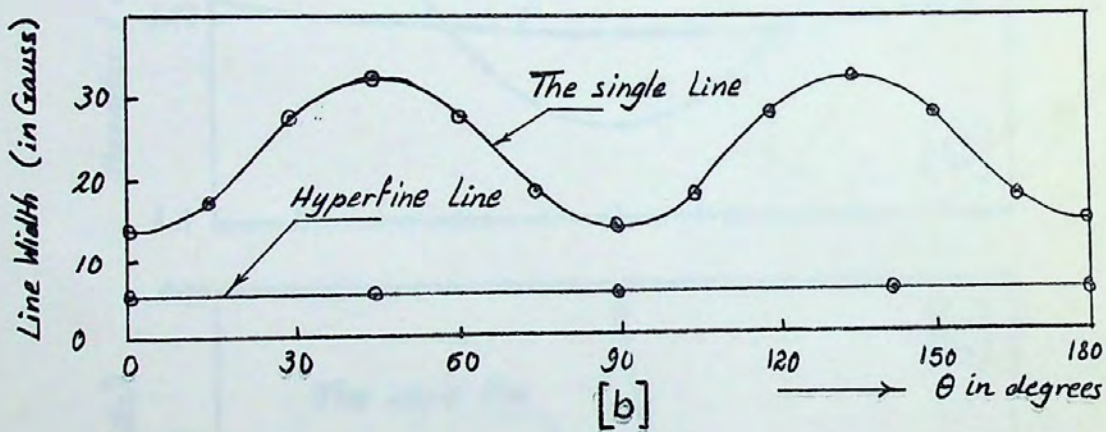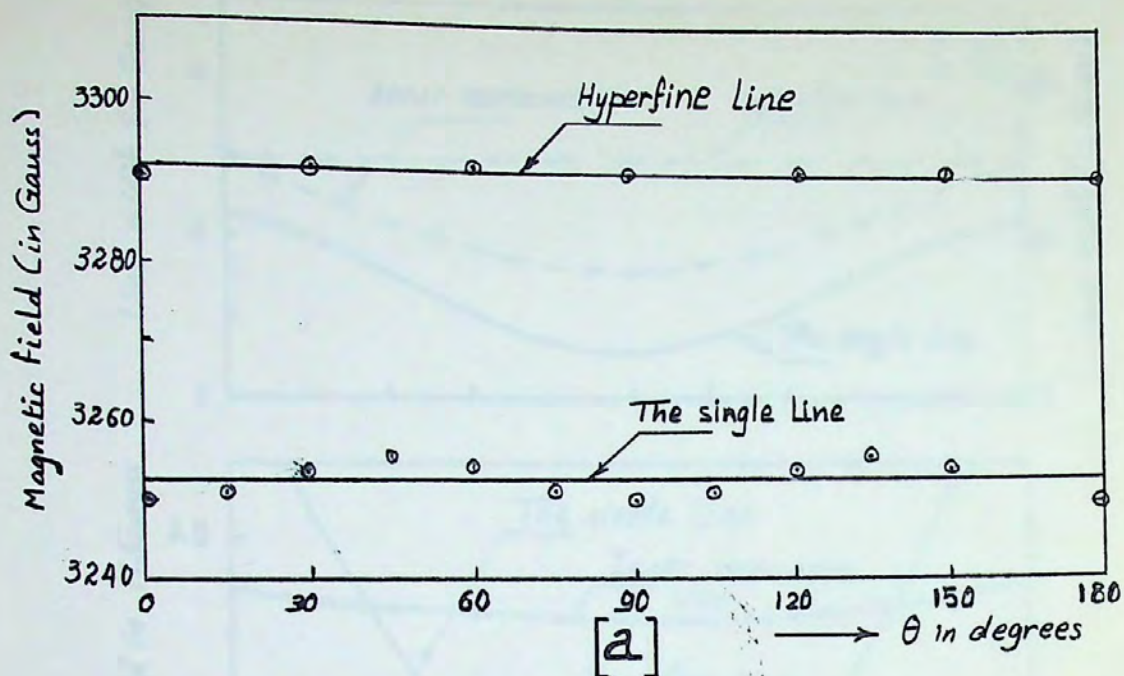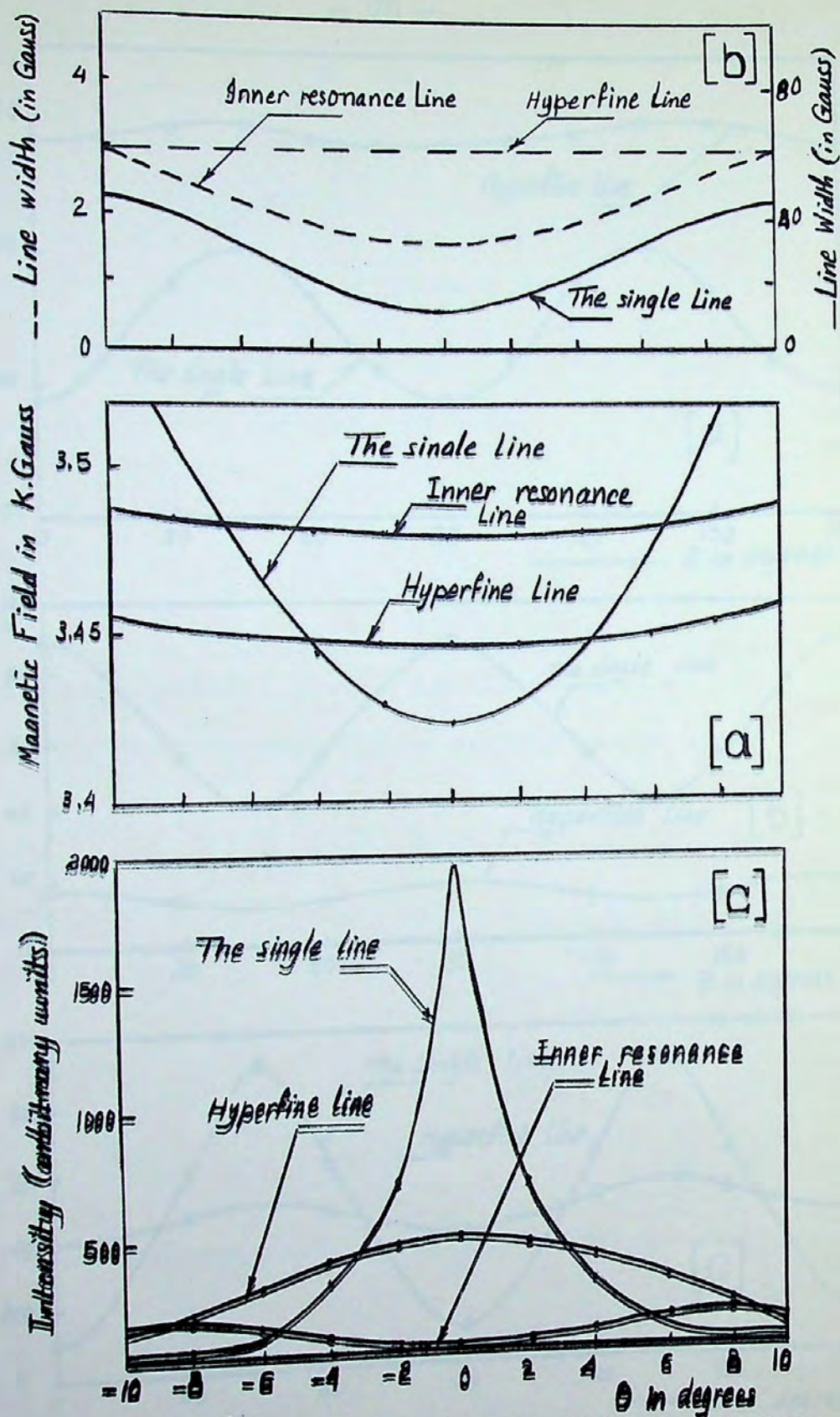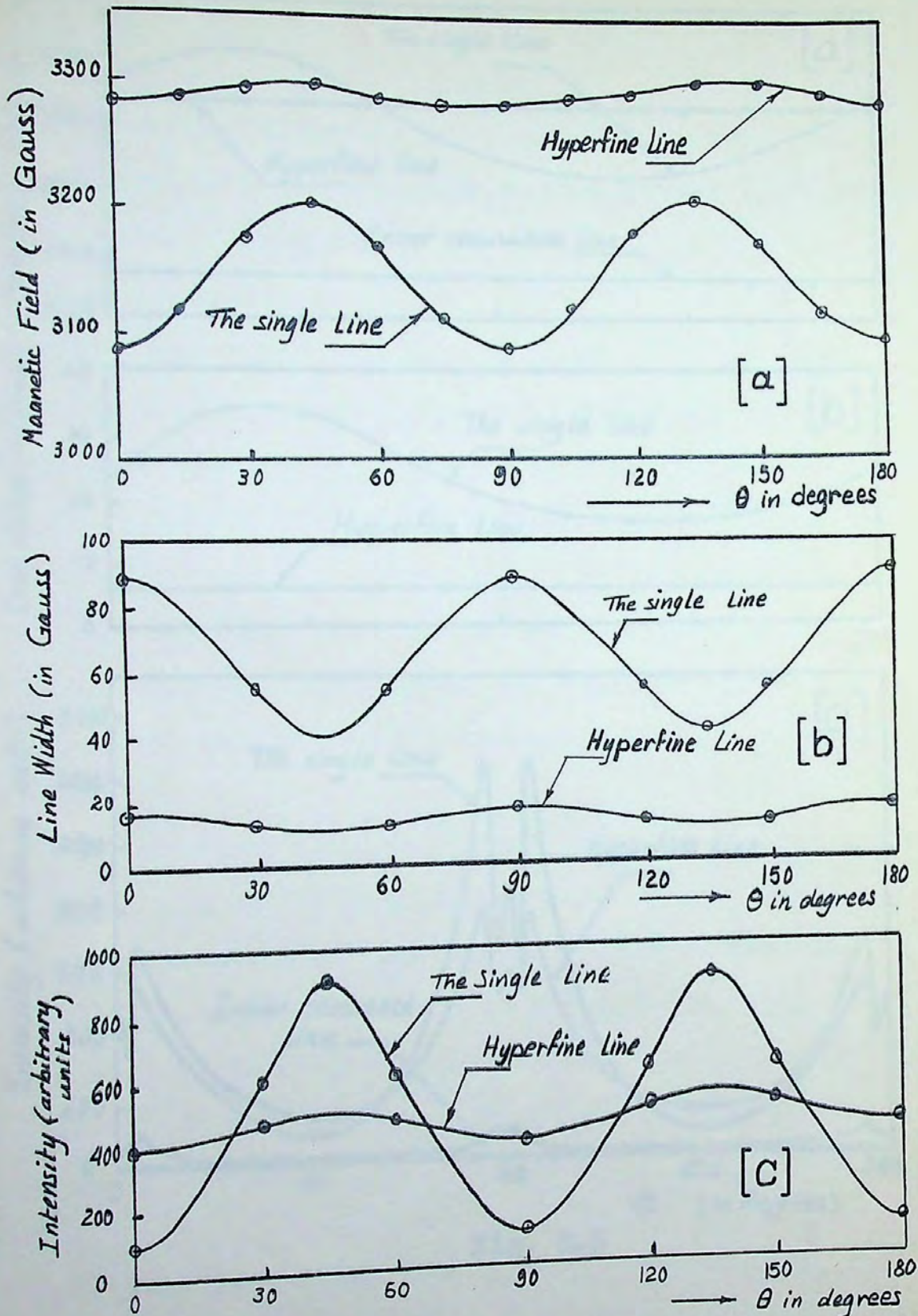Fig. 5-5c, show the variation of the intensity of each of the three components of the EPR spectra versus the angle $\emptyset$ at room temperature and $\Theta = 0^\circ$.

b- The six-line spectrum

Since the BaTiO$_3$ crystal is known to be doped with Manganese, a spectrum of Mn^{2+} ion is expected. The Mn^{2+} ion has a ^{6}S spectroscopic state, with five unpaired electrons giving $S = \frac{5}{2}$. The isotopic abundance of ^{55}Mn, $I = \frac{5}{2}$ is 100% and hence each fine structure line is split into six equally spaced lines (in first order) of equal intensity. Recalling the theory in Chapter II, we expect to see five sets of lines each of six hyperfine lines, i.e. a total of 30 lines.

The actual spectrum obtained is not composed of five sets each having six lines, but it comprises only six equally spaced lines with equal intensities, which is presumed to be the six lines belonging to the $M_s = + \frac{1}{2} \leftrightarrow M_s = - \frac{1}{2}$ transition. A scan of the magnetic field from 0 to 10 kilo-gauss was made to see whether there are other transition sets but no other transitions or other spectral components were detected.

From Fig. 5-1, it is seen that the six-line spectrum has separations of about 80 gauss between lines, and the g-value

of the center of gravity of the 6 lines is equal to $2.004\pm$ 0.001. Since no line is detected at the center of gravity of the six-line spectrum, then the isotopic species producing the six-line spectrum has a natural abundance of 100%. This spectrum is comparable to that observed for Mn^{2+} in similar crystals[1,3]. Thus on the basis of doping the crystal with Mn and the similarity in hyperfine splitting and isotopic abundance it is assumed that the six line spectrum is the hyperfine structure of the $M_s = + \frac{1}{2} - M_s = -\frac{1}{2}$ transition of the Mn^{2+} ion.

This observed hyperfine spectrum fits the spin Hamiltonian with the following measured parameters, listed in Table 5-1, in the cubic, tetragonal and orthorhombic phases :-

Table 5-1

Spin Hamiltonian parameters of Mn^{2+} in $BaTiO_3$ single crystal

	Cubic phase	Tetragonal phase	Orthorhombic phase
g	2.004 ± 0.001	2.004 ± 0.001	2.004 ± 0.001
A	$(75 \pm 3) \times 10^{-4}$ cm^{-1}	$(72\pm2) \times 10^{-4}$ cm^{-1}	$(72\pm2) \times 10^{-4}$ cm^{-1}
D & E	cannot be calculated since the other transitions of the Mn^{2+} ion (namely $+\frac{5}{2} \leftrightarrow +\frac{3}{2}$, $+\frac{3}{2} \leftrightarrow +\frac{1}{2}$, $-\frac{1}{2} \leftrightarrow -\frac{3}{2}$ & $-\frac{3}{2} \leftrightarrow -\frac{5}{2}$) were not detected.		

Figs. 5-2a, 5-3a & 5-4a show the orientation dependence
(for Θ - rotation about the a-axis of the crystal), of the
magnetic field value (H) for any of the lines of the hyperfine
structure at the temperatures 140°C, 25°C & -40°C respectively.
It is seen that the value of H for each spectral component
is independent of the rotation angle Θ at 140°C. At 25°C,
H has a minimum value at $\Theta = 0°$ and then increases with
increasing Θ up to $\Theta = \pm 12°$, above 12° the absorption lines
disappear$. At -40°C, H follows nearly a cos 2 Θ relation
versus Θ, with minimum values at $\Theta = 0°$, 90° & 180°. Fig. 5-5a
shows the orientation dependence (for $\emptyset$ - rotation about the
c-axis of the crystal), of the magnetic field value (H) for
any of the lines of the hyperfine structure at 25°C & $\Theta = 0°$.
It is seen from Fig. 5-5a, that H is independent of the
rotation angle $\emptyset$, at 25°C with $\Theta = 0°$.

From Figs. 5-2b, 5-3b & 5-4b, it is seen that the line
width of any line of the hyperfine structure lines is indepen-
dent of the orientation angle Θ at 140°C and at 25°C. At -40°C,
the line width changes within small limits ($\pm$ 2 gauss) follow-
ing a cos 2 Θ function with respect to the angle Θ. Fig. 5-5b
shows that the line width of the hyperfine lines is independent
of the orientation angle $\emptyset$ at 25°C & $\Theta = 0°$.

From Figs. 5-2c, 5-3c & 5-4c, it is clear that the
intensity of any line of the hyperfine lines is dependent

upon the orientation angle θ. At $140^\circ C$, it changes according to a cos 2θ relation with a maximum value at $\theta = 0^\circ$, 90° & 180°. At $25^\circ C$, the intensity has a minimum at $\theta = 0^\circ$ and decreases to zero intensity for $\theta > 12^\circ$. At $-40^\circ C$, the intensity changes according to a cos 2θ relation with minimum value at $\theta = 0^\circ$, 90° & 180°. Fig. 5-5c, show the variation of the intensity of any line of the hyperfine structure lines with respect to the rotation angle $\emptyset$ at $25^\circ C$ and $\theta = 0^\circ$. It is seen from Fig. 5-5c that the intensity is maximum at $\emptyset = 0^\circ \pm 5^\circ$ and $\emptyset = 180^\circ \pm 5^\circ$ and is minimum at $(\emptyset = 0^\circ \pm 5^\circ$ & $\emptyset = 180^\circ \pm 5^\circ$ and is minimum at$)$ $\emptyset = 90^\circ$, 270°.

c- The inner resonance lines

On the basis of the hypothesis that the six-line spectrum is the hyperfine spectrum of Mn^{2+} ion, the resonance lines appearing between these hyperfine structure lines, Fig. 5-1, cannot be hyperfine lines too.
H. Ikushima in 1965[4] identified these inner resonance lines as due to the forbidden transitions of Mn^{2+} ions in $BaTiO_3$ single crystals for which Δm_1 (of the nucleus) $= \pm 1$ & ± 2. He observed these forbidden doublets only in the central electronic transition $M_s = +\frac{1}{2} \leftrightarrow M_s = -\frac{1}{2}$ when the crystal was in the tetragonal phase. Folen[5], Shneider and Sircar[6],

Walder[7], and Odehnal[8] have considered the forbidden
doublet splittings in the central electronic transition.
Bleaney and Rubins[9] concluded from a formula they gave
that the five doublets at the central transition should
have the relative intensity ratios 5: 8 : 9 : 8 : 5 to
each other.

Tables 5-2 & 5-3 shows a comparison between the experimental
doublet splittings and intensities with those obtained
experimentally by H. Ikushima[4] and the theoretical calcul-
ations of Bleaney[9] and Odehnal[8].

Table 5-2

The splittings of the forbidden doublets of the types
$\Delta M_s = \pm 1$ and $\Delta m_I = \pm 1$

m_1	$- 5/2$	$- 3/2$	$- \frac{1}{2}$	$+ \frac{1}{2}$	$+ 3/2$
H (in gauss) Theor.[4]	17.5	19.3	21.1	22.9	24.7
H Exp. by Ikushima[4]	15.5	18.2	20.5	22.8	26
H This Exp.	15.0	18.0	21.0	22.0	25.0

Table 5-3

Relative intensity of the five starred forbidden doublets

$$\left(\Delta M_s = \pm 1, \Delta m_1 = \pm 1 \right)^{*}$$

m_1	-5/2	-3/2	-1/2	+1/2	+3/2
Theor.[4]	5	8	9	8	5
Exp. by Ikushima[4] ($\theta = +5^o$)	5	7	9	8	6
This Exp. ($\theta = +5^o$)	5	8	9	7	6

* The five unstarred doublets have different intensities,
  but the same intensity ratio.

The parameters of the inner forbidden lines are measured
at 25^oC only, since in the cubic and orthorhombic phases they are
negligibly weak in intensity compared with the allowed ones.
From Fig. 5-2a, it is seen that the magnetic field resonance
value for any of the forbidden lines has a minimum value at
$\theta = 0^o$ and then increases with increasing θ up to $\theta = 12^o$,
above 12° the forbidden lines intensity goes to zero and the
lines disappear.
From Fig. 5-2b, it is clear that the line width of the inner
transition lines increased from a minimum value of 3 gauss at
$\theta = 0^o$ to 6 gauss at $\theta = 12^o$.
From Fig. 5-2c, it is seen that the intensity of the inner
transition lines increase from a minimum value at $\theta = 0^o$ to a

maximum value around $\theta = 6 - 10^{\circ}$ and then decreases again to reach zero intensity for $\theta > 12^{\circ}$.

Fig. 5-5c, shows the variation of the intensity of any line of the inner transition lines with respect to the rotation angle $\emptyset$ at $25^{\circ}C$ and $\theta = 0^{\circ}$. It is seen from Fig. 5-5c, that the intensity is maximum at $\emptyset = 0 \pm 5^{\circ}$ & $\emptyset = 180 \pm 5^{\circ}$, and is minimum at $\emptyset = 90^{\circ}$ & 270°.

d- The single line

Single crystals of pure $BaTiO_3$ do not exhibit any EPR spectra. The EPR spectrum appears only when a crystal contains paramagnetic ions either doped in it or present as an impurity. Since the six line spectrum has been attributed to Mn^{2+} ion, then the single line appearing at $H = 3.410$ K.Gauss for H parallel to the c-axis and having an intensity of approximately four times the intensity of one of the components of the hyperfine structure spectrum, must belong to some other impurity in the $BaTiO_3$ crystal. This single line has a g-value of 2.000 when H is parallel to the c-axis of the crystal at room temperature.

Figs. 5-2a, 5-3a & 5-4a shows the behaviour of the magnetic field resonance value H of the single line, as a function of the orientation angle θ (rotation about the a-axis of the crystal), at the temperatures $140^{\circ}C$, $25^{\circ}C$ & $-40^{\circ}C$.

At 140°C, it is seen that H of the single line is independent of orientation.

At 25°C, H has a minimum value at $\theta = 0°$ and then increases with increasing θ up to $\theta = \pm 12°$, above 12° the absorption line disappears.

At -40°C, H follows a cos 2θ relation with minimum value at $\theta = 0°$, 90° & 180°.

Fig. 5-5a, shows the orientation dependance (for $\emptyset$ - rotation about the c-axis of the crystal), of the magnetic field value H of the single line at 25°C and $\theta = 0°$. It is seen from Fig. 5-5a, that H follows a sin $\emptyset$ relation with respect to the rotation angle $\emptyset$ at 25°C & $\theta = 0°$.

From Figs. 5-2b, 5-3b & 5-4b, it is clear that the line width of the single line follows a cos 2θ relation at 140°C, with a minimum value of 13 gauss at $\theta = 0°$, 90° & 180°, and a maximum value of 34 gauss at $\theta = 45°$ & 135°. At 25°C the single line has a line width of 11 gauss at $\theta = 0°$, and then increases with increasing θ up to 46 gauss at $\theta = 10°$, and then disappears for $\theta > 12°$. At -40°C the line width follows a cos 2θ relation with a maximum of 90 gauss at $\theta = 0°$, 90° & 180°, and a minimum value of 41 gauss at $\theta = 45°$ & 135°. Fig. 5-5b shows that the line width of the single line follows a sin $\emptyset$ relation with respect to the rotation angle $\emptyset$ at 25°C and $\theta = 0°$.

Figs. 5-2c, 5-3c & 5-4c show that the intensity of
this line follows a cos 2θ relation versus θ at 140°C with
a maximum value at $\theta = 0^{\circ}$, 90° & 180°. At 25°C the intensity
has a maximum value at $\theta = 0^{\circ}$, and then decreases with
increasing θ to reach zero intensity for $\theta > 12^{\circ}$. At -40°C,
the intensity follows a cos 2θ relation with a minimum value
at $\theta = 0^{\circ}$, 90° & 180°. Fig. 5-5c, show the variation of the
intensity of the single line with respect to the rotation
angle $\emptyset$ at 25°C and $\theta = 0^{\circ}$. It is seen from Fig. 5-5c that
the intensity is maximum at $\emptyset = 0^{\circ}$ & 180° and is minimum at
$\emptyset = 90^{\circ}$, & 270°, and that around $\emptyset = 0 \pm 5^{\circ}$ and $180^{\circ} \pm 5^{\circ}$ there
are two other minima, and around $\emptyset = 0 \pm 10^{\circ}$ and $180^{\circ} \pm 10^{\circ}$
there are two other maxima.

e- Effect of x-ray irradiation

EPR measurements of the x-ray irradiated crystal revealed
a decrease in the intensity of the single line, ~~attributed to~~
~~Fe^{3+}~~, to about 20% of its original intensity. The Mn^{2+} hyper-
fine lines and forbidden doublets decreased in intensity to
about 80% of their original value.

f- Effect of thermal annealing

After thermal annealing of the crystal at a temperature
of 300°C, the EPR spectra of the crystal observed prior to
irradiation was found.

II- Discussion

A discussion of the above results reveals the following:

1) Since the hyperfine spectrum is independent of the rotation θ about the a-axis at a temp. of $140^{\circ}C$, it is assumed that the Mn^{2+} ion occupies a site of cubic symmetry. And since at $140^{\circ}C$ the $BaTiO_3$ crystal is in the cubic phase with Ba^{2+} and Ti^{4+} ions occupying sites of cubic symmetry, it is expected that the Mn^{2+} would exhibit an orientation independence in their site.

2) The hyperfine spectrum disappears at $25^{\circ}C$ for $\theta > 12^{\circ}$, and it goes to higher fields on changing θ from $\theta = 0^{\circ}$ by positive or negative values, indicating that we are at the low field extremal, and that at $\theta = 0^{\circ}$ we are around one of the magnetic axes of the crystal, and when $\theta > 12^{\circ}$ we are off that magnetic axis[3].

3) At $25^{\circ}C$, the crystal is in the tetragonal phase, with the Ba^{2+} ion in a cubic site, while Ti^{4+} is in a cubic site with tetragonal distortion.

Thus it is expected that if Mn^{2+} ion were in the Ba site no orientation dependence of the spectrum would be observed. Since orientation dependence is observed for θ-rotation (see Fig. 5-2a); it is suggested that the Mn^{2+} ions occupy the Ti^{4+} sites.

It should be noted that the ionic radius of the Ti
site is 0.602 Å while the ionic radius of Mn^{2+} is 0.8 Å.
Hence in addition to the tetragonal distortion of the Ti
site, when the crystal is in the ferroelectric phase, there
will be additional distortion due to the excess radius of
Mn^{2+}.

4) At $-40^{\circ}C$, the crystal is in the orthorhombic phase, and
the Ti^{4+} site will have C_2 symmetry, (the spectrum of Mn^{2+}
exhibits just this orientation dependence).

5) The c-axis of the crystal is a symmetry axis of the Ti^{4+}
site at $25^{\circ}C$, hence the H value of the spectrum is independent
of the rotation angle $\emptyset$ around the c-axis.

6) The variation of intensity of any line of the hyperfine
structure with respect to $\emptyset$-rotation in the way shown in
Fig.5-5c, is attributed to the change of phase of the absorp-
tion lines according to the following steps:

    i- around $\emptyset = 0$ and within $\pm 5^{\circ}$ the phase of the absorpt-
       ion lines is in its normal case.

    ii- from $\emptyset = 5^{\circ}$ to $\emptyset = 20^{\circ}$ there is gradual phase inversion
       taking place.

    iii- from $\emptyset = 20^{\circ}$ to 160° the absorption lines have fixed
       inverted phase.

    iv- from $\emptyset = 160^{\circ}$ to 175° gradual phase inversion takes
       place again.

v- around $\emptyset = 180^\circ$ within $\pm 5^\circ$ the phase returns back
to its normal case.

This behaviour of the change of phase of the absorption
lines is attributed to the change in spectrometer cavity-
impedance when the direction of the polarization axis of the
crystal changes with respect to the direction of the electric
component of the R.F field in the cavity.

7) One possible reason for the absence of the $M_s = \pm \frac{1}{2} \leftrightarrow$
$M_s = \pm 3/2$ and the $M_s = \pm 3/2 \leftrightarrow M_s = \pm 5/2$ transitions is
that the D and E terms in the Hamiltonian equation (2-45),
have a distribution of values. Such a distribution would not
affect the $M_s = + \frac{1}{2} \leftrightarrow M_s = \leftrightarrow \frac{1}{2}$ transition to first order but
could cause the $M_s = \pm \frac{1}{2} \leftrightarrow M_s = \pm 3/2$ and the $M_s = \pm 3/2 \leftrightarrow$
$M_s = \pm 5/2$ transitions to become so broad that they would not
be detectable.

8) The g-value of the single line is very close to the free
spin value, a property of the ions of the d^5 system. Inspect-
ion of the g-values of the ions of the d system, tabulated
in table 5-4 below, shows that:

Table 5-4

Ion	Isotope	Natural abundance %	Nuclear spin	g-values
Ti^{3+}	^{47}Ti	7.75	5/2	1.1 - 1.98
V^{2+}	^{51}V	99.76	7/2	1.98
Cr^{3+}	^{53}Cr	9.55	3/2	1.98
Mn^{2+}	^{55}Mn	100	5/2	2.0
Fe^{3+}	^{57}Fe	2.17	1/2	2.0
Ce^{2+}	^{53}Co	100	7/2	4.3
Ni^{2+}	^{61}Ni	1.25	3/2	2.2
Cu^{2+}	^{63}Cu	69.09	3/2	2.0 - 2.3
	^{65}Cu	30.91	3/2	2.0 - 2.3

All these d-system ions will be disregarded for having a
g-value either less or bigger than that of the single line
except Mn^{2+}, Fe^{3+} and Cu^{2+}, which have g-values approximately
equal to 2.0. Mn^{2+} will also be disregarded since it has been
discussed before and was seen to give six line spectrum. ^{63}Cu
has natural abundance of 69.09% and nuclear spin of 3/2, which
means that the fine structure of Cu^{2+} will be split to four
hyperfine components each of intensity 17% of the central
line. Since the spectrum we have is only of a single line
and not a central line flanked by four components two on
each side, Cu^{2+} ion must also be disregarded. The only ion
which would have a spectral transition similar to the one
observed is Fe^{3+} and in this case the observed line is due
to the $M_s = + \frac{1}{2} \leftrightarrow M_s = - \frac{1}{2}$ transition. ^{57}Fe has natural

abundance of 2.17 % and $I = \frac{1}{2}$, which means that the spectrum of Fe^{3+} will consist of a central line flanked by two hyperfine components one on each side of intensity $\approx 1\%$ of the central line. Because of the relative low intensity compared to the unsplit line and the width of this line they would not be detected. It is to be noted that in the above discussion we considered only the middle transition $(M_s = + \frac{1}{2} \leftrightarrow M_s = - \frac{1}{2})$ on the basis of the same argument given for the six-line spectrum in item 7 above.

9) Since the single line spectrum is independent of the orientation angle Θ at $140^\circ C$, it is assumed that the Fe^{3+} impurity ion occupies a site of cubic symmetry. And since at $140^\circ C$ the $BaTiO_3$ crystal is in the cubic phase with Ba^{2+} and Ti^{4+} ions occupying sites of cubic symmetry. An orientation independence in either site is expected. It is suggested that Fe^{3+} will prefer the Ti^{4+} site by virtue of their ionic radii, that of $Fe^{3+} = 0.64$ Å and of Ti^{4+} site $= 0.602$ Å.

10) At $25^\circ C$, the crystal is in the tetragonal phase with the Ba^{2+} ion in a cubic site, while Ti^{4+} is in a cubic site with tetragonal distortion. Since orientation dependence of the single line for Θ-rotation at $25^\circ C$ is clear, then the assumption of Fe^{3+} occupying the Ti^{4+} site is supported.

11) At $-40^\circ C$, the crystal is in the orthorhombic phase, and the Ti^{4+} site will have C_2 symmetry. The spectrum of the single

line exhibits just this orientation dependance at $-40°C$ for the Θ-rotation.

12) The decrease in intensity after x-ray irradiation is explained as a conversion of the Fe^{3+} to Fe^{2+} by capturing an electron excited by the x-ray photons. Similar effects have been observed in other oxide crystals when Fe^{3+} is present as an impurity. The decrease in the intensity of the Mn^{2+} spectrum is explained by a similar process. These two processes may be represented thusly:

$$BaTiO_3 + \text{x-rays} \rightarrow 2e + (BaTiO_3)^{2+}$$

$$Fe^{3+} + e \longrightarrow Fe^{2+}$$

$$Mn^{2+} + e \longrightarrow Mn^{1+}$$
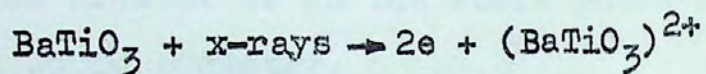
and upon heating the reaction is reversed.

Another possible reaction is:

$$Mn^{2+} + \text{x-ray} \longrightarrow Mn^{3+} + e$$

and hence,

$$Fe^{3+} + e \longrightarrow Fe^{2+}$$
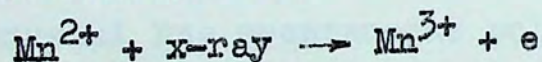
However, the relative change in the intensity of the Fe^{3+} spectrum and the Mn^{2+} spectrum are not in agreement with this reaction.

III- Summary

1- EPR spectra of $BaTiO_3$ single crystal doped with Mn^{2+} ion have the following components:

a- Mn^{2+} Hyperfine structure of the $M_S = +\frac{1}{2} \leftrightarrow M_S = -\frac{1}{2}$ transition.

b- Mn^{2+} forbidden transition for $\Delta M_S = \pm 1, \Delta m_I = \pm 1$.

c- Single line spectrum attributed to Fe^{3+} impurity.

2- It is suggested that both the Mn^{2+} and Fe^{3+} ions occupy Ti^{4+} sites on the basis of:-

a- At $140^{\circ}C$ the crystal is in the cubic phase and the Ti^{4+} site has a cubic symmetry.

b- At $25^{\circ}C$ the crystal is in the tetragonal phase and the Ti^{4+} site has a cubic symmetry with tetragonal distortion.

c- At $-40^{\circ}C$ the crystal is in the orthorhombic phase and the Ti^{4+} site exhibits a C_2 symmetry.

d- The $BaTiO_3$ crystal has spontaneous polarization along the a-axis of the crystal at $25^{\circ}C$, and its c-axis coincides with one of the magnetic axes of the crystal at that temperature.

3- Hence both Fe and Mn impurities are ordered with respect to the two sites which they might occupy.

4- The relative intensities of the Fe^{3+} line and the Mn^{2+} spectrum are approximately the same. Hence it can be assumed that Mn^{2+} and Fe^{3+} ions have approximately the same concentrations in the crystal.

B- Mg_2SiO_4 synthetic crystal

I- Results

a- The orientation dependence of the EPR spectrum of the Mg_2SiO_4 single crystal at $25°C$ in the ab plane was obtained. The rotation about the c-axis was from an angle $\theta = 0$ (when the b-axis is parallel to the magnetic field) to $\theta = 90°$ (when the a-axis is parallel to the magnetic field) and then to $\theta = 180°$.

Fig. 5-6 shows the spectrum for the above rotation about the c-axis when $\theta = 0°$. It is seen from Fig. 5-6 that the spectra comprise five absorption lines with unequal intersities and unequal splitting between any two of them, and different line widths, having the g-values 6.2, 4.65, 4.29, 1.81 & 1.005 respectively. As θ is changed from $0°$ by any small amount $\geqslant \pm 0.5°$ the five absorption lines split to ten absorption lines, Fig. 5-7. As θ is varied from $\theta \geqslant 0.5$ to $180°$ these ten lines move apart and at the same time their intensity varies. Fig. 5-8 shows the variation of the magnetic field value at which each one of these absorption lines occur as a function of the θ angle rotated from the b-axis at $25°C$. It is seen from Fig. 5-8 that the magnetic field value for any line is the same at the angle θ and $(180° - \theta)$. It is also seen that minimum
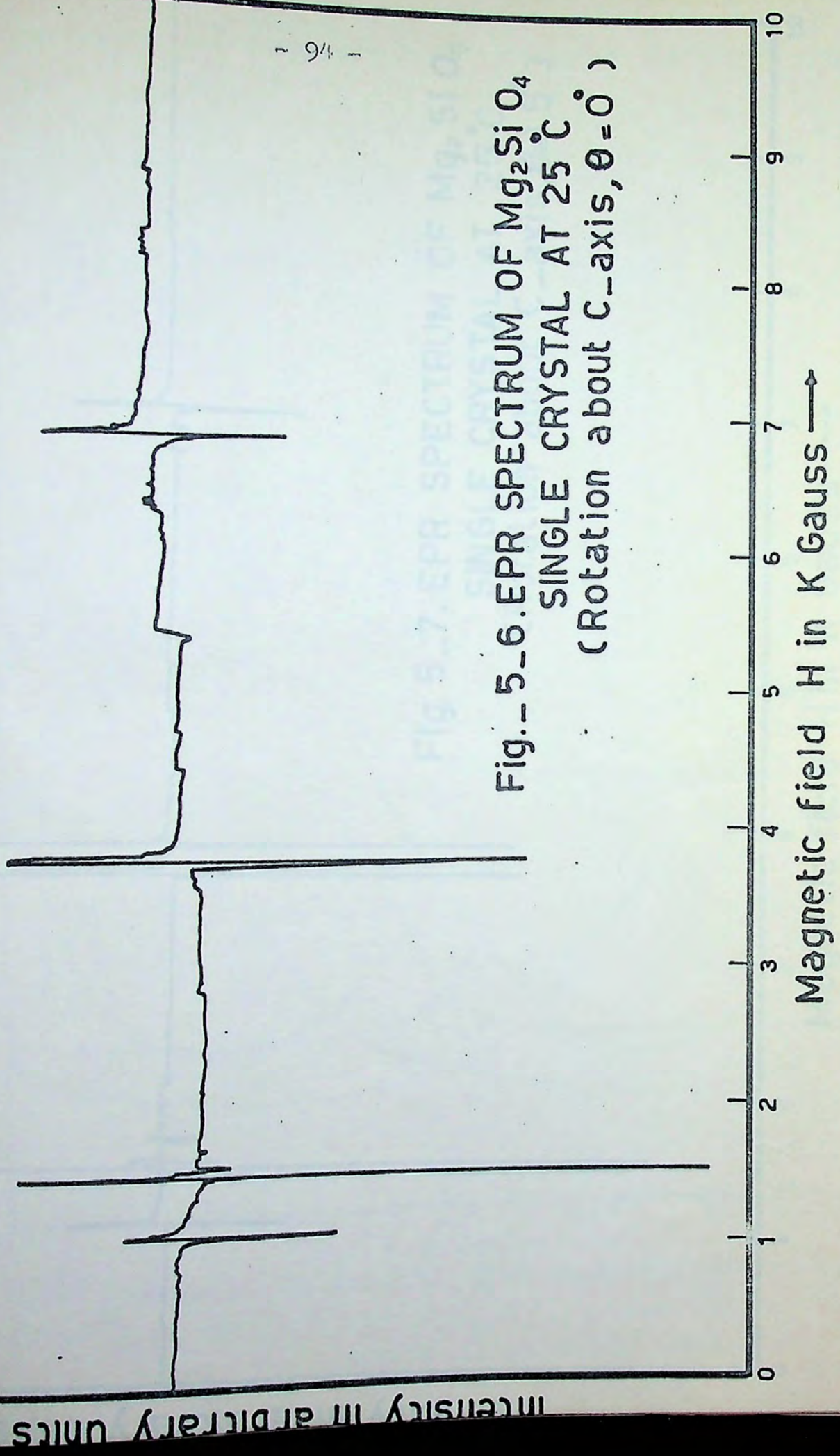
Fig._5_6.EPR SPECTRUM OF Mg₂SiO₄
SINGLE CRYSTAL AT 25 °C
(Rotation about C_axis, θ=0°)

Magnetic field H in K Gauss →

Intensity in arbitrary units

Fig. 5_7. EPR SPECTRUM OF Mg$_2$SiO$_4$
SINGLE CRYSTAL AT 25°C
(Rotation about C_axis, θ=1.5°)

Magnetic field H in K Gauss ⟶
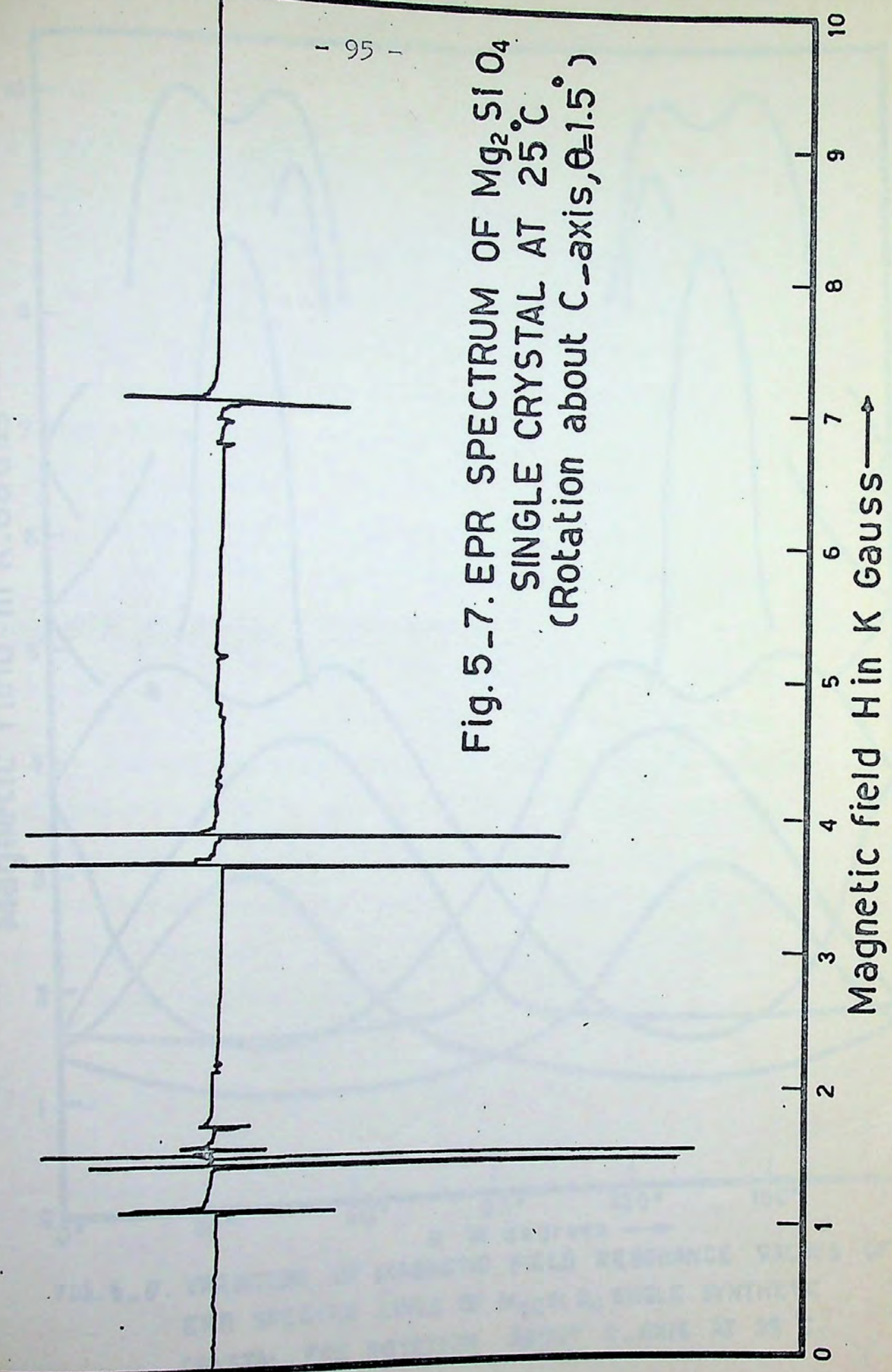
Intensity in arbitrary units

FIG. 5_8. VARIATION OF MAGNETIC FIELD RESONANCE VALUES OF
EPR SPECTRA LINES OF Mg₂SiO₄ SINGLE SYNTHETIC
CRYSTAL, FOR ROTATION ABOUT C_AXIS AT 25 °C.

splitting between the lines is observed at $\theta = 0^\circ$ and 180° i.e. when the b-axis is parallel to the magnetic field. It is to be noted that the position of maximum splitting between the lines is within the range of $\theta = 45 \pm 5^\circ$, Fig. 5-9. It is to be noted also that when the intensity of any of the absorption lines goes to zero this is represented, in Fig. 5-8, by a break in the graph representing the change of its magnetic field value vs θ. And so at some angles, only five or six absorption lines may appear and the others have zero intensity. It is seen in Fig. 5-9 that a spectrum of Mn^{2+} ion, of about 5% of the considered absorption lines, appear in between the lines of the spectra.

b- The second experiment done for the Mg_2SiO_4 single crystal is EPR measurements at $25^\circ C$, while rotating the crystal in the ac plane around its b-axis from an angle $\theta = 0$ (when the a-axis is parallel to the magnetic field) to $\theta = 90^\circ$ (when the c-axis is parallel to the magnetic field) and then to θ 180°.

Fig. 5-10 shows the spectrum for this rotation about the b-axis when θ 90°. It is seen from Fig. 5-10 that the spectra comprise:-
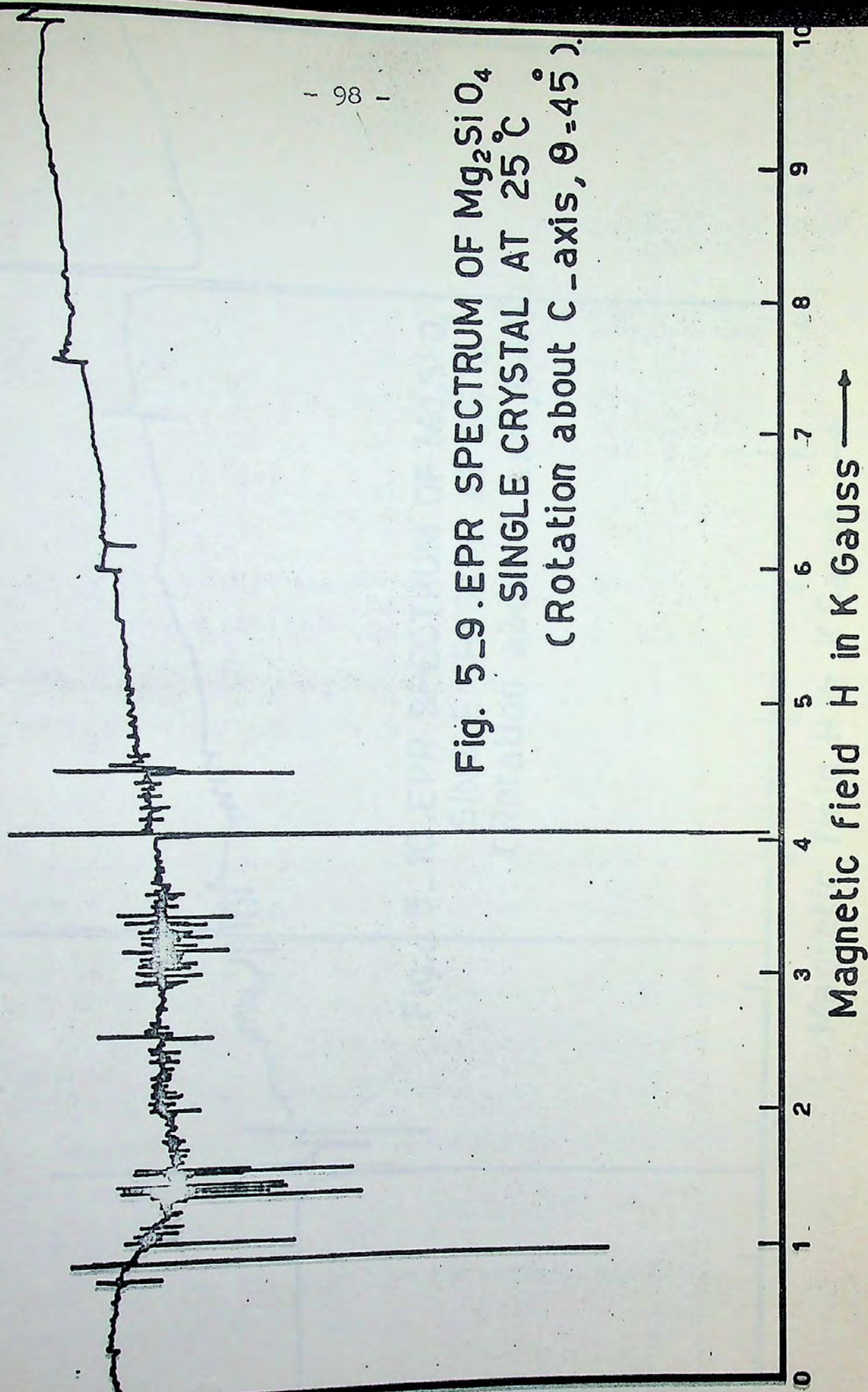
Fig. 5_9. EPR SPECTRUM OF Mg_2SiO_4 SINGLE CRYSTAL AT 25°C (Rotation about C_axis, θ =45°).

Magnetic field H in K Gauss ⟶

Intensity in arbitrary units ,
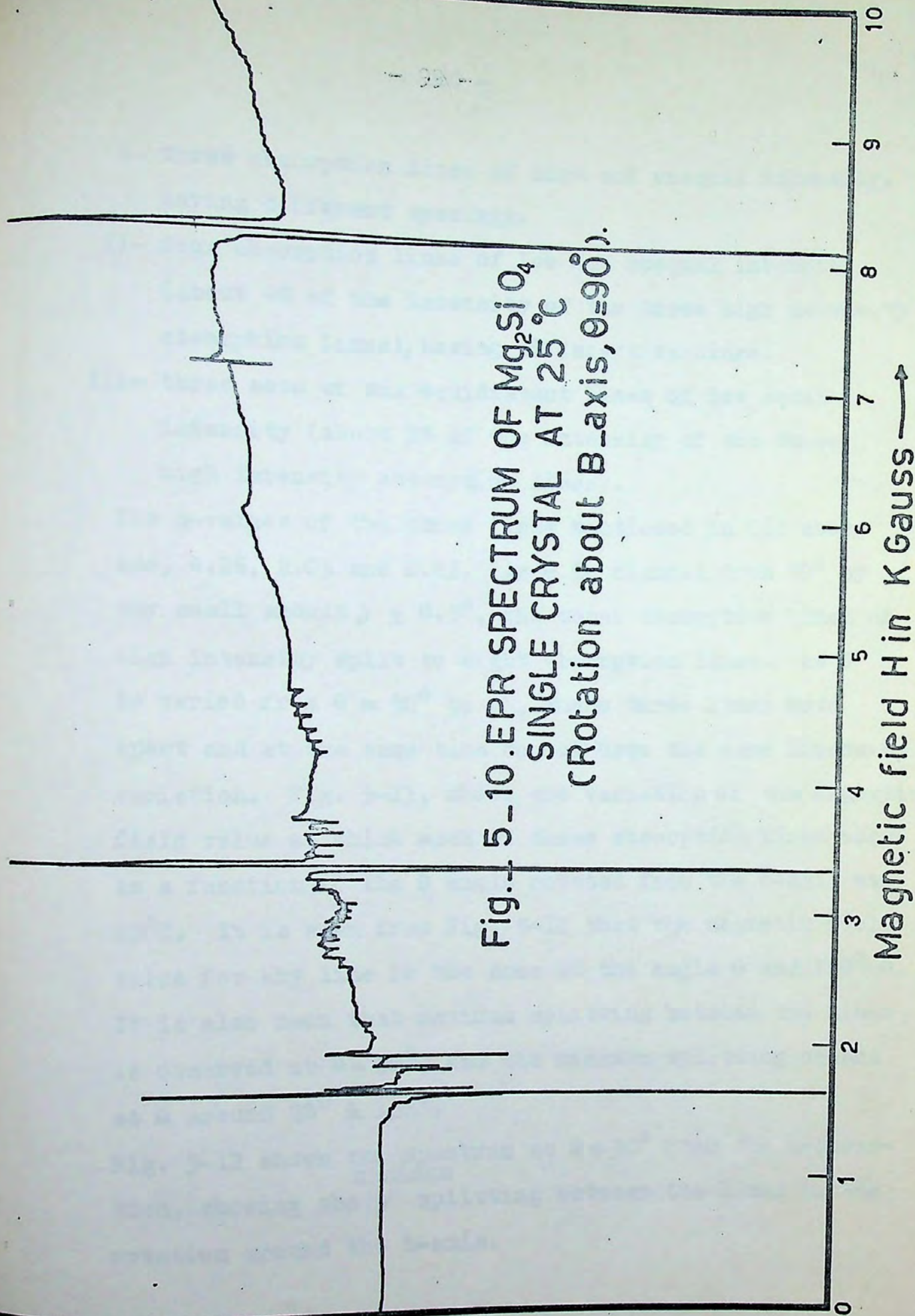
Fig._ 5_10. EPR SPECTRUM OF Mg₂Si O₄
SINGLE CRYSTAL AT 25°C
(Rotation about B_axis, θ=90°).

Magnetic field H in K Gauss ⟶

intensity in arbitrary units

i- three absorption lines of high and unequal intensity,
   having different spacings.

ii- four absorption lines of low and unequal intensity
   (about 6% of the intensity of the three high intensity
   absorption lines), having different spacings.

iii- three sets of six equidistant lines of low equal
   intensity (about 3% of the intensity of the three
   high intensity absorption lines).

The g-values of the three lines mentioned in (i) above
are, 4.26, 2.05 and 0.82. As Θ is changed from 90° by
any small amount $\geqslant \pm 0.5^{\circ}$, the three absorption lines of
high intensity split to eight absorption lines. As Θ
is varied from $\Theta = 90^{\circ}$ to 0°, these three lines move
apart and at the same time do not have the same intensity
variation. Fig. 5-11, shows the variation of the magnetic
field value at which each of these absorption lines occur
as a function of the Θ angle rotated from the c-axis at
25°C. It is seen from Fig. 5-11 that the magnetic field
value for any line is the same at the angle Θ and $180^{\circ} - \Theta$.
It is also seen that maximum splitting between the lines
is observed at $\Theta = 90^{\circ}$, and the minimum splitting occurs
at Θ around 28° & 152°.

Fig. 5-12 shows the spectrum at $\Theta = 30^{\circ}$ from the a-direc-
tion, showing the / minimum splitting between the lines in the
rotation around the b-axis.

FIG. 5-11. VARIATION OF MAGNETIC FIELD VALUE OF THE LINES OF
THE EPR SPECTRUM OF Mg_2SiO_4 SYNTHETIC SINGLE
CRYSTAL FOR ROTATION ABOUT B-AXIS AT 25 °C.

Fig.5_12. EPR SPECTRUM OF $Mg_2 Si O_4$ SINGLE CRYSTAL AT 25℃ (Rotation about B_axis, $\theta = 30°$)

Magnetic field H in K Gauss →
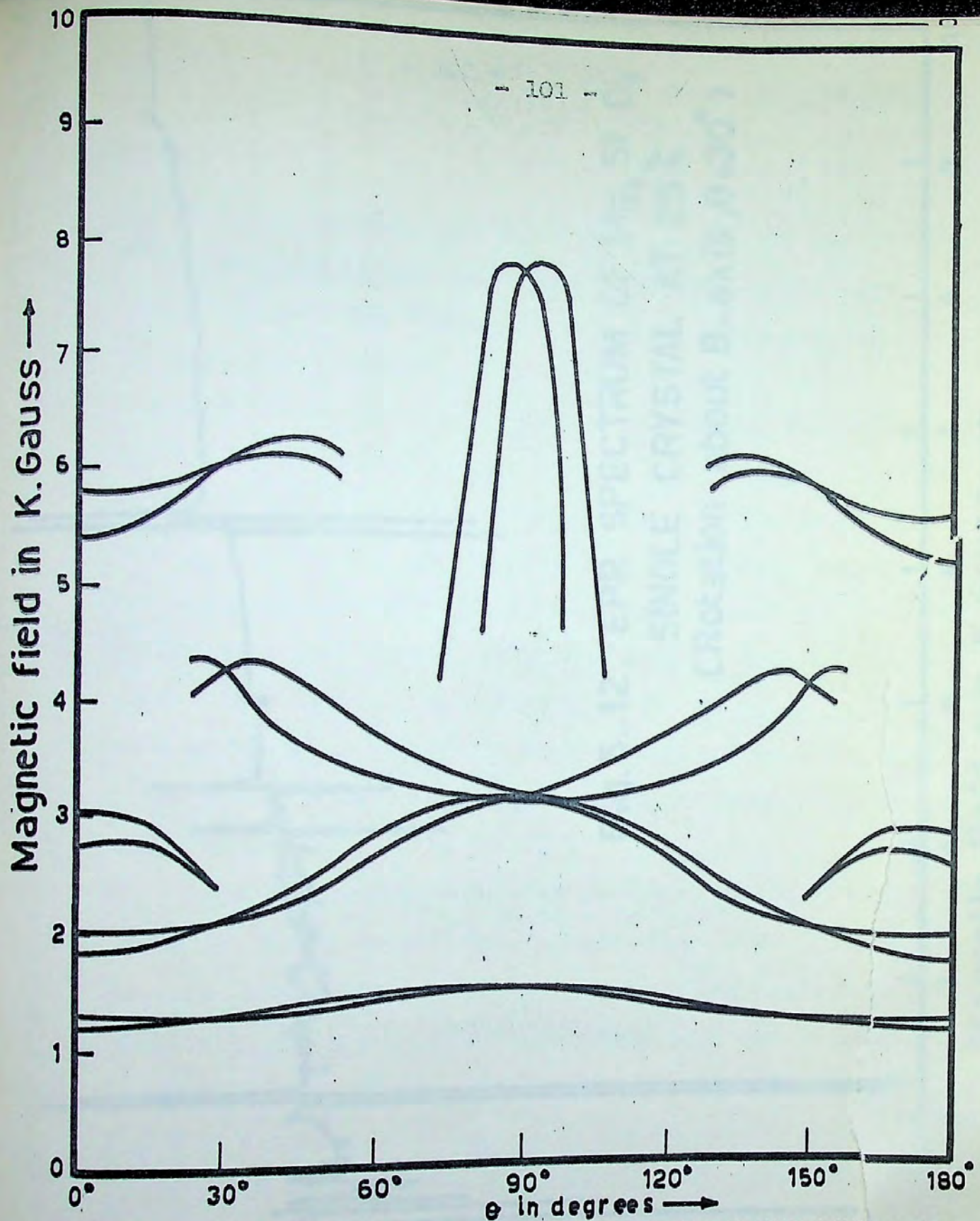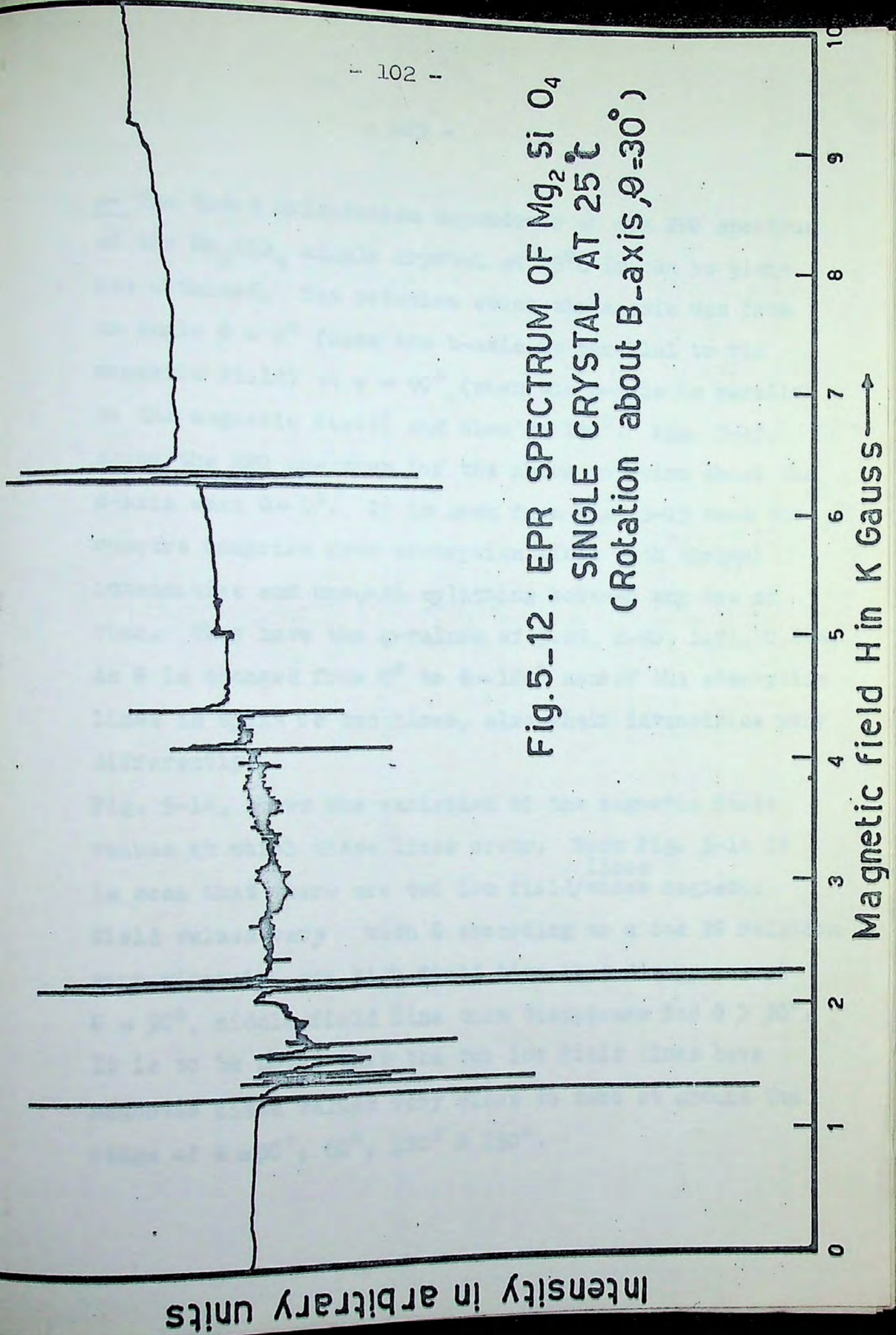
Intensity in arbitrary units

c- The third orientation dependence of the EPR spectrum of the Mg_2SiO_4 single crystal at 25^oC in the bc plane was obtained. The rotation about the a-axis was from an angle $\Theta = 0^o$ (when the b-axis is parallel to the magnetic field) to $\Theta = 90^o$ (when the c-axis is parallel to the magnetic field) and then to 180°. Fig. 5-13, shows the EPR spectrum for the above rotation about the a-axis when $\Theta = 0^o$. It is seen from Fig. 5-13 that the spectra comprise four absorption lines with unequal intensities and unequal splitting between any two of them. They have the g-values of 3.89, 2.00, 1.31, 0.694. As Θ is changed from 0° to $\Theta = 180^o$ none of the absorption lines is split to two lines, also their intensities vary differently.

Fig. 5-14, shows the variation of the magnetic field values at which these lines occur. From Fig. 5-14 it is seen that there are two low field/whose magnetic field values vary with Θ according to a cos 2Θ relation approximately, one high field line that disappears at $\Theta = 90^o$, middle field line that disappears for $\Theta > 50^o$. It is to be noted that the two low field lines have magnetic field values very close to zero at around the range of $\Theta = 30^o$, 60°, 120° & 150°.

Fig. 5_13. EPR SPECTRUM OF Mg_2SiO_4 SINGLE CRYSTAL AT 25°C (Rotation about A_axis, $\theta = 0°$)

Magnetic field H in K Gauss →

Intensity in arbitrary units
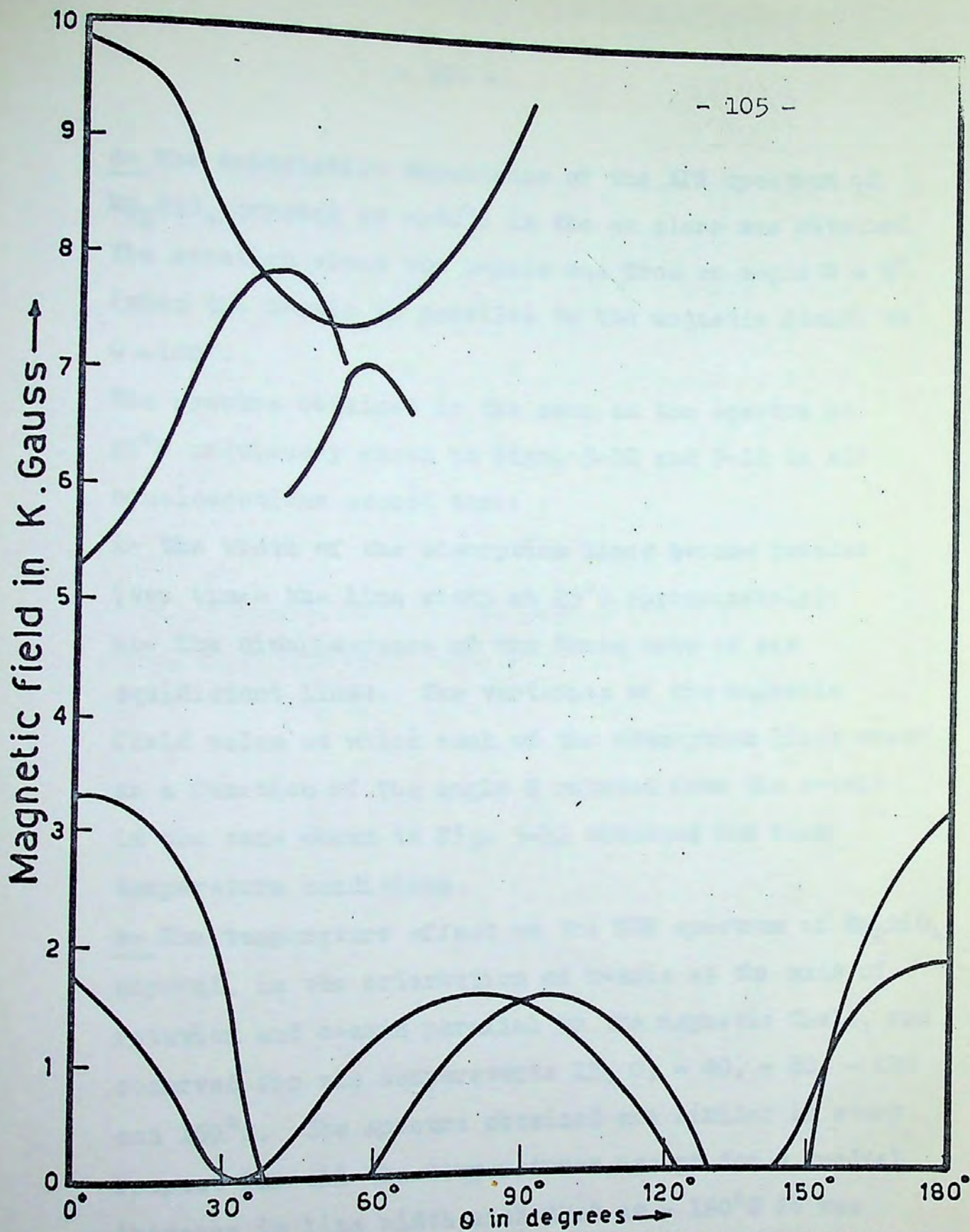
FIG. 5-14. VARIATION OF MAGNETIC FIELD RESONANCE VALUE OF EPR SPECTRA LINES OF Mg_2SiO_4 SINGLE SYNTHETIC CRYSTAL FOR ROTATION ABOUT A-AXIS AT 25 °C.
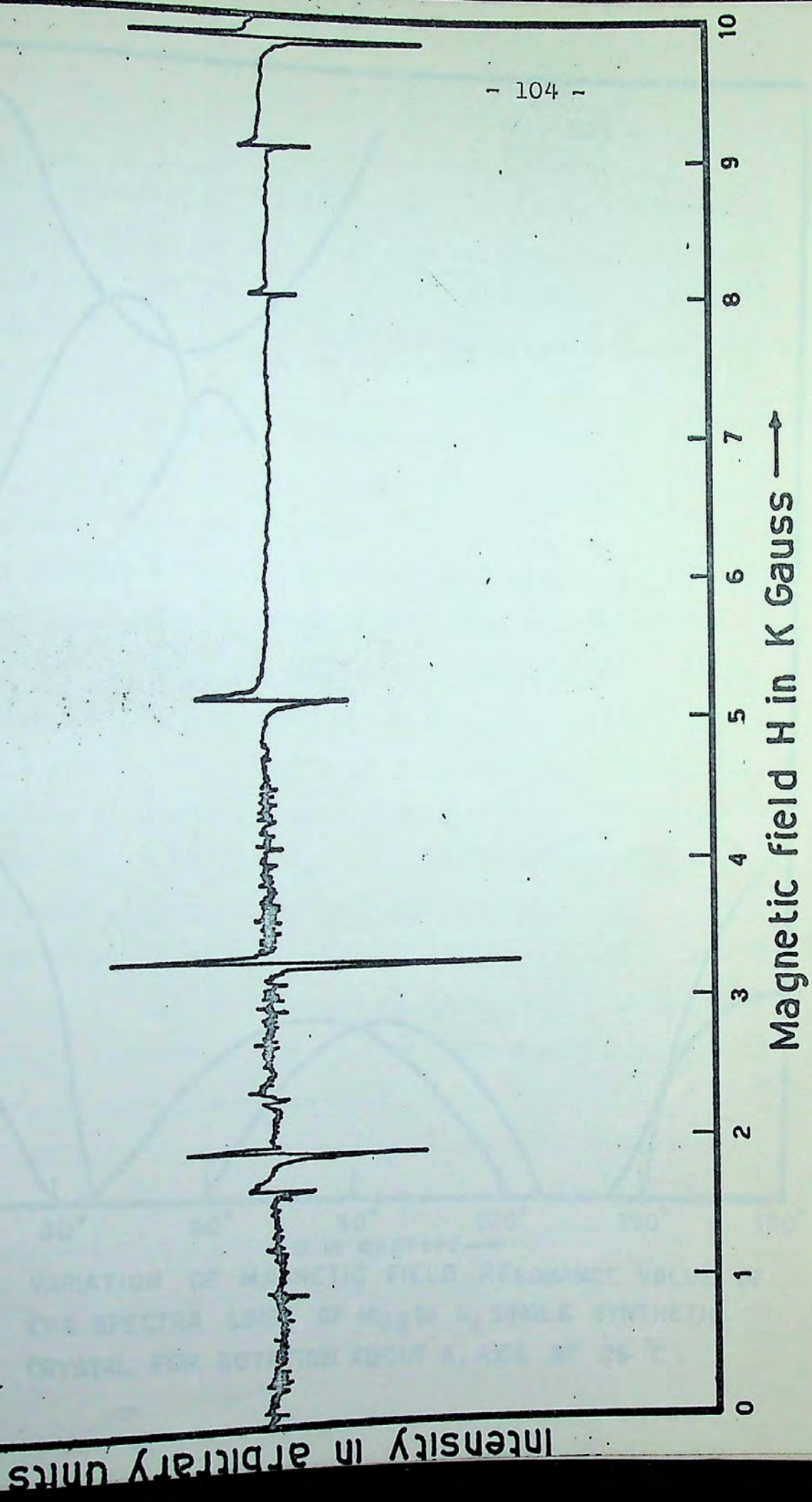
d- The orientation dependence of the EPR spectrum of Mg_2SiO_4 crystal at $-160^{\circ}C$ in the ac plane was obtained. The rotation about the b-axis was from an angle $\Theta = 0^{\circ}$ (when the c-axis is parallel to the magnetic field) to $\Theta = 180^{\circ}$.

The spectra obtained is the same as the spectra at $25^{\circ}C$ previously shown in Figs. 5-10 and 5-12 in all considerations except that:

i- the width of the absorption lines became broader (two times the line width at $25^{\circ}C$ approximately).

ii- The disappearance of the three sets of six equidistant lines. The variation of the magnetic field value at which each of the absorption lines occur as a function of the angle Θ rotated from the c-axis is the same shown in Fig. 5-11 obtained for room temperature conditions.

e- The temperature effect on the EPR spectrum of Mg_2SiO_4 crystal, in the orientation of b-axis as the axis of rotation and c-axis parallel to the magnetic field, was observed for the temperatures 25, 0, - 40, - 80, - 120 and $160^{\circ}C$. The spectra obtained are similar in every respect for all the temperatures except for a gradual increase in line width such that at $- 160^{\circ}C$ it was double the value of the line widths at $25^{\circ}C$.

f- EPR measurements of the powdered synthetic crystal were made. At room temperature one broad signal was obtained, shown in Fig. 5-15, having a g-value of 2.83, and a line width of 160 gauss. EPR spectra obtained for the powder at lower temperatures 0, -80° and $-160^\circ C$ are shown in Fig. 5-15. It is seen from Fig. 5-15, that the temperature variation does not affect the EPR spectrum of the powdered synthetic crystal.

g- EPR spectrum of the Mg_2SiO_4 crystal, with the crystal b-axis perpendicular to the magnetic field and the c-axis parallel to the magnetic field, obtained after irradiating the crystal by x-rays for 60 minutes, showed no absorption lines except one small peak at $g = 2.07$ (observed at a signal level of 4000).

The EPR spectrum of the x-irradiated crystal after subsequent annealing at $300^\circ C$ recovered its original features of the spectrum before x-ray irradiation. Heating to higher temperatures $400^\circ C$ & $500^\circ C$ revealed decreased intensity of the absorption lines and introduced distortion in the shape of the absorption lines.

Fig. 5_15. EPR SPECTRUM OF POWDERED Mg₂Si O₄ SYNTHETIC FORSTERITE, AT DIFFERENT TEMPERATURES.

Intensity in arbitrary units

Magnetic field H in K Gauss →
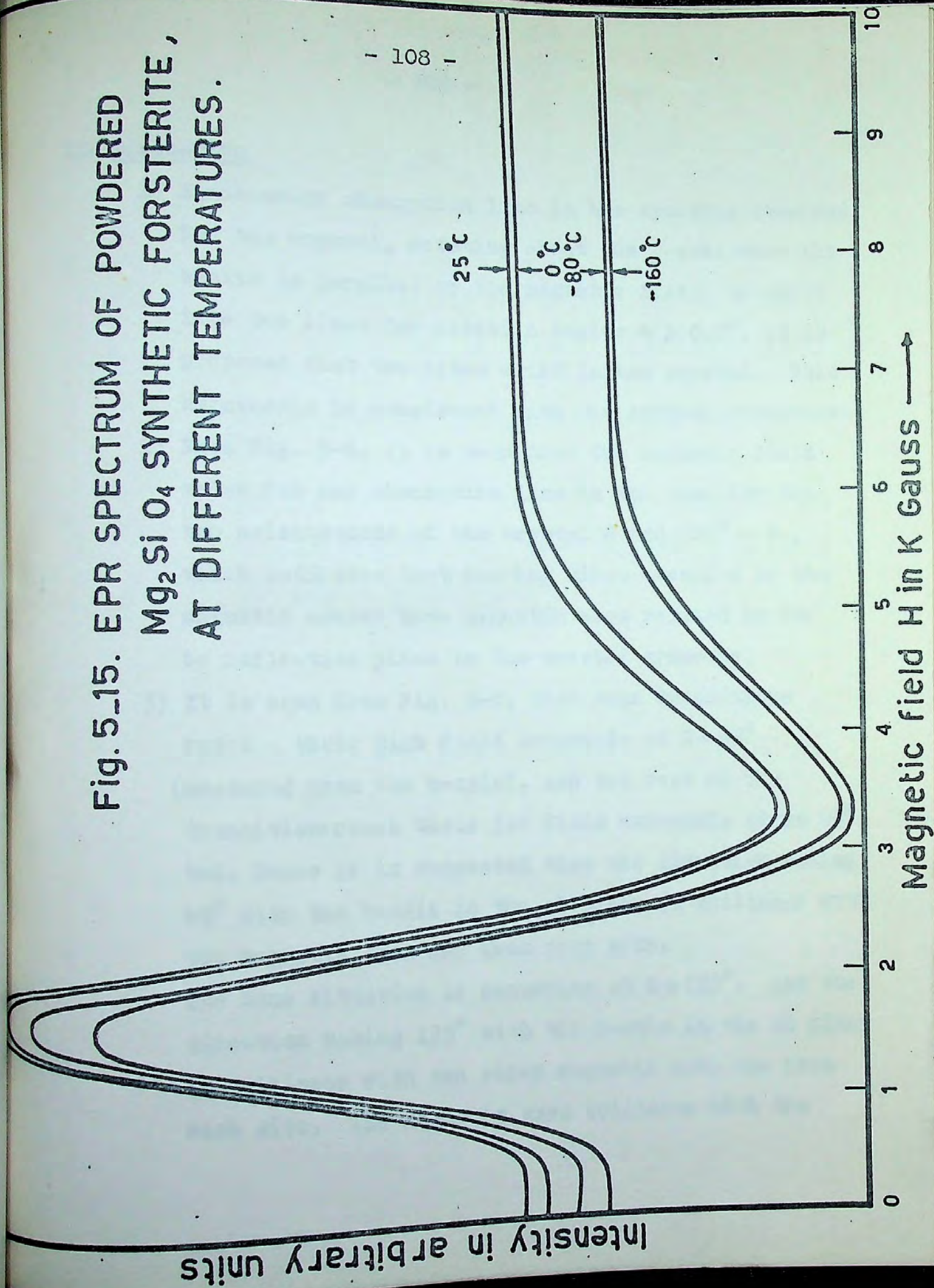
II- Discussion

1) Since every absorption line in the spectrum observed for the crystal, rotating about the c-axis when the b-axis is parallel to the magnetic field, is split into two lines for rotation angles $\theta \geqslant 0.5°$, it is proposed that two sites exist in the crystal. This hypothesis is consistent with the crystal structure.

2) From Fig. 5-8, it is seen that the magnetic field value for any absorption line is the same for the two orientations of the crystal θ and $180° - \theta$, which indicates that the two sites occupied by the magnetic center have magnetic axes related by the bc reflection plane in the crystal symmetry.

3) It is seen from Fig. 5-8, that some transitions reach their high field extremals at $\theta = 45°$ (measured from the b-axis), and the rest of the transitions reach their low field extremals at $\theta = 45°$ too. Hence it is suggested that the direction making $45°$ with the b-axis in the ab plane is collinear with two magnetic axes one from each site.
The same situation is occurring at $\theta = 135°$. And the direction making $135°$ with the b-axis in the ab plane is collinear with two other magnetic axes one from each site. The magnetic axes collinear with the

direction of $\theta = 45^\circ$ are 90° away from the magnetic axes collinear with the direction of $\theta = 135^\circ$, and are related by the bc reflection plane.

The conclusion of suggesting two sites related by 90° rotation around the c-axis can be compared to the result given by A. Chatelain and R.A. Weeks for Mn^{2+} in Mg_2SiO_4[2] of equivalent sites related by 67.5° rotation around the c-axis.

4) The splitting of the absorption lines observed for crystal rotation around the b-axis in the ac plane at $25^\circ C$ when the c-axis is $\pm 0.5^\circ$ off the magnetic field supports the postulate of having two sites in the crystal.

5) From Fig. 5-11, it is seen that the magnetic field value for any absorption line is the same for the angle θ and for the angle $180^\circ - \theta/$ thus the ab plane is a reflection plane in the crystal symmetry.

6) Since it is seen from Fig. 5-11, that all transitions observed for H at $\theta = 90^\circ$ (i.e. when the c-axis is parallel to the magnetic field) reaches either a low field or high field extremal value it is suggested that the crystallographic c-axis is collinear with the magnetic axes of sites 1 & 2.

7) From Fig. 5-14 it is seen that rotating the crystal
around its a-axis in the bc plane gives no symmetry
of the lines, which suggests that there is a mis-
orientation in fixing the (a) crystallographic axis
of the crystal during the experiment within $\pm 10^{\circ}$
that caused the field extremals to be off their
expected positions.

8) An effort was made to fit the magnetic field values of
the observed spectrum lines for the rotations around
(a), (b) & (c) directions to the graphs given by Dowsing
& Gibson[3] for a d^5 system. This effort suggests
that

  i) $\lambda = 0.267$

  ii) $D = 0.11$ cm^{-1}

  iii) The c-crystallographic axis of the crystal
    coincides with its z-magnetic axis.

  iv) The line $+45^{\circ}$ from the b direction
    in the ab plane of the crystal coincides
    with its x-magnetic axis.

  v) The y-magnetic axis of the crystal is in the
    ab plane of the crystal coinciding with the
    line -45° from the b-direction of the crystal.

Suggestions (iii), (iv) & (v) are supported by the
reasonings given in items 3 and 6 above.

9) It is suggested that some of the observed lines in the EPR spectra of Mg_2SiO_4 observed at $25^\circ C$ for rotation about its a, b & c crystallographic axes, are forbidden transitions ($\Delta M_s = 2, 3, 4..$). The intensity of these lines are exactly zero for directions of H parallel to the principal axes, but can be of the same order of magnitude as that of the normal transitions for H parallel to aribtrary directions.

10) The EPR spectra obtained for Mg_2SiO_4 crystal at different orientations do not have any hyperfine structure. Hence the paramagnetic ion causing these EPR spectra must have a small or zero abundance of an isotope with nuclear magnetic moment. Hence the transition ions Ti^{3+}, V^{2+}, Cr^{3+}, Mn^{2+}, Co^{2+} and Cu^{2+} are excluded, and thus the only ion left of the 3d-system is Fe^{3+}. The 4d and 5d systems have quite different transitions. Hence Fe^{3+} is the most probable ion which can account for the observed spectra.

The agreement of our results to the Dowsing and Gibson paper[3] indicates that the paramagnetic ion present is a d^5 ion. Hence the hypothesis of having Fe^{3+} ion is supported.

11) The decrease in intensity of all of the absorption
   lines with x-ray irradiation is similar to effects
   observed for Fe^{3+} in other crystals, attributed to
   Fe^{3+} trapping an electron causing its valency to
   change. Thermal annealing to $300^{o}C$ of the Mg_2SiO_4
   crystal, after x-ray irradiation, showed that the
   EPR spectrum of the crystal recovered its original
   feature before x-ray irradiation, indicating the
   reversibility of the valency change. This behaviour
   also is similar to that observed for Fe^{3+} in other
   oxides.

12) Heating to temperatures higher than $300^{o}C$ caused
   local disordering in the crystal structure revealed
   by the EPR spectrum.

III- Summary

* The Mg_2SiO_4 synthetic single crystal studied has Fe^{3+} impurity in it.

* The crystal has two site symmetries related by 90° rotation around the C axis.

* The magnetic axes of the two sites are related to the crystallographic axes of the crystal as follows:

$$(x_1,b) = 45^\circ \qquad (x_2,b) = 135^\circ$$

$$(y_1,b) = 135^\circ \qquad (y_2,b) = 45^\circ$$

$$z_1 \equiv C\text{-axis} \qquad z_2 \equiv C\text{-axis}$$

* The Fe^{3+} impurity is suggested to occupy the M(2) sites.

* Orientation dependence of the EPR lines was consistent with the M(2) site which has a C_v symmetry.

* X-ray irradiation causes Fe^{3+} to trap an electron following the reaction:

$$Fe^{3+} + X\text{-rays} \longrightarrow Fe^{2+}$$

* Heating to $300^\circ C$ causes the crystal to recover its conditions prior to X-ray irradiation.

* Crystal undergoes local/disorder upon heating to temperatures higher than $300^\circ C$.

Appendix I

V-4502 EPR Spectrometer System

The spectrometer used has the features outlined in the block diagram shown in Fig. I   It is a standard Varian V-4502 EPR Spectrometer system. Its magnet is a Varian V-3400 9 in. magnet and associated power supply.

A- They have the following specifications:

1- Performance Specifications

|	
Operating frequency	: 9.5 g.c. nominal (X-band)
Field Modulation frequency	: 100 Kc.
Klystron power output	: 300 mw maximum.
Klystron frequency stability	: 1 part in 10^6 with automatic frequency control (AFC).
Modulation field intensity	: No less than 35 gauss peak-to-peak maximum.
Field scanning rates	: 30 seconds, 1, 2.5, 5, 10, 25 and 50 minutes,
Magnetic field regulation	: 5 parts in 10^7 for a $\pm$ 10% change of line voltage or load impedance from mean.
Air Gaps	: 2.625 clearnace air gap.
Environment	: V-4502 EPR Spectrometer systems are highly stable. Normal variations in room temp,, assuming reasonable precautions against hot and cold air flow, and normal variations in inlet water temp. do not affect performance.
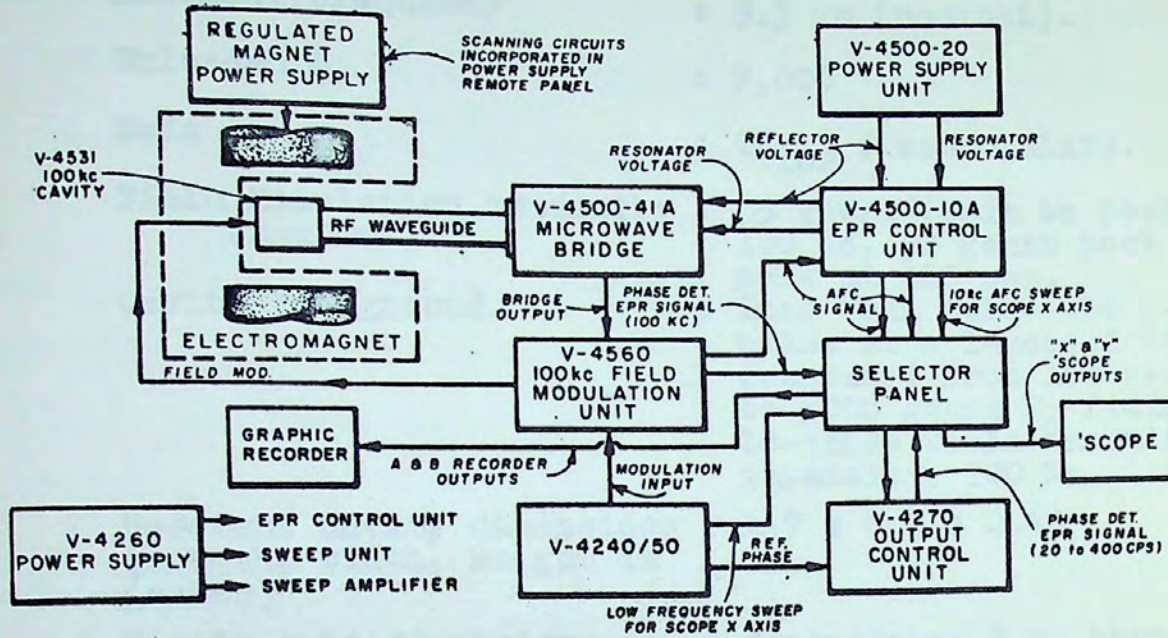
Fig. I
Block diagram of EPR spectrometer.

2- EPR Cavity Performance Specifications

Resonant Frequency	: 9.5 gc (nominal).
Unloaded Q	: 7,000
Mode	: TE_{102} (rectangular).
Field Modulation intensity (maximum)	: 35 gauss (peak to peak) at 100 Kc, 50 gauss peak to peak at 400 cps.
Cavity Background	: Less than twice the p-p noise at a 1-second time constant, from 100 gauss to 5000 gauss H_o field at 10-gauss field modulation intensity, 100 Kc.
Resonant Cavity dimensions (length, width, height in inches)	: 1.7 x 0.9 x 0.45
Sample tube dimensions	: Accomodates 5 mm thru 11.5 mm OD tubing by means of collets.
Required Magnetic Gap	: 1.75 inches.

B- Description of system components

1. V-4500 - 10A EPR control unit.

The EPR control unit provide the following functions in the operation of V-4502 EPR Spectrometer Systems: it indicates the deviation of Klystron frequency from cavity frequency when these frequencies differ; it monitors the Klystron resonator current; it indicates the current flowing through the crystal detector in the microwave bridge; it monitors the Klystron reflector voltage; and provides ON-OFF, Coarse, and Fine reflector voltage control; it controls the amplitude of the AFC

(automatic frequency control) modulation voltage applied to the Klystron reflector; it controls the AFC gain, and provides ON-OFF control of the AFC signal.

2. V-4500 - 41A X-Band Microwave Bridge.

The bridge contains a Klystron, the microwave distribution system, and a crystal detector. Absorption of microwave power in the sample as a result of resonance, unbalances the bridge. The unbalanced condition is detected by the crystal detector.

The bridge permits selection of either the dispersion or absorption mode. The absorption mode is more easily saturated by microwave power than the dispersion. The ability to observe the dispersion is often of great advantage in locating weak, unknown resonance signals, while observation of absorption mode is an aid in the interpretation of complex, multi-line resonances. The dispersion mode is often of great advantage in locating weak, unknown resonance signals, while observation of the absorption mode is an aid in the interpretation of complex, multi-line resonances.

3. V-4531 Multi-purpose cavity

The V-4531 cavity is termed a multi-purpose cavity because it can be used for fixed and variable temperature

studies, low-and high-power operation studies requiring either audio or 100 - Kc field modulation, and studies involving sample irradiation by u-v, visible, and other irradiation sources. In addition, it will accept sample tubes up to 11.5 mm in diameter.

The field sweep coils of the V-4531 cavity are designed for 100-Kc field modulation and will provide 35 gauss peak-to-peak field modulation at this frequency. Slots expose the sample for irradiation studies, and have a transmission of 50%. When not in use, they may be covered. The careful attention given to the electrical properties and mechanical construction of the V-4531, plus the high Q obtained, is in no small part responsible for the high-sensitivity of the V-4502 EPR spectrometer systems.

4- V-4250 Sweep Unit

The V-4250 sweep unit generates selectable frequencies of 20, 40, 80, 200 and 400 cps which are then amplified by the V-4240 sweep amplifier and applied to the cavity modulation coils. These frequencies also drive the X-axis of the oscilloscope, and the phase detector of the V-4270 Output Control Unit.

5- V-4270 Output Control Unit

Designed to provide recorder display of EPR signals for audio field modulation studies. Its functions are duplicated for 100 - Kc studies by the V-4560 100 - Kc Field Modulation and Control Unit.

6- V-4240 Sweep Amplifier Unit

This unit amplifies the modulation frequencies produced by the V-4250 Sweep unit, providing sufficient power to drive the cavity sweep coils and the phase detector of the V-4560 Output Control Unit.

7- V-4560 100 - Kc Field Modulation and Control Unit.

It contains a 100 - Kc crystal controlled oscillator which generates the field modulation frequency, and a high-gain amplifier and phase detector of the EPR signal.

The sensitivity of the EPR spectrometer when using 100 - Kc field modulation is approximately 15 times that obtained with 400 - cps modulation.

8- Fieldial Magnetic Field Regulator

Varian's Fieldial Magnetic Field Regulator and sweep unit, a standard component of V-4502 EPR Spectrometer Systems, provides a very high degree of flux regulation in the air gap, and a means of accurately dialing desired field values by a

calibrated front panel control/indicator. The Fieldial regulator also provides a field-proportional voltage for injection into the x-channel of an x-y recorder.

9- V-4595 Selector Panel

The selector panel, controls the presentation to the oscilloscope from both the V-4560 100 - Kc Field Modulation and Control Unit, and the V-4270 Output Control Unit. It also selects signals from either unit for presentation to the graphic recorder with the further choice of 1st or 2nd derivative display.

10- Graphic Recorder

A graphic recorder is required for readout of the EPR signal. The Varian Model G-14 Graphic Recorder is supplied with the systems. The unit supplied has 100-mv span, 0.6-second full-scan balancing time, and chart speeds of 1 inch and 4 inches per minutes.

11- Oscilloscope

A Hewlett-Packard Model 120A Oscilloscope is included in the spectrometer console for rapid initial setup and adjustment, and for signal observation. It is also used for check-out and adjustment of system components.

12- Magnet Systems

The 9-inch magnet system of the V-4502-12 system is offered as a relatively small, compact, and convenient component. It has 2.625-inch clearance air gap. The maximum field strength is 10 kilogauss. The field is controlled by a semiconducting device, according to the Hall effect.

13- Variable temp. accessory

The Model V-4557 Variable Temp. Accessory automatically controls the temperature of an EPR sample within the range of - 185°C to + 300°C. The temperature at the sample is controlled by passing a controlled current through an electric heater in the gas stream that is directed to the sample in the EPR cavity. A resistance - type temperature sensor near the sample monitors the gas stream temperature.

Appendix II

Crystal Orientation Goniometer

The goniometer parts are:

1- The sample holder (a) to which the sample is glued.

2- The goniometer tube (b) to which the sample holder is attached.

3- The goniometer cylinder (c) with the reference disc (d) and the fastening nut (e). The reference disc has a reference notch to which the crystal directions and the rotation angles are related.

4- The protractor disc (f) with spring bracket (g). It works as a protractor and is divided to 360 degrees by marked lines every 5 degrees.

5- The protractor wheel (h). It works also as a protractor and is divided in the same way to 360° as disc (f).

For working with the goniometer, the following steps are followed:

Case-A: Rotation in a horizontal plane (containing the magnetic field), around a vertical crystal axis (θ-rotation).

1- The sample is glued to the sample holder adequate for the type of rotation required.

2- The sample holder is screwed to the goniometer tube (b) and passed through the goniometer cylinder (c).

GONIOMETER

for EPR studies of crystals and their angular variations.

Labels in figure:
- WHEEL PROTRACTOR
- GONIOMETER TUBE
- REFERENCE DISC
- DISC PROTRACTOR
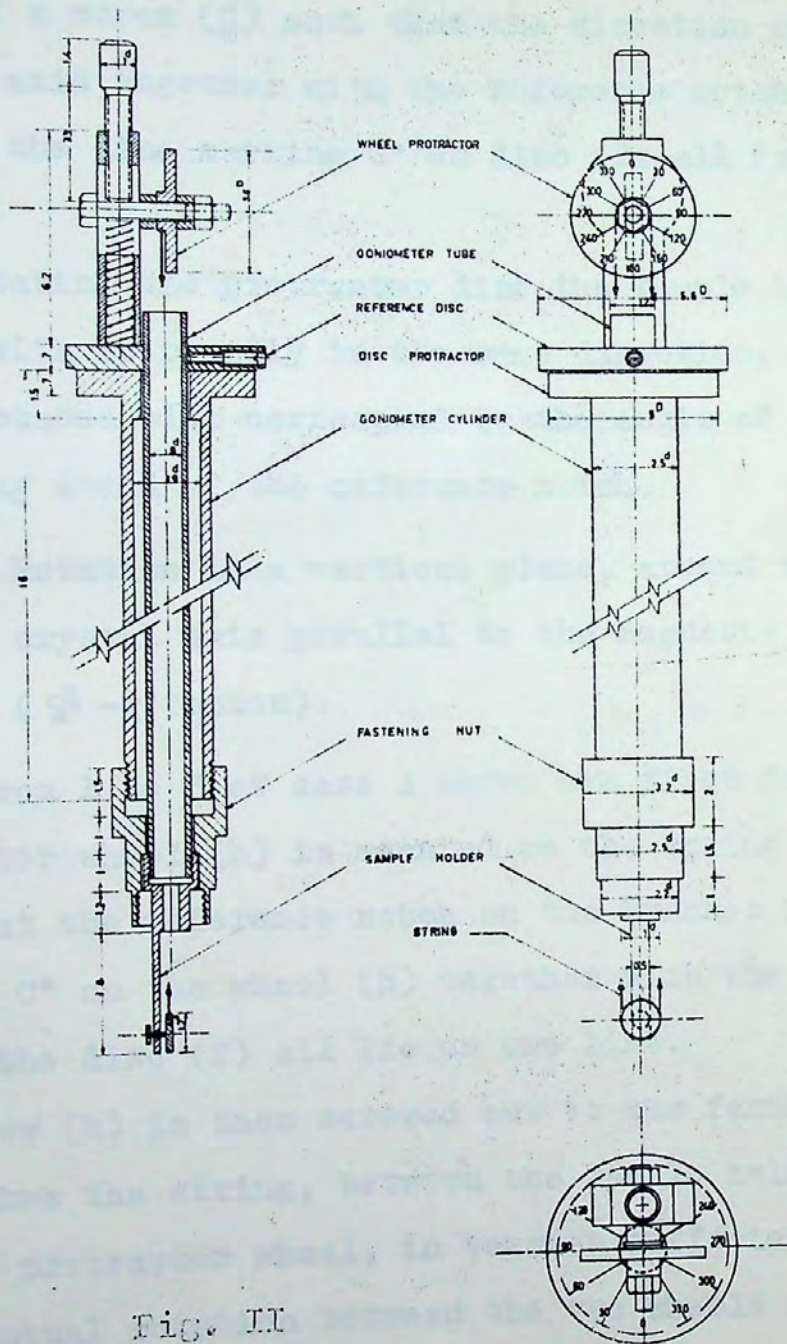- GONIOMETER CYLINDER
- FASTENING NUT
- SAMPLE HOLDER
- STRING

Fig. II

cm.

3- The protractor disc is then fastened to the end of the goniometer tube coming out of the goniometer cylinder by means of a screw (j) such that the direction of the crystal axis together with the reference notch on disc (d) and the line marking 0° on disc (f) all fall on one lines.

4- When rotating the protractor disc the sample holder will rotate with it rigidly in the same direction, and the angle rotated will correspond to the angle of the line now lying ahead of the reference notch.

Case-B: Rotation in a vertical plane, around a horizontal crystal axis parallel to the magnetic field (ϕ-rotation).

1- Steps from 1 to 3 of case A above are first followed.

2- Protractor wheel (h) is mounted on the spring bracket (g), such that the reference notch on the bracket (g), the line marking 0° on the wheel (h) together with the line marking 90° on the disc (f) all lie on one line.

3- The screw (k) is then screwed out to the farthest extent that makes the string, between the sample holder wheel and the protractor wheel, in tension sufficient enough to cause mutual rotation between the two wheels when rotating the wheel (h).

4- Rotating the wheel (f) the crystal will rotate in the
same direction giving us the ϕ-rotation required.

After prepairing the goniometer for work as in cases
A & B above, it is mounted to the cavity head with the
sample holder inserted inside the cavity, and the fastening
nut screwed to the cavity head. The fastening nut screwing
is adjusted such that the reference notch on the reference
disc lies on the vertical line passing through the middle of
the cavity and consequently the middle of the air gap of the
magnet poles.

Appendix III
Character tables of representative
crystallographic point groups
of Cubic System.

T_d	E	$8C_3$	$3C_2$	$6S_4$	$6\sigma_d$		
A_1	1	1	1	1	1		$x^2+y^2+z^2$
A_2	1	1	1	-1	-1		
E	2	-1	2	0	0		$(2z^2-x^2-y^2,$ $z^2-y^2)$
T_1	3	0	-1	1	-1	(R_x, R_y, R_z)	
T_2	3	0	-1	-1	1	(x, y, z)	(xy, xz, yz)

O_h	E	$8C_3$	$6C_2$	$6C_4$	$3C_2(=C_4^2)$	i	$6S_4$	$8S_6$	$3\sigma_h$	$6\sigma_d$		
A_{1g}	1	1	1	1	1	1	1	1	1	1		$x^2+y^2+z^2$
A_{2g}	1	1	-1	-1	1	1	-1	1	1	-1		
E_g	2	-1	0	0	2	2	0	-1	2	0		$(2z^2-x^2-y^2,$ $x^2-y^2)$
T_{1g}	3	0	-1	1	-1	3	1	0	-1	-1	(R_x, R_y, R_z)	
T_{2g}	3	0	1	-1	-1	3	-1	0	-1	1		(xz, yz, xy)
A_{1u}	1	1	1	1	1	-1	-1	-1	-1	-1		
A_{2u}	1	1	-1	-1	1	-1	1	-1	-1	1		
E_u	2	-1	0	0	2	-2	0	1	-2	0		
T_{1u}	3	0	-1	1	-1	-3	-1	0	1	1	(x, y, z)	
T_{2u}	3	0	1	-1	-1	-3	1	0	1	-1		

References

Chapter I.

1- B. Bleaney and K.W.H. Stevens, Rept. Prog. Phys. 16, 108 (1953).

2- R.D. Dowsing and J.F. Gibson, J. Chem. Phys. vol. 50, No.1 (1969), 294.

3- A. Chatelain and R.A. Weeks, J. Chem. Phys. vol. 52 No. 7, 3758, April 1970.

4- A. Chatelain and R.A. Weeks, J. Chem. Phys. vol. 52 No. 11, 5682, June 1970.

5- A.W. Hornig and E.T. Jaynes, Phys. Rev. vol. 96 (1954) pp 1703.

6- Sakudo, J. Phys. Soc. Japan, vol. 18 (1963), p. 1626.

7- Sakudo, Unoki and Mackaw, J. Phys. Soc. Japan, vol. 18 (1963) p 913.

8- Denis J.A. Gainon, J. App. Phys. vol. 36 pp 2325, July 1965.

9- H. Ikushima and S. Hayakawa, J. Phys. Soc. Japan 20 (1965) 1517.

10- Hiroshi Ikushima. J. Phys. Soc. Japan, vol. 21, No. 10, Oct. 1966.

11- J.D. Birle, G.V. Gibbs, P.B. Moore, and J.V. Smith, Am. Mineralogist 53, 807 (1968).

12- H. Onkon, Mineral. Petrog. Mitt. 1965, 34.

13- S. Geller and J.L. Durand, Acta Cryst. 13, 325 (1960).

14- E.N. Eliseev, Sov. Phys. Cryst. 3, 163 (1958).

15- J. Michoulier, J.M. Gaite, and B. Maffeo, compt. Rend.
269, 535 (1969).

Chapter II

1- E. Zavoisky, J. Phys. USSR, 9, 211, 245 (1945).

2- Bruce R. McGarvey, J. Chem. Phys. (1968).

3- H.M. Assenheim, Introduction to electron spin resonance
(Hilger & Watts, Ltd., London 1960).

4- G.E. Pake, Paramagnetic Resonance (W.A. Benjamin, Inc.,
New York, 1962).

5- Juan A. McMillan, Electron Paramagnetism (Reinhold Book
Corporation, New York, 1968).

6- R.D. Dowsing and J.F. Gibson, J. Chem. Phys. 50, 294
(1969).

7- D.J.E. Ingram, Spectroscopy at Radio and Microwave
Frequencies (Butterworths Scientific Publications, Ltd.,
London, 1967) 2nd ed.

8- J.E. Bennett, J.F. Gibson, D.J.E. Ingram, T.M. Haughton,
G.A. Kerkut, and K.A. Munday, Proc. Roy. Soc. (London)
A 262, 395 (1961).

9- E.S. Kirkpatrick, K.A. Muller, and R.S. Rubins, Phys. Rev.
135, A86 (1964).

10- T. Castner, Jr., G.S. Newell, W.G. Holton, and C.P. Slichter, J. Chem. Phys. 32, 668 (1960).

11- J.S. Griffith, Mol. Phys. 8, 213, 217 (1964).

12- H.H. Wickman, M.P. Klein, and D.A. Shirley, J. Chem. Phys. 42, 2113 (1965).

13- F. Holluj, Can. J. Phys. 44, 503 (1966).

14- G.J. Troup and D.R. Hutton, Brit. J. App. Phys. 15, 1493 (1964).

15- Bleaney, B., Phil. Mag. 42, 441 (1951).

16- W. Low, Paramagnetic Resonance in Solids, Academic, New York, 1960.

17- F. Albert Cotton, Chemical Applications of Group Theory, John Wiley & Sons, Inc. (1963).

Chapter III

1- P.W. Forsbergh, Phys. Rev. vol. 76, No. 8 (1949), 1187.

2- B. Motthias and A. von Hipple, Phys. Rev. 73 (1948), 1378.

3- J. K. Hulm, Nature 160, 126 (1947).

4- H.F. Kay, Acta Cryst. 1 (1948), 229.

5- C. Kittel, Introduction to Solid State Physics, John Wiley & Sons, Inc. (1966)

6- L. Pauling, The nature of the chemical bond, Cornell University Press, N.Y., 1960, 3rd ed.

7- J.D. Birle, G.V. Gibbs, P.B. Moore, and J.V. Smith, The American Mineralogist, vol. 53 (1968), 807.

Chapter V

1- A. Chatelain and R.A. Weeks, J. Chem. Phys. vol. 52 No.7 (1970), 3758.

2- A. Chatelain and R.A. Weeks, J. Chem. Phys. vol. 52 No.11 (1970), 5682.

3- R.D. Dowsing and J.F. Gibson, J. Chem. Phys. vol. 50 No. 1 (1969), 294.

4- H. Ikushima, J. Phys. Soc. Japan, vol. 21 No. 8 (1965),1517.

5- V.F. Folen, Phys. Rev. 125 (1962), 1581.

6- V.J. Schneider and S.R. Sircar, Z. Naturforsch, 17a (1962), 651.

7- P. Walder, Helv. Phys. Acta, 35 (1962), 756.

8- M. Odehnal, Czech. J. Phys. 13 (1963), 566.

9- B. Bleaney & R.S. Rubins, Proc. Phys. Soc (London) 77 (1961), 103.

10- H.M. Assenheim, Introduction to electron spin resonance, Hilger & Watts Ltd. London (1966).